Fall 2015

Localization and tracking of electronic devices with their unintended emissions

Nurbanu Guzey

Department: Electrical and Computer Engineering

LOCALIZATION AND TRACKING OF ELECTRONIC DEVICES WITH THEIR UNINTENDED EMISSIONS

by

NURBANU GUZEY

A DISSERTATION

Presented to the Faculty of the Graduate School of the

MISSOURI UNIVERSITY OF SCIENCE AND TECHNOLOGY

In Partial Fulfillment of the Requirements for the Degree

DOCTOR OF PHILOSOPHY

In

Electrical Engineering

2015

Approved by:
Dr. Jagannathan Sarangapani
Dr. Maciej Zawodniok
Dr. Steve Grant
Dr. Mohammad Tayeb Ahmad Ghasr
Dr. Sanjay Madria

PUBLICATION DISSERTATION OPTION

This dissertation consists of the following five articles that have been submitted for publication. The papers are formatted according to Missouri University of Science and Technology specifications

Pages 13-41, "Localization of Near-Field Radio Controlled Unintended Emitting Sources in the Presence of Multipath Fading, were published in IEEE Transactions on Instrumentation and Measurement, in Nov. 2014.

Pages 42-76, "Localization of Near-Field Sources in Spatially Colored Noise," were published in IEEE Transactions on Instrumentation and Measurement, in August 2015.

Pages 77-105, "Tracking of Radio-controlled Sources using Unintended Emissions" under review with Elsevier Measurement journal.

Pages 106-146, "Analysis of Localization and Tracking Methods for Unintended Emitting Sources*"* were submitted to the Journal of Signal Processing Systems.

Pages 147-179, "Localization and Tracking of Unintended Emitting Sources in 3D Environments" were submitted to the IEEE Transactions on Instrumentation and Measurement.

ABSTRACT

The precise localization and tracking of electronic devices via their unintended emissions has a broad range of commercial and security applications. Active stimulation of the receivers of such devices with a known signal generates very low power unintended emissions. This dissertation presents localization and tracking of multiple devices using both simulation and experimental data in the form of five papers.

First the localization of multiple emitting devices through active stimulation under multipath fading with a Smooth MUSIC based scheme in the near field region is presented. Spatial smoothing helps to separate the correlated sources and the multipath fading and results confirm improved accuracy. A cost effective near-field localization method is proposed next to locate multiple correlated unintended emitting devices under colored noise conditions using two well separated antenna arrays since colored noise in the environment degrades the subspace-based localization techniques.

Subsequently, in order to track moving sources, a near-field scheme by using array output is introduced to monitor direction of arrival (DOA) and the distance between the antenna array and the moving source. The array output, which is a nonlinear function of DOA and distance information, is employed in the Extended Kalman Filter (EKF). In order to show the near- and far-field effect on estimation accuracy, computer simulation results are included for localization and tracking techniques.

Finally, an L-shaped array is constructed and a suite of schemes are introduced for localization and tracking of such devices in the three-dimensional environment. Experimental results for localization and tracking of unintended emissions from single and multiple devices in the near-field environment of an antenna array are demonstrated.

ACKNOWLEDGEMENTS

I would like to express my sincere thanks to my advisor, Professor Jagannathan Sarangapani, for his close supervision, help and support during the entire research duration. Without his patient and constant guidance, this dissertation would not have been possible. I would like to thank Dr. Hao Xu, for his timely help, valuable suggestions concerning to my research. I would also like to thank Dr. Tayeb Ghasr, who gave me many helpful discussions and suggestions regarding my dissertation work. In addition I would like to thank my committee members Dr. Steve Grant, Dr. Maciej Zawodniok and Dr. Sanjay Madria for their valuable comments and suggestions.

Finally, I want to thank my husband, Haci Mehmet Guzey, my sons, Fatih and Melih Guzey, my parents, Nesrin and Cemal Akyuz, and parents in-law, Munure and Servet Guzey, as well as the rest of my family for their infinite love, care and encouragement, without which I would have not been at this stage of my life. In addition, I would like to extend my deepest thanks to my dear friend Havva Malone for her help and support, and many other friends in Rolla who made my Ph.D. life more fun and interesting.

TABLE OF CONTENTS

Page

LIST OF ILLUSTRATIONS

Page

PAPER I

PAPER II

PAPER V

LIST OF TABLES

Page

1. INTRODUCTION

Detection and localization of multiple RC electronic devices through their unintended emissions can play a critical role in security and surveillance applications. These devices can be detected via their unintended emissions, a technique referred as passive detection [1]. However, [2] and [3] have determined that the super heterodyne or super regenerative receivers in these RC devices are responsive to radio frequency stimulation. The unintended emissions due to active stimulation signals are stronger, have a predictable response [4] and also provide a better detection range [5]. [3] used second order self-similarity characteristics to detect unintended emissions from a super regenerative receiver whereas a matched filter was utilized in [6].

The methods introduced in [2] and [6] used a single antenna, but did not provide the direction of arrival (DOA) of the unintended emissions. However, array antennas not only provide DOA information but also increase the received signal-to-noise ratio (SNR) [3]. With the increased SNR, the detection range can be enhanced; furthermore, the DOA information can help to locate the device. Therefore, the array processing techniques used in radar, sonar and acoustic applications can be employed for locating the unintended emitting devices.

Received signal strength (RSS) based localization techniques are also popular due to their ease of implementation with the received power information. However, in order to determine the signal propagation model, accurate channel estimation is needed [7]. To overcome this condition, fingerprinting of the area is completed first by using RSS measurements; then, location estimation of the device is evaluated by online matching of current measurements with the fingerprints [8]. However, the RSS is affected by

reflections, diffraction or scattering, necessitating new fingerprinting, which can be time consuming.

Another array processing method presented in the literature is the time of arrival (TOA) based schemes. The TOA and time difference of arrival (TDOA) methods require accurate synchronization between a transmitter and receiver pair, which is not always possible. Also, a time-stamp needs to be included on the transmitting signal to measure the distance that the signal has traveled. The TOA can be calculated with different techniques such as direct sequence spread-spectrum (DSSS) [9], [10] or ultra-wide band measurements [11].

The DOA is defined as the angle between the direction of the incident signal propagation and a reference direction on the antenna array. The phase difference between the antenna elements is used to determine the DOA and no other information is needed from the transmitter [12]. From the geometry, the localization performance also depends upon the distance between the source and the antenna array. If the source is placed further from the receivers, the inaccuracy in the DOA estimation will result in higher localization error.

In the delay and sum method given in [13], the angle which results in maximum power is considered as DOA. The resolution of the estimation is related with the number of antennas in the array. To increase the accuracy, widely used high resolution techniques such as MUSIC [14] and ESPRIT [15] are developed. These subspace based methods apply eigenvalue decomposition (EVD) to the covariance matrix of the array output and use the orthogonality property between the noise and signal subspaces. The computational complexity of MUSIC and EPRIT based methods leads to the

development of DOA schemes such as matrix pencil [16], which does not require the covariance matrix of the array output or methods such as SUMWE [17] where EVD is not calculated.

The existing methods [13]-[17] are considered as far-field localization schemes where the DOA information to each antenna element is assumed to be same, since the incident signal has a planar characterization when the device is placed in the far-field region of the antenna array. However, due to the weak nature of the emissions, it is more appropriate to use near-field localization schemes where the DOA to each antenna cannot be assumed to be the same at each antenna due to the spherical shape of the incident signal in near-field. The phase difference is also a function of the distance between the source and the antenna array which makes the localization process more challenging. Fresnel approximation [18], which is the second order Taylor series expansion of the phase between antennas, is the most preferred method to mitigate this deficiency.

The near-field method such as in [19] uses the higher order statistics for location estimation. A maximum likelihood estimator is proposed in [20] and an ESPRIT-like least square scheme is developed in [21] to approximate the location of near-field devices. On the other hand, these methods [19]-[21] provide near-field location estimation in a computationally expensive manner and are sensitive to correlation among sources and multipath fading signals.

The efficiency of both near- and far-field subspace-based localization methods [13]-[17] and [19]-[21] mentioned above depends on the separation of the signal and noise subspaces. These subspaces are orthogonal and separated efficiently when the noise is white as assumed in [13]-[17] and [19]-[21]. However, the noise may not be always

white Gaussian due to cross talk among channels, random radiation from sources or the presence of undesired interference. When the noise in the environment has colored characteristics, the overlapping subspaces cannot be separated since the colored noise prevents a subspace rotation. The comprehensive effect of colored noise on location estimation is discussed in [22].

There are two main methods presented in the literature to whiten the noise if it is colored. The first approach parametrizes the noise covariance matrix such that both noise parameters and DOA are estimated. As an example, the noise is parametrized as an auto-regressive (AR) model in [23] and [24]. Alternatively, in [25] and [26], the noise covariance matrix is written as a sum of known basis functions. Rather than noise covariance estimation, signal covariance is approximated by modeling it as a combination of known basis functions assuming that the signal model is partially known [27]. Although the techniques mentioned in [23]-[27] do not require a prior knowledge of the noise covariance matrix, they require partial information about noise or signal modeling. In the second approach, noise-only data is used to whiten the colored noise and estimate the noise covariance matrix [28]. In this approach, the efficiency of the whitening filter depends on the number of noise-only data samples.

Another challenge to locate the unintended emitting devices appears if the device is non-stationary, then it can be critical to track these devices for security reasons. The angle tracking algorithms in [29] and [30] assume that that the sources are stationary during a limited integration time, and apply a conventional angle estimation method such as MUSIC in that interval to track the angle and the device.

However, a data association problem occurs for the DOAs estimated from the two successive time intervals in these methods [29]-[30] if there is more than one device to track. This problem is efficiently solved in [31] with a recursive tracking technique where the DOA is estimated based on the most recent array output, which is used to update the predicted DOA. The distance between the estimated and the true covariance matrix of the array output is minimized to associate the multiple devices with their corresponding DOA in [32]; however, the method assumes that the signal powers of all devices are different, which may not be possible in practice.

In [32]-[35], a Kalman filter is utilized to increase the estimation accuracy and to solve the data association problem. In these methods [32]-[35], during the prediction step of the Kalman filter, the current state vector is estimated from the previous state vector, and later in the correction step, current measurements are used to enhance the estimated state vector. In [35], Park's method [34] is improved by estimating angle innovations from signal subspace instead of the output covariance matrix.

DOA estimation methods mentioned in [14]–[28] focused solely on estimating the azimuth angle. However, if an airborne array is used to locate ground-based sources, the elevation angle of arriving signals should also be estimated for localization. In [38], many array configurations are analyzed and the L-shaped array is found superior to other configurations for two- dimensional (2D) DOA (azimuth and elevation angles) estimation. The preference for the L-shaped array is due to its simpler configuration when compared to others and an improved accuracy due to its larger aperture, which can accommodate the largest distance among sensors [38].

Therefore, L-shaped arrays have become very popular for solving 2D DOA estimating problems. Tayem and Kwon [39] proposed a computationally efficient 2D DOA estimation technique based on the propagator method by employing one or two L-shaped arrays. They proved that the 2D problem can be decomposed into two independent 1D problems with an L-shaped array, which means the method is computationally inexpensive. However, two independent sets of angles have to be paired together properly by using a pairing algorithm such as in [40]. A cross-correlation technique is presented in [41] to obtain correct DOA pairs by constructing a Toeplitz matrix. Unfortunately, the pair matching is inefficient when the difference of the corresponding azimuth and elevation angle is small and the signal to noise ratio (SNR) is low. A simple maximum likelihood method was proposed in [38] for 2D DOA estimation; however, it requires good initial estimates.

The performance of each proposed method can be studied by computer simulations by considering different cases; such as different antenna numbers and SNR, however; this can be very costly if performed through an experimental setup. Motivated by the above facts, in this dissertation, a suite of novel localization and tracking schemes for unintended emitting devices are presented. The organization of the thesis follows.

1.1 ORGANIZATION OF THE DISSERTATION

Localization of multiple RC electronic devices through their unintended emissions can have an important role in security and commercial applications. Theoretically, RC devices emit low power unintended emissions in the presence of an active stimulation signal. The major challenges to detecting and localizing these devices are high noise conditions, multipath fading and correlation between sources if there are

multiple devices. Reliable localization methods are required to determine the exact location of the devices under practical conditions. Furthermore, the unintended emitting device can be nonstationary, and tracking of these devices under these major challenges is also needed.

Since the initial power of the unintended emissions is not known, received signal strength (RSS) based methods cannot satisfactorily locate the RC device through its unintended emissions, and time of arrival (TOA) techniques require high synchronization performance; therefore, DOA-based estimation techniques have been developed since they are more suitable for this topic.

First, a MUSIC based DOA estimation method is presented to locate correlated RC devices in the near-field region of an antenna array under multipath fading conditions. Antenna elements are divided into overlapping subarrays in order to separate multiple correlated sources or multipath fading from the obstacles in the environment. The mean of the output covariance matrix of overlapping subarrays are then calculated to estimate both DOA and the distance between an antenna array and the source.

Second, a localization method to estimate DOA and the distance between antenna array and the source in colored noise conditions is developed. Most existing theoretical DOA estimation methods assume a white noise environment, but they degrade the performance in practice when the noise is colored. Two well-separated antenna arrays are employed to use the spatial diversity between the arrays for localization of the unintended emitting device.

The unintentional emitting sources may not always be stationary; therefore a tracking method is proposed in this dissertation to track both DOA and the distance

between the antenna array and the source using an extended Kalman filter with the array output directly instead of covariance matrix of the array output.

In order to provide a broad analysis, computer simulation results of the proposed methods are given. Therefore, the effectiveness and performance of the methods are also verified with computer simulations in near- and far-fields of the antenna array besides experimental measurements.

Finally, near-field, three-dimensional (3D) localization and tracking schemes are demonstrated for unintended emissions from electronic devices by using an L-shaped array. Most of the methods [14]-[28] where both azimuth and elevation angles are estimated do not work satisfactorily in the near-field region of the antenna array. The 3D localization and tracking of electronic devices are developed by using the difference in the phase characteristics of the arrays, which are placed at different axes.

Traditional far-field localization techniques [13]-[17] assume that the DOA information to each antenna element in the array is similar. In addition, the unintended emissions from RC devices have very weak power; therefore, detecting and locating them in the far-field region of the array may not be efficient. Hence, near-field localization techniques are required where both DOA and the distance between the source and the array are estimated, which makes the localization more challenging. However, existing near-field localization techniques [19]-[21] do not consider the correlation among sources or they assume perfect environmental conditions. Therefore the main goal of this dissertation is to locate and track the unintended emitting devices accurately with active stimulation using linear antenna arrays in the presence of correlation among the sources or multipath fading for different environmental conditions.

1.2 CONTRIBUTIONS OF THE DISSERTATION

The contributions in this dissertation are summarized as follows. The first contribution is the development of a near-field localization technique based on the MUSIC method for multiple correlated sources. The existing near-field localization techniques [19]-[21] degrade the performance when the sources are correlated; moreover, they perform the localization at a high computational expense. In order to separate the correlated sources or the multipath fading signals from the environment, a spatial smoothing process is applied and the antenna array is divided into overlapping subarrays. This smoothing provides random phase modulation, which in turn targets the decorrelation of the sources. Instead of the covariance matrix of the array output, the mean of the covariance matrices of the subarrays is employed in the two dimensional search. Furthermore, most of the localization schemes such as [19]-[21] provides computer simulations to demonstrate the effectiveness of their methods. However the conditions in the real environment are not as perfect as they are in computer simulations; therefore, the hardware evaluation of the proposed method, symmetric subarray based near-field localization technique [36] and conventional 2D-MUSIC [37] is provided to depict the real performance of the methods.

The near-field localization methods, [19]-[21] and [36]-[37], use the orthogonality between the signal and noise subspaces when the noise is white. However, the assumption of noise being white may not be valid especially for practical applications. The effect of colored noise is also considered in [22]. The second paper extends the idea of near-field localization by relaxing the assumption of white noise in the environment. To discard the effects of colored noise, two well-separated arrays resulting in spatial

diversity among the arrays is used. Instead of conventional eigenvalue decomposition, generalized correlation decomposition is utilized for subspace estimation from the separated arrays. Also, since this method does not require noise statistics, it is more adaptive to the environmental conditions. Furthermore, since the unintended emissions are generated with a stimulating signal, before applying the stimulation signal, noise-only samples are collected. These samples are used to construct a whitening filter. When this filter is applied to the covariance matrix of the array output with unintended emissions, the noise becomes white and subspace based methods can be used. Also, as in the first paper, hardware evaluation of both methods is provided to show more realistic results and the efficiencies of the methods are compared.

The main contribution of the third paper is the development of a near-field tracking algorithm for the nonstationary unintended emitting devices which is very important for security reasons. In contrast to the tracking methods as discussed in [29]-[35], where the covariance matrix of the array output is constructed for every time instant. Finally, the array output is directly used in the extended Kalman filter to estimate the states, which are the DOA and the distance between the antenna array and the source. This property makes the method more convenient for the practical applications since to estimate the covariance matrix, multiple snapshots of the array output are needed for every time instant which may not be possible especially for practical applications.

The tracking techniques in [34]-[35] uses a linear measurement model for the Kalman filter; however, the measurement model is a nonlinear function of the state variables. Therefore, instead of a linear measurement model, a nonlinear measurement model is used to increase the accuracy of the tracking method. Experimental results for

the tracking of single and multiple devices are presented for different scenarios; also, the hardware evaluation of Park's method [34] is provided, and the effectiveness of different measurement and evaluation methods is compared.

The contributions of the fourth paper include a broad analysis of the proposed methods by computer simulations. Due to the low power of targeted emissions, near-field techniques are developed in this dissertation. Computer simulations will prove that the near-field approach is the best way to locate and track unintended emissions. By this analysis, the effectiveness and the performance of each method will be checked with computer simulations. Furthermore, simulation results for different array and source configurations will be provided to see how the methods perform if these configurations were implemented by hardware.

The contributions of the last and most recent paper of this work include the development of near-field, 3D localization and tracking schemes by an L-shaped array. When the array and the sources are not in the same level, besides the azimuth angle, the elevation angle should also be estimated. Methods proposed for the 2D DOA (e.g., azimuth and elevation angles) estimation [38]–[41] assume the source to be in the far-field region of the antenna array; however, the distance between the array and the source should also be estimated if the source is placed in the near-field of the array.

The proposed 3D localization method uses the difference in the phase characteristics of the arrays located at different axes and provides the localization without a pair matching algorithm. The same property is also used with 2-stage EKF to track the unintended emissions if they are nonstationary. Further, the received signal by the ULA is modeled with free space Green's function instead of DOA; therefore, using the new

model in a MUSIC scheme provides the estimation of Cartesian coordinates directly. In this way, the errors in the DOA estimation will not affect the location estimation because a small error in DOA can lead to a huge error in localization if the device is placed far away from the array. Also the array is placed at a height to reduce reflections from the environment. The effectiveness of the proposed methods for localization and tracking of unintended emitting sources are presented with experimental results.

PAPER

I. LOCALIZATION OF NEAR FIELD RADIO CONTROLLED UNINTENDED EMITTING SOURCES IN THE PRESENCE OF MULTIPATH FADING

ABSTRACT

Localization of near field unintended emitting radio controlled (RC) devices under a multipath environment is considered in this paper by using a uniform linear antenna array (ULA). Since received signals are dependent on both angle of arrival (AoA) and distance from the RC devices to the ULA in the near-field scenario [12], traditional localization schemes based on received signal strength indicator (RSSI), time difference in arrival (TDOA), which only estimate either AoA or distance, are unsuitable. Therefore, a novel smooth 2-D MUSIC near-field localization scheme is developed to locate RC devices under a multipath environment with a possible location error of $\pm 0.5m$. Experimental results are provided to show the effectiveness and feasibility of the Smooth 2-D MUSIC near-field localization scheme and it is contrasted with other methods such as symmetric subarray and 1-D MUSIC based schemes.

1. INTRODUCTION

Radio controlled (RC) devices which have either super heterodyne or super regenerative receivers are responsive to radio frequency stimulation [1], [2]. This stimulation leads the devices to emit unintended radiation. For instance, in [2] a second order self-similarity representation is used for detecting the signals emitted by a super-regenerative receiver from a single unknown device. Array detector with directional antennas is employed for the detection of such devices in [3] whereas matched filter is utilized in [4]. In passive detection [5], unintended emissions without stimulation are used for detection and identification. However, by active stimulation, the unintended emissions from the devices are stronger, have a predictable frequency response [6] and in addition as indicated in [7] a better detection range provided the device responds to the stimulation.

The available detection methods from [1-2] and [4] use a single antenna where the angle of arrival (AOA) information is not available. Array antennas, on the other hand, not only increase the received SNR [3] but also they provide AoA information. Increased SNR enhances the detection range while the AoA information can help locate the device.

In addition, array antennas can separate and classify multiple devices and multipath fading signals in comparison with a single antenna. Therefore array processing techniques and array antennas have been used to detect and locate multiple active sources [8-11]. Active sources have a higher SNR when compared to the passive unintended emissions and they likely get detected. In addition, the devices are placed and located in the far-field region of the array antennas.

Existing localization schemes [8-11] for the far-field region assume that the angle of arrival (AoA) information to each antenna element is same as that of the other, a stringent assumption when the RC devices are in the near field region. In the far field region, the phase difference between antennas is a function of AoA whereas in the near field region, the distance between the antennas and the source is also included in both phase difference between antennas and near field signal representation.

Therefore, the near field localization of a RC device is more challenging than locating a device in the far field region since the near-field received signals are an implicit nonlinear function of AoA and distance between the RC devices and the antenna array which makes it difficult to infer either AoA or distance. To overcome this deficiency, a well-known Fresnel approximation [12] can be utilized to represent the implicit function with the second order Taylor expansion.

Recently, Challa and Shamsunder [13] proposed a least square ESPRIT-like algorithm to estimate the near-field location of the device. A novel localization scheme is introduced based on the fourth order cumulants of the near field sources in [14]. In contrast, authors in [15] developed a novel maximum likelihood estimator (MLE) to approximate the location of devices in the near-field region. However, these methods [13-15] provide the near-field location at the expense of significant computational cost and are sensitive to multipath effects degrading the location accuracy.

To mitigate this deficiency, in the literature [18], a near-field localization scheme, referred to as the 2-D MUSIC, has been introduced to estimate both the AoA and distance between the near-field RC devices and the antenna array. However, this method is found to be sensitive to the multipath fading.

To mitigate the multipath fading which degrades the performance of the localization in the near-field scenario, a spatial smoothing procedure has been incorporated into the 2-D MUSIC scheme [18] in order to de-correlate the received signals. Thus the proposed Smooth 2-D MUSIC localization scheme can locate the near-field RC devices even in the presence of multipath signals. Further, the experiment results are given to demonstrate the effectiveness and feasibility of the proposed 2-D Smooth MUSIC scheme and contrasted with symmetric subarray based near-field localization and 1-D MUSIC by using the linear antenna array to evaluate the effectiveness of the proposed schemes.

Therefore, the main contributions of the proposed work include: 1) the development of the Smooth 2-D MUSIC near field localization scheme for RC devices in the presence of multipath fading by extending the work of 2D-MUSIC scheme [18]; 2) performance evaluation of the symmetric subarray based near field localization, 2-D MUSIC and proposed Smooth 2-D MUSIC schemes using experimental data; and 3) comparison of these schemes with 1-D MUSIC scheme.

The rest of this paper is organized as follows. Section 2 formulates the near field signal representation. Subsequently, symmetric subarray based near-field localization scheme without multipath fading is introduced. Next, the novel smooth 2-D MUSIC scheme in the presence of multipath fading is developed. Experimental details and evaluation results for smooth 2-D MUSIC and symmetric subarray based near-field methods by using data collected from a RC device are provided for AoA and range estimation in Section 3.

Moreover, localization results for near field technique is compared with a far field method (1-D MUSIC) in order to show the effectiveness. Section 4 concludes the paper by giving the future directions.

2. METHODOLGY AND EXPERIMENTAL SETUP

In this section, the near field signal representation is introduced first. Subsequently, the symmetric subarray based near-field localization scheme is given. Eventually, the Smooth 2-D MUSIC scheme is proposed to locate a near-field passive source in the presence of multipath fading. The localization of a source with unintended emissions from a device by using an antenna array is depicted in Figure 2.1.

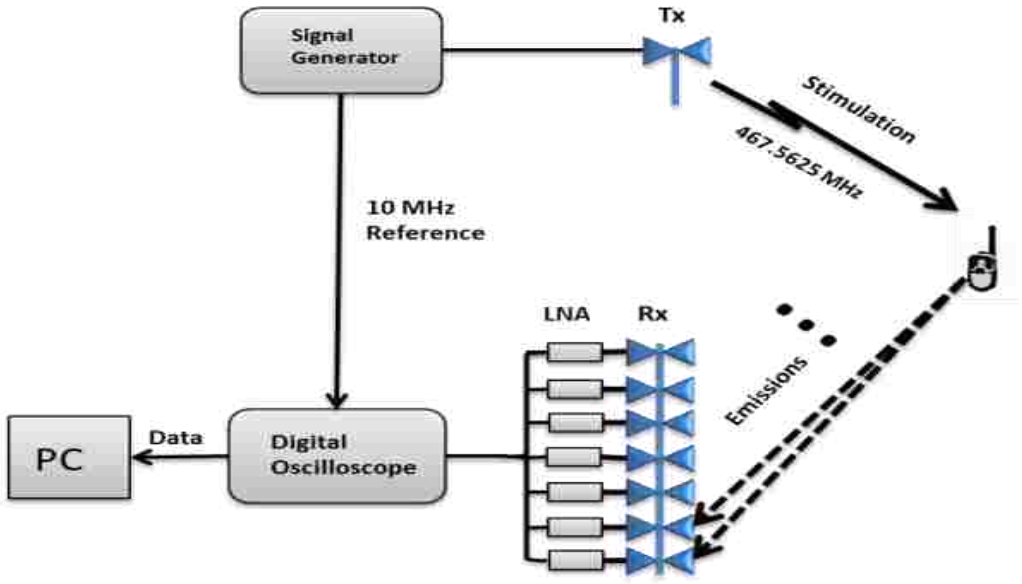

Figure 2.1. Schematic view of detection and localization process from unintended emissions.

2.1 NEAR FIELD SIGNAL MODEL

Consider a uniform linear array (ULA) consisting of $P = 2K + 1$ antenna element with spacing *d* wherein the center element of the array is assigned as the reference point. Moreover, since there are *M* near-field and narrowband passive radiating RC sources, the signal received at the ULA can be represented as

$$\mathbf{x}(t) = \sum_{m=1}^{M} \mathbf{a}(\theta_m, r_m) s_m(t) + \mathbf{n}(t) \tag{2.1}$$

$$= \mathbf{A}\mathbf{s}(t) + \mathbf{n}(t) \quad t = 1, \ldots N$$

where N is the number of snapshot, $s_m(t) \in \Re$ is the received signal power from the m^{th} passive source, $\mathbf{s}(t) = [s_1(t), s_2(t), \cdots s_M(t)] \in \Re^M$ denotes the received signal power vector, $\mathbf{n}(t) = [n(-K), \ldots n(K)] \in \Re^P$ is the additive white Gaussian noise vector and $\mathbf{A} = [\mathbf{a}(\theta_1, r_1), \mathbf{a}(\theta_2, r_2), \ldots, \mathbf{a}(\theta_M, r_M)] \in \Re^{P \times M}$ is the $P \times M$ steering matrix. This steering vector, $\mathbf{a}(\theta_m, r_m)$, can be represented as

$$\mathbf{a}(\theta_m, r_m) = \left[e^{j\tau_{-K}(\theta_m, r_m)}, e^{j\tau_{-K+1}(\theta_m, r_m)}, \cdots, e^{j\tau_K(\theta_m, r_m)} \right]^T, m = 1, .., M \tag{2.2}$$

Where T denotes the matrix transpose, θ_m, r_m are AoA and distance between the m^{th} passive source and ULA respectively, and $\tau_k(\theta_m, r_m)$ denotes the phase shift between k^{th} antenna and reference point. This term $\tau_k(\theta_m, r_m)$ is expressed as

$$\tau_k(\theta_m, r_m) = \frac{2\pi d}{\lambda} \left(\sqrt{r_m^2 + (kd)^2 - 2 r_m kd \sin\theta_m} - r_m \right) \quad k = -K, \ldots, K \tag{2.3}$$

Where d denotes the spacing between antenna elements, λ is the wavelength of the transmitter and k is k^{th} antenna element.

Since near-field sources are located in the Fresnel region, phase shift can be approximated by using Fresnel approximation [12] as

$$\tau_k(\theta_m, r_m) \approx \frac{2\pi d}{\lambda} \left(kd \sin\theta_m - \frac{k^2 d^2 \cos\theta_m}{2 r_m} \right), \quad k = -K, \ldots, K \tag{2.4}$$

Substituting (2.4) into (2.1), received signals from k^{th} antenna element is given by

$$x_k(t) = \sum_{m=1}^{M} e^{j\left(-\frac{2\pi d}{\lambda}\sin\theta_m\right)k + j\left(-\frac{\pi d^2}{\lambda r_m}\cos^2\theta_m\right)k^2} s_m(t) + n(t) \quad k = -K, \ldots, K \tag{2.5}$$

The received signal can be expressed in the form of $\mathbf{X}(t) = \left[x_{-K}(t),\ \ldots..\ , x_K(t)\right]^T \in \Re^P$ as

$$\mathbf{X}(t) = \mathbf{A}\mathbf{S}(t) + \mathbf{N}(t) \quad t = 1, \ldots N \tag{2.5}$$

where T denoting transpose, $\mathbf{S}(t) = \left[s_1(t), \cdots, s_M(t)\ \right]^T \in \Re^M$ is the vector of received signal power, $\mathbf{N}(t) = [n_{-K}(t),\ \ldots\ , n_K(t)]^T \in \Re^L$ is the additive Gaussian noise vector and $\mathbf{A} = [\mathbf{a}(r_1, \theta_1), \cdots, \mathbf{a}(r_M, \theta_M)] \in \Re^{P \times M}$ denotes antenna array manifold matrix where the steering vector $\mathbf{a}(r_m, \theta_m) \in \Re^M$ for m^{th} passive source is now expressed as

$$\mathbf{a}(r_m, \theta_m) = \begin{bmatrix} a_{m,-K} \\ \vdots \\ a_{m,K} \end{bmatrix} = \begin{bmatrix} e^{j\left(-\frac{2\pi d}{\lambda}\sin\theta_m\right)K + j\left(-\frac{\pi d^2}{\lambda r_m}\cos^2\theta_m\right)K^2} \\ \vdots \\ e^{-j\left(-\frac{2\pi d}{\lambda}\sin\theta_m\right)K + j\left(-\frac{\pi d^2}{\lambda r_m}\cos^2\theta_m\right)K^2} \end{bmatrix} \quad m = 1, \ldots M \tag{2.7}$$

In the next subsection, the symmetric subarray based near-field localization and 2-D MUSIC localization schemes are introduced.

2.2 SYMMETRIC SUBARRAY BASED NEAR FIELD LOCALIZATION

It is important to note that the second term in the exponential in (2.7) does not change for $-k^{th}$ and k^{th} antenna element, only the sign of first component changes. This property is used to construct two subarrays which are symmetric to each other as demonstrated in Figure 2.2.

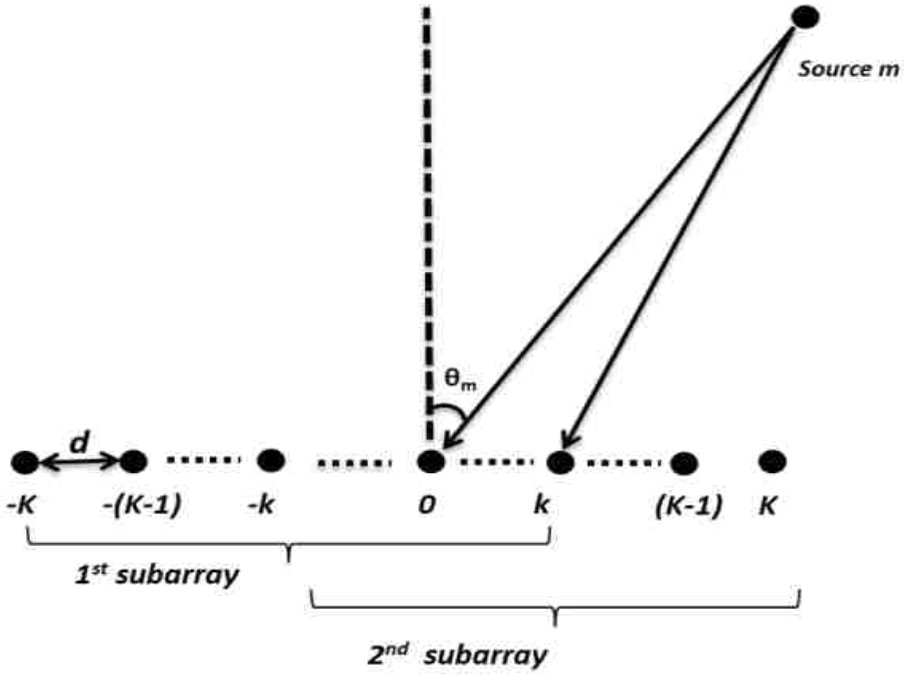

Figure 2.2. Construction of two symmetric subarrays.

By using this property, both AoA and distance between the passive source and ULA can be estimated at the same time. First, the ULA is divided into two subarrays: the 1st subarray is constructed with L sensors in the ascending order and 2nd subarray is constituted with the last L sensors in the descending order [16]. Subsequently, received signal from these two subarrays can be represented respectively as

$$\mathbf{X}_1(t) = \mathbf{A}_1\mathbf{S}(t) + \mathbf{N}_1(t), \qquad \mathbf{X}_2(t) = \mathbf{A}_2\mathbf{S}(t) + \mathbf{N}_2(t) \tag{2.8}$$

with $M < L < 2K+1$, $\mathbf{N}_1 \in \Re^L$ and $\mathbf{N}_2 \in \Re^L$ are noise vectors of 1st and 2nd subarrays respectively, $\mathbf{A}_1 \in \Re^{L\times M}$ is constructed with first L rows of $\mathbf{A}$ and $\mathbf{A}_2 \in \Re^{L\times M}$ is constituted with last L rows of $\mathbf{A}$ in the reverse order. Therefore, the relationship between $\mathbf{A}$ and $\mathbf{A}_1, \mathbf{A}_2$ can be represented as

$$\mathbf{A} = \begin{bmatrix} \mathbf{A}_1 \\ \text{last } (P-L) \text{ rows} \end{bmatrix} = \begin{bmatrix} \text{first } (P-L) \text{ rows} \\ \mathbf{JA}_2 \end{bmatrix} \tag{2.9}$$

With **J** is the anti-identity matrix satisfying $\mathbf{J}^2 = \mathbf{I}$. Moreover, $\mathbf{A}_1$ can be represented as

$$\mathbf{A}_1 = \left[\mathbf{a}_1(r_1, \theta_1), \cdots, \mathbf{a}_1(r_M, \theta_M) \right] \in \Re^{L \times M} \tag{2.10}$$

with

$$\mathbf{a}_1(r_m, \theta_m) = \begin{bmatrix} a_{m,-K} \\ \vdots \\ a_{m,-K+L-1} \end{bmatrix} \tag{2.11}$$

Next, using symmetry property, $\mathbf{A}_2$ is represented as

$$\mathbf{A}_2 = \left[\mathbf{C}(\theta_1)\mathbf{a}_1(r_1, \theta_1), \cdots, \mathbf{C}(\theta_M)\mathbf{a}_1(r_M, \theta_M) \right] \tag{2.12}$$

where

$$\mathbf{C}(\theta_m) = diag\left[e^{-j\left(\frac{4\pi d}{\lambda}\sin\theta_m\right)K}, \ldots, e^{-j\left(\frac{4\pi d}{\lambda}\sin\theta_m\right)(K-L+1)} \right] \in \Re^{L \times L} \tag{2.13}$$

which is a function dependent on angle θ_m. Moreover, covariance matrix of the received signal is defined as $\mathbf{R} = E\left[\mathbf{X}(t)(\mathbf{X}(t))^H \right]$ and eigen decomposition of the covariance matrix can be expressed as

$$\mathbf{R} = \mathbf{U}_s \mathbf{\Lambda}_s (\mathbf{U}_s)^H + \mathbf{U}_n \mathbf{\Lambda}_n (\mathbf{U}_n)^H \tag{2.14}$$

where $\mathbf{U}_s \in \Re^{P \times M}$ denotes eigenvectors in signal subspace, and $\mathbf{U}_n \in \Re^{P \times (P-M)}$ represents $P-M$ eigenvectors of noise subspace. $\mathbf{\Lambda}_s \in \Re^{M \times M}$ is eigen-values in signal space and $\mathbf{\Lambda}_n \in \Re^{(P-M) \times (P-M)}$ denotes the eigen-values in noise space while *H* symbolizes as complex-conjugate transpose.

Next, generalized ESPRIT [7] method is utilized into the covariance matrix for estimating AoA. There exists a $M \times M$ full rank matrix **D** such that

$$\mathbf{U}_S = \mathbf{AD} = \begin{bmatrix} \mathbf{U}_{S1} \\ \text{last } (P-L) \text{ rows} \end{bmatrix} = \begin{bmatrix} \text{first } (P-L) \text{ rows} \\ \mathbf{U}_{S2} \end{bmatrix} \tag{2.15}$$

where

$$\mathbf{U}_{S1} = \mathbf{A}_1\mathbf{D}, \qquad \mathbf{U}_{S2} = \mathbf{JA}_2\mathbf{D} \tag{2.16}$$

Moreover,

$$\mathbf{JU}_{s2} = \mathbf{J}^2\mathbf{A}_2\mathbf{D} = \mathbf{A}_2\mathbf{D} \tag{2.17}$$

Then, introducing a diagonal matrix in generalized ESPRIT scheme [9] results in

$$\mathbf{\Delta}(\theta) = diag\left[e^{-j\left(\frac{4\pi d}{\lambda}\sin\theta\right)K}, \ \cdots, e^{-j\left(\frac{4\pi d}{\lambda}\sin\theta\right)(K-L+1)} \right] \tag{2.18}$$

According to (2.14) and (2.16), we have

$$\mathbf{JU}_{s2} - \mathbf{\Delta}(\theta)\mathbf{U}_{s,1}^{S1} = [\left(\mathbf{C}(\theta_1) - \mathbf{\Delta}(\theta)\right)\mathbf{a}_1(r_1,\theta_1),...,\left(\mathbf{C}(\theta_M) - \mathbf{\Delta}(\theta)\right)\mathbf{a}_1(r_M,\theta_M)]\mathbf{D} \tag{2.19}$$

It is important to note that k^{th} column of matrix $\mathbf{JU}_{s2} - \mathbf{\Delta}(\theta)\mathbf{U}_{s1}$ will be zero when $\theta = \theta_k$. Therefore, selecting an arbitrary $K \times M$ full column rank **F** matrix, the term $\mathbf{F}^H\mathbf{JU}_{s2} - \mathbf{F}^H\mathbf{\Delta}(\theta)\mathbf{U}_{s1}$ becomes singular. Therefore, spectrum function can be used to estimate the angles for multiple passive sources as

$$P(\theta) = \frac{1}{\det\left|\mathbf{F}^H\mathbf{JU}_{s2} - \mathbf{F}^H\mathbf{\Delta}(\theta)\mathbf{U}_{s1}\right|} \tag{2.20}$$

where $\mathbf{U}_{s1}, \mathbf{U}_{s2}$ are defined in (2.17), and $\mathbf{\Delta}(\theta)$ is defined in (2.19).

Remark 1: Spectrum function peaks (2.20) provide estimated AoAs. Moreover, substituting estimated $\hat{\theta}_m$, $m = 1, 2, ..., M$ into steering vector (2.9) and utilizing 1-D MUSIC, the distance between passive sources and ULA can be estimated. Therefore, these passive sources can be located by using estimated AoA and distance information.

2.3 PROPOSED SMOOTH 2-D MUSIC NEAR-FIELD LOCALIZATION

Although symmetric subarray based localization is considered in the previous subsection, it will be deficient under multipath fading since the signals will be correlated with each other which in turn can reduce the rank of the received signal covariance matrix. Therefore, to overcome this deficiency, a novel spatial smoothing 2-D MUSIC-based near-field localization scheme or simply Smooth 2-D MUSIC, illustrated in Figure 2.3, is proposed in this section. Before proceeding, the following assumption is needed.

Assumption 1 [8]: The number of multipath, N_p is considered known.

According to traditional 2-D MUSIC method [18], signal and noise subspaces are considered orthogonal. Then, by using this orthogonal property, the AoA and distance between the source and antenna array can be estimated based on the covariance matrix of the received signals that is expressed as

$$\mathbf{R} = E[\mathbf{x}\mathbf{x}^H] = E[\mathbf{A}\mathbf{s}\mathbf{s}^H\mathbf{A}^H] + E[\mathbf{n}\mathbf{n}^H] = \mathbf{A}\mathbf{S}\mathbf{A}^H + \sigma^2\mathbf{I} = \mathbf{R}_s + \sigma^2\mathbf{I} \tag{2.21}$$

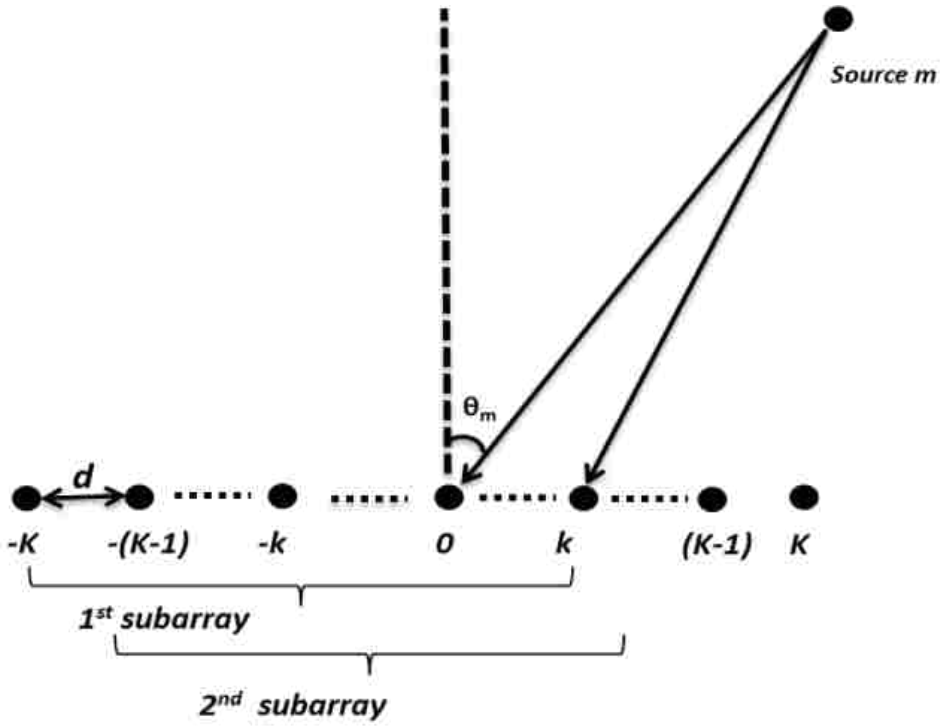

Figure 2.3. Spatial smoothing process with overlapping subarrays in the near field region [17].

where $\mathbf{R}_s \in \Re^{P\times P}$ is a $P\times P$ matrix with rank M. Since M sources are orthogonal, the covariance matrix $\mathbf{R}$ has $P-M$ zero eigenvectors corresponding to zero eigenvalues. Moreover, when $\mathbf{q}_m$ is an eigenvector for noise subspace of **R**, we have

$$\mathbf{R}_s\mathbf{q}_m = \mathbf{A}\mathbf{S}\mathbf{A}^H\mathbf{q}_m = 0 \quad \text{and} \quad \mathbf{A}^H\mathbf{q}_m = 0 \tag{2.22}$$

Next, 2-D MUSIC [18] finds the pseudo spectrum as

$$P_{MUSIC}(\theta, r) = \frac{1}{\sum_{m=1}^{P-M} \left|\mathbf{a}^H(\theta, r)\mathbf{q}_m\right|^2} \tag{2.23}$$

where P is the number of antennas in the antenna array and M being the number of sources.

Remark 2: The peaks of pseudo spectrum, $P_{MUSIC}(\theta, r)$, represent the locations of the near-field sources i.e. $(r_m, \theta_m), m = 1, 2, ..., M$. Similar to traditional MUSIC scheme [8], the 2-D MUSIC is based on the orthogonal property between the signal steering vector, $\mathbf{a}(\theta_m, r_m)$, and the noise eigenvector of the covariance matrix **R**.

However, since sources can be correlated in the presence of multipath fading, the matrix rank of R_s will decrease. Therefore, P_{MUSIC} in (2.23) cannot be utilized to locate these correlated sources. To overcome this challenge, spatial smoothing procedure has been included.

In the smooth 2-D MUSIC scheme, the *P* element antenna array is divided into multiple overlapping subarrays containing *q* antennas each. In order to decorrelate the multipath, the number of subarrays, *b*, should be greater than the number of multipath components, N_p. According to Assumption 1, it indicates that $b > N_p$. Next, the covariance matrix of the received signal at ULA is constructed by averaging the covariance matrices of the received signal from all the subarrays which is represented as

$$\mathbf{R}_S = \frac{1}{b}\sum_{i=0}^{b-1}\mathbf{R}_i \tag{2.24}$$

Remark 3: Using the spatial smoothing procedure, the new covariance matrix of the received signal, $\mathbf{R}_S$, (2.24) can be proven to be of full rank which is utilized to separate correlated sources i.e. signals from the multipath.

2.4 HARDWARE SETUP

The channel 8 of the Family Radio Service (FRS) of a walkie-talkie is employed for the experiment. A -40 dB, continuous stimulating signal at 467.5625 MHz is generated with Agilent MXG-N5182A signal generator. The walkie-talkie is left in standby mode and cycled on-off. It is placed on the ground and RF stimulating signal kept the walkie-talkie on [1] due to external stimulation. The hardware setup for this experiment as shown in Figure 2.4 consists of two 7-element uniform antenna array which is built with broadband, omnidirectional UHF BW 350-450MHz, Pharad lightweight wearable antennas.

Figure 2.4. Measurement setup for the experiment.

The antenna elements are connected to 40 dB low noise amplifiers (LNA) in order to amplify the weak signals from the source and also to mitigate the effects of noise. These are connected to 4-channel Agilent MSO6104A and Agilent MSO7104B

oscilloscopes for data acquisition. The signal frequency from the walkie-talkie is given by 445.862 MHz whereas the wavelength is obtained as

$$\lambda = c / f = \frac{3\times10^{8}\ m/s}{445.8625\times10^{6}\ 1/s} = 0.67m \tag{2.25}$$

where c is speed of light. Fresnel region for 7 element antenna array is given by $1.8\,m < r_k < 11\,m$. In this experiment, 200.000 data points are taken by repeating each measurement five times at any given position. After data collection, the proposed methods are applied and the location of the source is obtained within 32.3 seconds. Next the experimental results and discussion are introduced.

3. EXPERIMENT RESULTS AND DISCUSSION

3.1 ANGLE OF ARRIVAL AND DISTANCE ESTIMATION

First, the stimulated passive walkie-talkie is placed at 4.8m and 22^o from the source to ULA for the purpose of location determination. Desirable maximum localization error for this experiment is taken as $\pm 0.5\ m$, which is determined to be 5% of the length of the $10 \times 10\ m^2$ near field region. The data collected is utilized to evaluate the performance of the localization schemes. The localization performance of symmetric subarray based near-field localization and the proposed smooth 2-D MUSIC schemes have been evaluated.

As shown in Figure 3.1, the symmetric subarray based scheme can estimate the AoA satisfactorily thus indicating an acceptable localization performance. Next, prior measurements in the area indicate that there is significant multipath fading due to the presence of obstacles in the environment. In this scenario, the passive RC walkie-talkie is placed at the location of 110^o and 4.8m. However, multipath fading effects, which can degrade the localization performance significantly, have not been considered in the symmetric subarray based location scheme shown in Figure 3.1.

Under multipath fading, the proposed novel Smooth 2-D MUSIC based near-field localization scheme has been analyzed. By using the proposed Smooth 2-D MUSIC scheme, the AoA and distance are approximated. Subsequently, the device is located by using the estimated AoA and distance between the source and the antenna array.

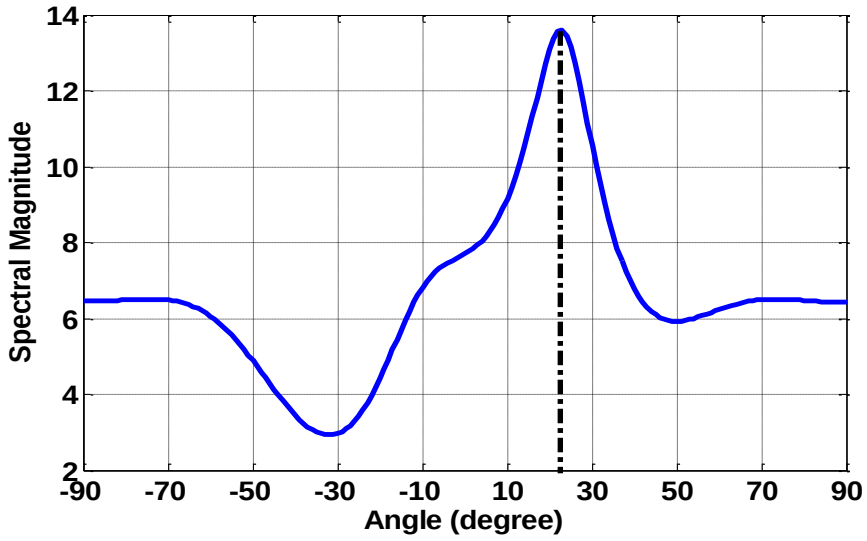

Figure 3.1. Bearing estimation of a near field source in real experiment environment.

Three remarkable peaks are observed in Figure 3.2 despite only one emitting source in the area. As shown in Figure 3.2, the estimation of both AoA and distance between the source and ULA are close to actual values of 110^{o} and 4.8m respectively even in the presence of multipath fading. It indicates that proposed Smooth 2-D MUSIC near-field localization scheme is able to deliver satisfactory performance for near-field localization with multipath fading signals.

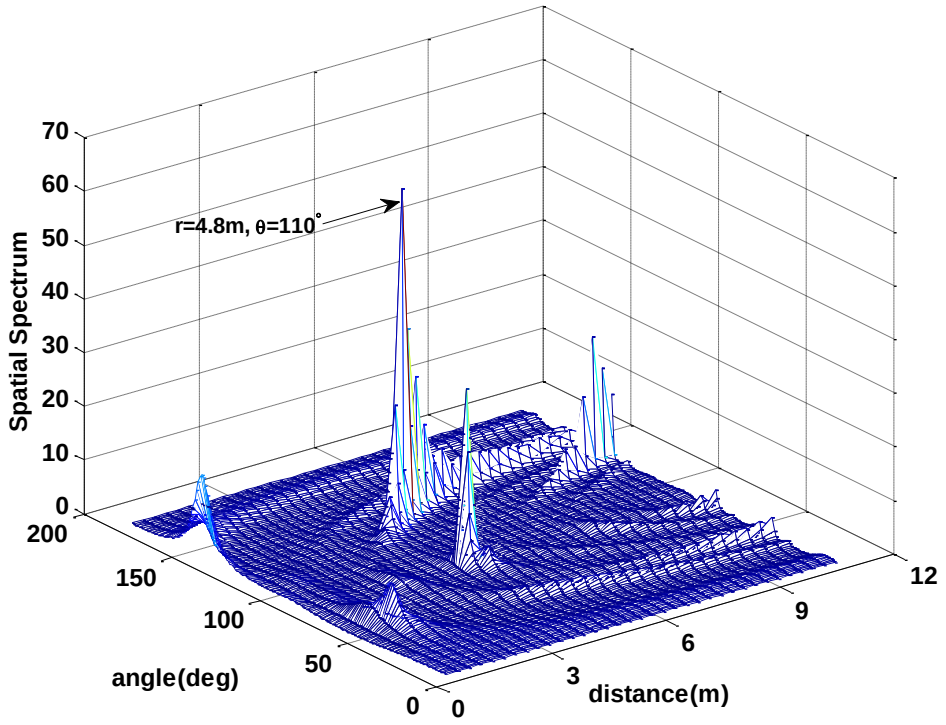

Figure 3.2. Angle and range estimation with Smooth 2-D MUSIC in multipath fading environment.

3.2 LOCALIZATION RESULTS IN MULTIPATH ENVIRONMENT

The AoA and distance estimation is repeated for many locations as shown in Figure 3.3. The 3rd dimension in Figure 3.3 represents the root mean square (RMS) localization error for each position. From Figure 3.3, the RMS localization error is less than 0.15m when the device is placed at (3.65m, 3.65m) whereas this RMS localization error will increase to 0.5m while the device is at (5.5m, 9.1m). It indicates that localization accuracy is higher when the passive source is placed at the center of the localization area.

According to [17], when the ULA is grouped into multiple subarrays, both the number of antennas in each subarray and number of subarrays will affect the performance

of the near-field localization scheme. Higher number of subarrays can locate more coherent sources or multipath components from the same source, while higher number of antenna elements in each subarray can locate more non-coherent RC sources [17]. However, in practice, increasing both the number of subarray groups and the number of antennas in each subarray is not possible since the number of antenna elements in the entire ULA is fixed. Therefore, identifying the optimum number of subarrays and number of antenna elements in each subarray is involved as shown in [19].

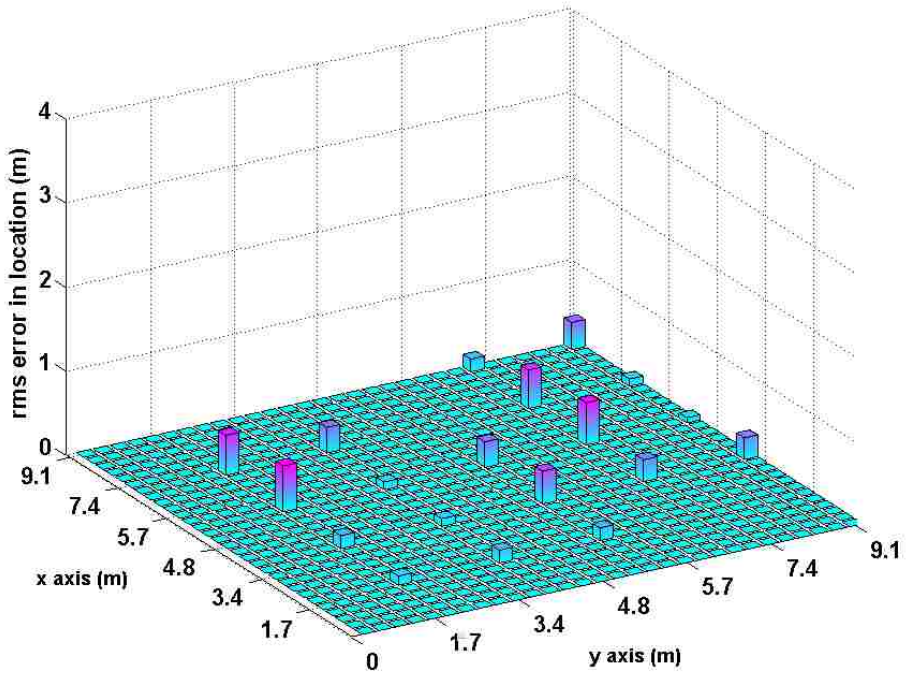

Figure 3.3. Localization of unintended emitting device with Smooth 2-D MUSIC for different positions.

Next, the traditional Smooth 1-D MUSIC localization scheme has been utilized for the sake of comparison. As shown in Figure 3.4, the localization performance of traditional smooth 1-D MUSIC is much worse when compared to the proposed Smooth 2-D MUSIC scheme since distance effects have been ignored in the Smooth 1-D MUSIC.

It is important to note that the distance effects between the passive source and ULA will decrease when the distance is increased since reciprocal of distance and $-1 \le \cos(\theta) \le 1$ appears in the signal representation (2.4).

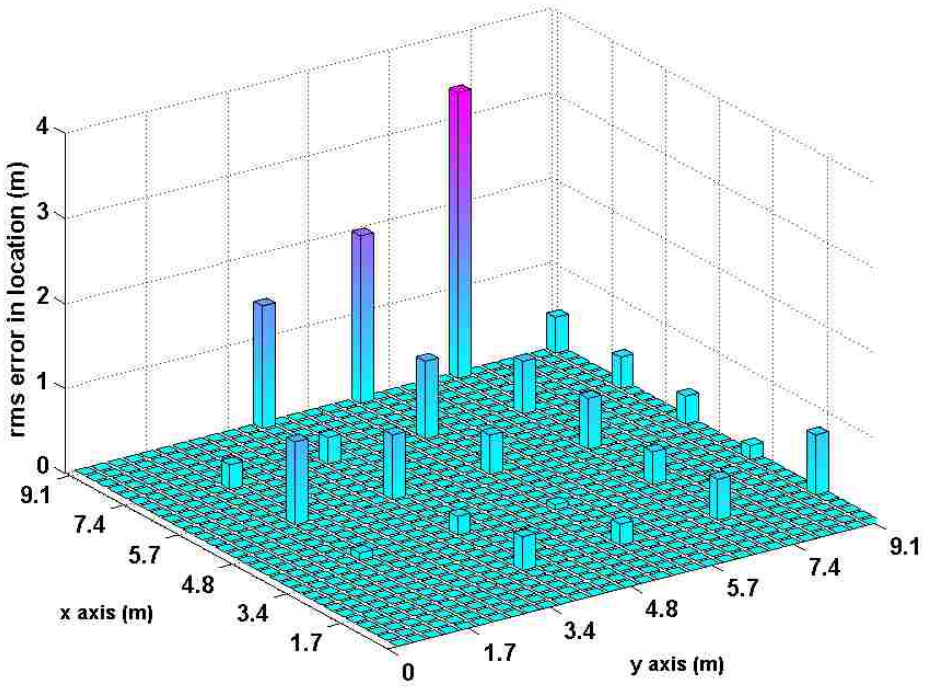

Figure 3.4. Localization of an unintended emitting device with Smooth 1-D MUSIC for different positions.

Next the performance of the ESPIRIT-like scheme is evaluated. Moreover, the localization result of traditional ESPRIT-like method is depicted in Figure 3.5. The root mean square (RMS) localization error is found to be less than 0.15m when the device is at (1.8m, 1.8m) whereas RMS will increase to 1.1m while the device is placed at (5.5m, 3.65m). Since multipath fading is ignored in the traditional ESPRIT-like method, its localization performance is inferior when compared to the proposed smooth 2-D MUSIC which considers the multipath fading effects.

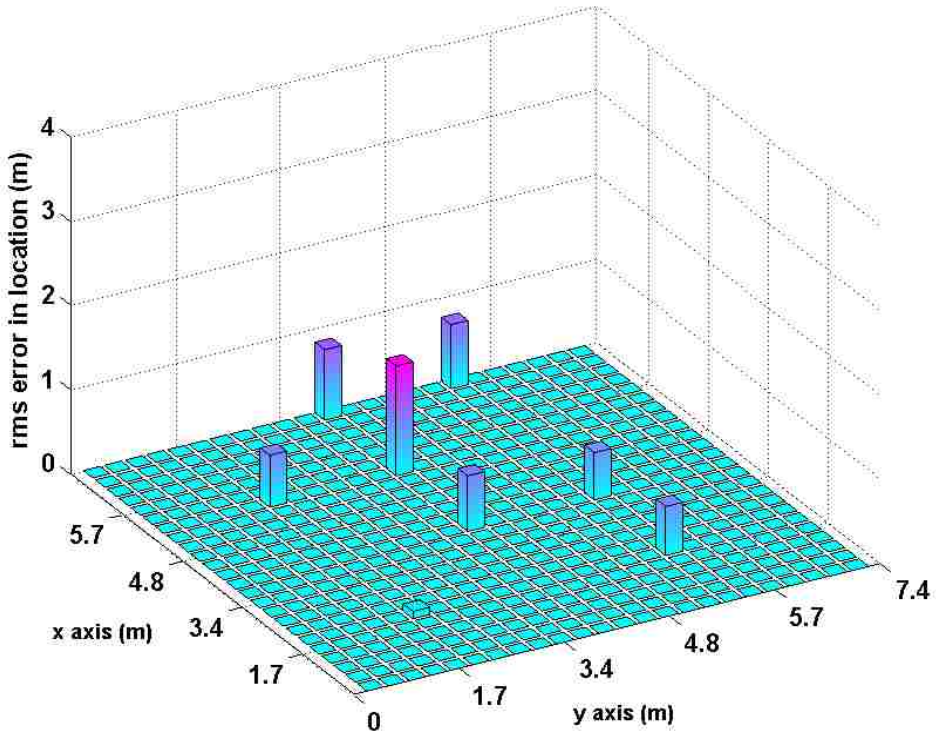

Figure 3.5. Localization results of an unintended emitting device by using ESPRIT-like localization technique.

In the array processing schemes [8-9], phase difference between the sensors is used for location estimation of a source. In the far field signal representation, phase difference between the sensors is a function of AoA to the sensors and inter-element spacing between the sensors. Since the source is far from the array, the AoA to each antenna is considered to be equal. Therefore the distance effects can be ignored [8-11] in the far field region since the distance between the antenna and the source does not have an effect on the phase difference between the sensors. By contrast, when the source is in the near field region of the sensor array, the phase difference will be a function of AoA to a reference point on the array and the distance between this reference point and the source.

Now, the traditional 1-D MUSIC is evaluated with the data collected in these experiments for the sake of comparison. As shown in Figure 3.6, the RMS localization errors increase significantly indicating that the localization performance of 1-D MUSIC degrades in the near-field region under the multipath fading since both distance effects and multipath fading are ignored in the traditional 1-D MUSIC scheme.

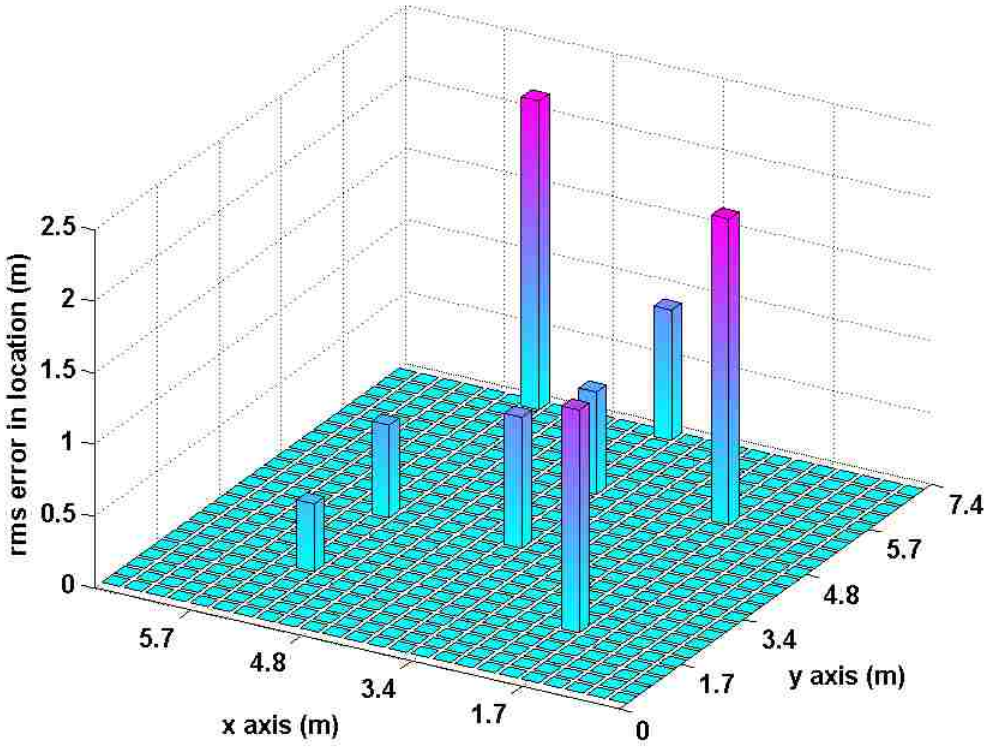

Figure 3.6. Localization results of one unintended emitting device with far field (1-D MUSIC) bearing estimation scheme.

Compared with 1-D MUSIC and symmetric subarray based near-field localization, schemes, experiment results depicted in Figures 3.1 to 3.6 indicate that the proposed Smooth 2-D MUSIC outperforms other schemes in locating a passive unintended emitting device in the near field and multipath fading environment. Experimental data provided in the following tables also indicate that the Smooth 2-D

MUSIC is better than traditional localization schemes such as 1-D MUSIC, and the ESPRIT-like scheme.

Table 3.1. Localization results with 2-D Smooth MUSIC

x(m)	y(m)	measured x (m)	measured y (m)	RMS error (m)
1.8	5.5	1.93	6	0.51
3.65	5.5	3.9	5.18	0.4
3.65	7.3	3.44	7.46	0.26

Table 3.2. Localization results with 1-D Smooth MUSIC

x(m)	y(m)	measured x (m)	measured y (m)	RMS error (m)
1.8	5.5	3.23	7.16	2.19
3.65	5.5	4.41	5.45	0.77
3.65	7.3	3.38	7.16	0.3

Table 3.3. Performance of near field localization with ESPRIT-like method

x(m)	y(m)	measured x (m)	measured y (m)	RMS error (m)
1.8	5.5	2.43	5.4	0.63
3.65	5.5	3.2	6.7	1.28
3.65	7.3	2.95	6.85	0.83

Table 3.4. Performance table for localization with far field assumption

x(m)	y(m)	measured x (m)	measured y (m)	RMS error (m)
1.8	5.5	3.96	5.5	2.16
3.65	5.5	3.2	4.93	0.72
3.65	7.3	2.95	7.89	0.91

With regards to computational complexity, the authors have considered the number of multiplications for matrix construction, eigen value decomposition (EVD) operation and two dimensional MUSIC search. The proposed algorithm constructs *b*

covariance matrices with a dimension of $q \times q$ for smoothing process and requires one EVD operation [20], where *b* is the number of subarrays, q is number of antennas in each subarray, and *N* is number of snapshots. If *K* points are searched for AoA and *Z* points for range estimation, the total computational cost is $O\left\{9bq^2N + 4/3q^3 + KZq^2\right\}$ where $O\{\bullet\}$ represents the number of operations. The computational cost without smoothing operation involves the construction of a $P \times P$ matrix, where *P* being the number of antennas in the array, one EVD operation and MUSIC search involves *K* points for the angle and *Z* points for the range. Therefore the computational cost for 2-D MUSIC will be $O\left\{9P^2N + 4/3P^3 + KZP^2\right\}$. Even though resolution decreases with the smoothing procedure, since $q \prec P$, the computational cost is reduced when compared to 2-D MUSIC algorithm without smoothing.

Experiments are performed in the front of McNutt Hall in Missouri University of Science and Technology campus. The performance of three localization schemes, smoothing 1-D and 2-D MUSIC algorithms, and traditional near field localization method [16] without spatial smoothing procedure, have been analyzed. As shown in the Figure 3.7, the Smooth 2-D Smooth MUSIC provides a larger localization area with acceptable error since it not only utilizes two dimensional search to estimate both AoA and distance between the near-field passive source and antenna array, but also it includes the spatial smoothing to deal with the effects of multipath signals.

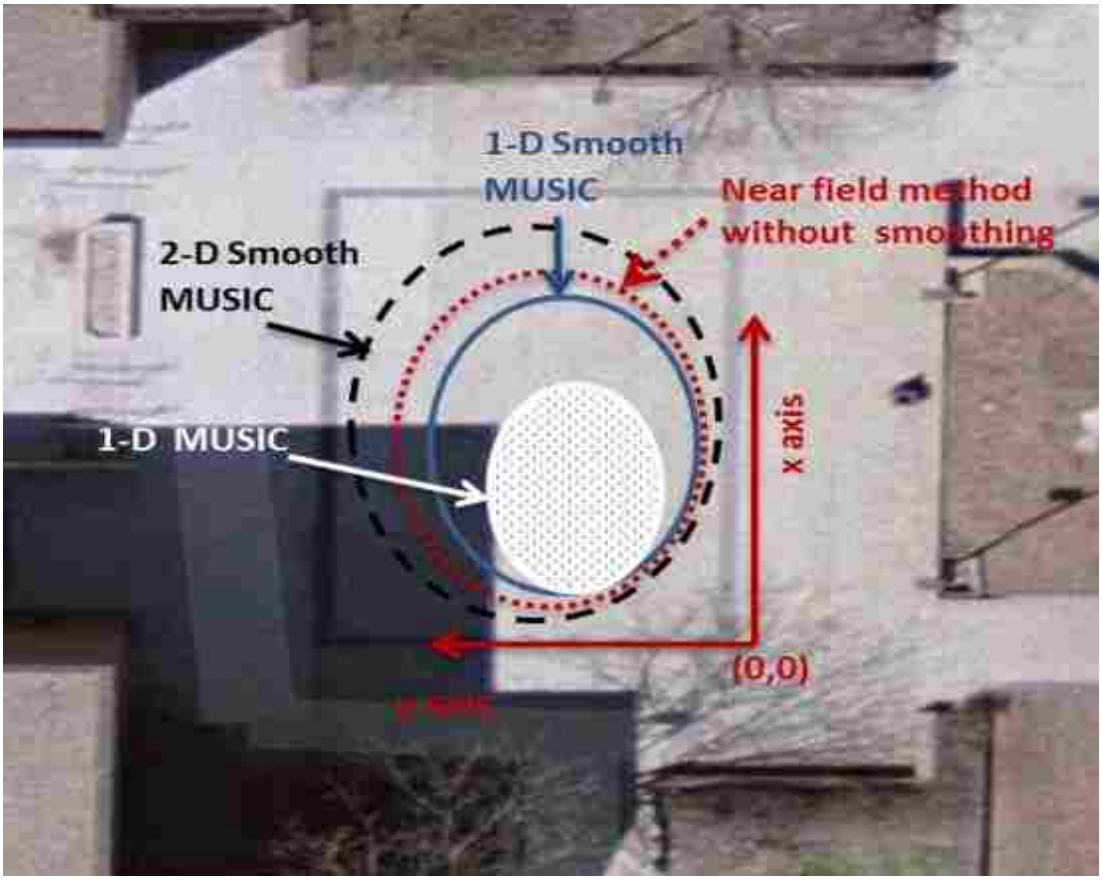

Figure 3.7. Performance of the near field and far field localization schemes when a source is placed in the near field region of the antenna array.

4. CONCLUSIONS

Near field localization of an unintended emitting passive source was analyzed by using a symmetric subarray based and 2-D MUSIC near-field localization schemes, where both AoA and distance from the source to the antenna array were estimated. Moreover, a smoothing scheme was included with 2D MUSIC [18] to obtain the covariance matrix of the received signals in order to de-correlate the coherency between the multipath and direct signals from the source. Eventually, the data from the experimental setup indicate that Smooth 2-D MUSIC is more efficient than other near-field localization methods especially in the presence of multipath fading. The future work includes the AoA estimation and localization of unintended emitting sources when the number of sources and multipath are unknown.

5. REFERENCES

[1] C. Stagner, A. Conrad, C. Osterwise, D. G. Beetner and S. Grant, "A practical superheterodyne-receiver detector using stimulated emissions," IEEE Transactions on Instrumentation and Measurement, Vol. 60, No. 4, April 2011.

[2] J. Hertenstein and S. Jagannathan, "Simulation and Detection of Unintended Electromagnetic Emissions From Super-Regenerative Receivers," IEEE Transactions on Instrumentation and Measurement, vol.62, no.7, pp.2093-2100, July 2013.

[3] V.Thotla, M.T.A. Ghasr, M. Zawodniok, S. Jagannathan and S. Agarwal, "Detection and localization of multiple R/C electronic devices using array detectors," 2012 IEEE International Instrumentation and Measurement Technology Conference (I2MTC), pp.1687-1691, 13-16 May 2012.

[4] A. Shaik, H. Weng, X. Dong, T.H. Hubing and D.G. Beetner, " Matched filter detection an identification of electronic circuits based on their unintentional radiated emissions," *IEEE International Symposium on In Electromagnetic Compatibility*, vol. 3, pages 853-856, August 2006

[5] D. G. Beetner, S. Seguin and T. Hubing, "Electromagnetic emissions stimulation and detection system," U.S. Patent 7,464,005, Dec. 9, 2008.

[6] V. Thotla, M.T.A. Ghasr, M. Zawodniok, S. Jagannathan and S Agarwal, "Detection of Super-Regenerative Receivers Using Hurst Parameter," *IEEE Transactions on Instrumentation and Measurement*, vol.62, no.11, pp.3006,3014, Nov. 2013

[7] Sarah Seguin, "Detection of low cost radio frequency receivers based on their unintended electromagnetic emissions and an active stimulation," Ph.D dissertation, Missouri University of Science and Technology, Rolla, MO 2009.

[8] R. Schmidt, " Multiple emitter location and signal parameter estimation," *IEEE Transactions on Antennas and Propagation*, vol.34, no.3, pp. 276- 280, March 1986

[9] F. Gao and A.B. Gershman, "A generalized ESPRIT approach to direction-of-arrival estimation," *IEEE Signal Processing Letters*, vol.12, no.3, pp.254-257, March 2005

[10] M.F. Khan and M. Tufail, "Comparative analysis of various Matrix Pencil methods for direction of arrival estimation," *International Conference on Image Analysis and Signal Processing (IASP)*, pp.496-501, 9-11 April 2010

[11] J. Xin and A. Sano, "Computationally efficient subspace-based method for direction-of-arrival estimation without eigendecomposition," *IEEE Transactions on Signal Processing*, vol.52, no.4, pp. 876-893, April 2004

[12] B. D. Steinberg, Principles of Aperture and Array System Design: Including Random and Adaptive Arrays. New York, NY, USA: Wiley, 1976, pp. 9–10.

[13] R.N. Challa and S. Shamsunder, "High-order subspace-based algorithms for passive localization of near-field sources," *Conference Record of the Twenty-Ninth Asilomar Conference on Signals, Systems and Computers, 1995.* vol.2, pp.777,781 vol.2, Oct. 30 1995-Nov. 1 1995

[14] N. Yuen and B. Friedlander, "Performance analysis of higher order ESPRIT for localization of near-field sources," *IEEE Transactions on Signal Processing*, vol.46, no.3, pp.709-719, Mar 1998.

[15] E, Cekli and H. A. Cirpan, "Unconditional maximum likelihood approach for near-field source localization," *8th IEEE International Conference on Electronics, Circuits and Systems*, vol.2, pp.753-756 Sep 2001

[16] W. Zhi and M. Y.W. Chia, "Near-Field Source Localization via Symmetric Subarrays," *IEEE Signal Processing Letters*, vol.14, no.6, pp.409,412, June 2007

[17] T. Shan, M. Wax and T. Kailath, "On spatial smoothing for direction-of-arrival estimation of coherent signals," *IEEE Transactions on Acoustics, Speech and Signal Processin*, vol.33, no.4, pp. 806-811, Aug 1985

[18] Y. D. Huang and M , Barkat, "Near-field multiple source localization by passive sensor array, " *IEEE Transactions on Antennas and Propagation*, vol.39, no.7, pp.968,975, Jul 1991

[19] A.B. Gershman and V.T. Ermolaev, "Optimal subarray size for spatial smoothing," *IEEE Signal Processing Letters*, vol.2, no.2, pp.28-30, Feb 1995.

[20] J. Liang and D. Liu, "Passive Localization of Mixed Near-Field and Far-Field Sources Using Two-stage MUSIC Algorithm," *IEEE Transactions on Signal Processing*, vol.58, no.1, pp.108-120, Jan. 2010

II. LOCALIZATION OF NEAR-FIELD SOURCES IN SPATIALLY COLORED NOISE

ABSTRACT

This paper presents near-field localization of unintended emitting radio-controlled (RC) sources in a colored noise environment by using a uniform linear array (ULA) antenna. Existing localization methods for RC devices perform satisfactorily under white noise, but they ignore multipath fading or correlation among the sources. Therefore, a suite of novel schemes, referred to as 2D MUSIC-Smooth Sparse Arrays (SSA) and 2D MUSIC-Whitened Noise (WN) is proposed to bring together correlation among the sources, multipath fading and color noise effects during near-field location estimation. Experimental evaluation of the proposed methods and the original Smooth 2D MUSIC compares both schemes while demonstrating their effectiveness.

1. INTRODUCTION

Radio-controlled (RC) devices are sensitive to stimulation and they emit low power unintended emissions [1]-[3]. Array processing techniques, which are intensively used in radar, sonar and acoustic applications, can be used to locate the RC devices with unintended emissions. Direction of arrival (DOA) estimation with array processing has been a highly popular topic in signal processing for the past few decades. High resolution estimators such as MUSIC [4], ESPRIT [5] and WSF [6] are efficient assuming that the DOA to each antenna is equal; however, this is not true when the sources are located in the near-field region of the antenna array since the received signals are a nonlinear function of the DOA. This near-field region also includes the distance between the sources and the antenna array, thereby complicating the location estimation.

The Fresnel approximation [7] is the most preferred method used to mitigate this deficiency; it is the second order Taylor series expansion of the phase between antennas, which depends upon DOA and distance between the array and the sources. The techniques for near-field DOA estimation in recent years have generally used higher order statistics [8]. Cekli and Cirpan [9] developed a maximum likelihood estimator. An ESPRIT-like least square scheme is proposed in [10] to approximate the location of near-field sources.

However, the location estimations in [8]-[10] are degraded when the sources are either correlated or in the presence of multipath fading. A subspace based method in [11] addresses the localization of near-field sources in the multipath environment in a computationally inexpensive way. The efficiency of the subspace-based methods from [4]-[6] and [11] depends upon the separation of signal and noise subspaces. In addition,

the overlapping subspaces cannot be separated from each other in the presence of colored noise thus preventing a subspace rotation. Therefore, the DOA-based estimation methods [4]-[11] do not locate well in the presence of colored noise, which occurs during cross talk among channels, random radiation from sources or in the presence of undesired interference. The comprehensive effect of colored noise on DOA estimation is reported in [12].

The literature presents two main ways to whiten colored noise. In the first approach, the noise covariance matrix is parameterized so that both noise parameters and direction of arrival (DOA) are estimated. For instance, in [13] and [14], the noise is parameterized as an auto-regressive (AR) model. Alternatively, the noise covariance is expressed as a sum of known basis functions in [15] and [16]. Instead of noise covariance estimation, the signal covariance is estimated in [17] by modeling it as a combination of basis functions under the assumption that the signal is partially known. While these techniques [14]-[17] have the advantage of not requiring prior knowledge of noise covariance matrix, they require information about noise or signal models. The second approach uses noise-only or signal-free data in order to whiten the colored noise and estimate the noise covariance matrix [18]. The effect of small statistical deviations on whitening filter estimation is reported in [19] and [20]. Here, the efficiency of the whitening filter depends on the number of signal-free snapshots.

In this paper, two near-field localization methods are developed for narrowband correlated and uncorrelated sources in spatially colored noise by extending the white noise based Smooth 2D MUSIC [11] scheme. In the 2D MUSIC-Whitened Noise (MUSIC-WN), a whitening filter is constructed with noise-only samples. The covariance

matrix of the noise becomes an identity matrix due to the whitening filter [21]; therefore, the noise and signal subspaces can be separated efficiently, and locations of RC devices are approximated in a colored noise environment.

However, since the number of noise-free samples will be limited in a practical environment, the estimation errors in the whitening filter will affect the location accuracy. Hence, a novel 2D MUSIC-Smooth Sparse Arrays (MUSIC-SSA) is introduced in order to efficiently estimate the signal and noise subspaces for location estimation. Two well-separated arrays are employed in 2D MUSIC-SSA. Instead of the conventional eigen-decomposition techniques, a generalized correlation decomposition (GCD) [22] is utilized for subspace estimation. Signal and noise subspaces are extracted from the cross covariance matrix of the sparse array outputs where it does not contain a noise component.

Therefore, in contrast to Smooth 2D MUSIC, the proposed methods consider the color effect of the noise, which is inevitable in practical applications. Unlike other estimation schemes in the literature [13]-[16], which require noise statistics of the environment, the proposed 2D MUSIC-SSA does not require noise statistics, which helps in the method's adaptive evaluation of the specific hardware needed for various environments.

To move on, the main contributions of this study include: 1) the development of a 2D MUSIC-SSA localization method for multiple near-field RC devices in multipath and unknown colored noise environments, 2) the construction of a whitening filter without stimulation and using that filter with Smooth 2D MUSIC, 3) the hardware evaluation of the proposed methods by using multiple correlated and uncorrelated sources

via data collection, and 4) comparison of 2D MUSIC-SSA with Smooth 2D MUSIC-WN and traditional Smooth 2D MUSIC [11]. Though the hardware evaluation of the proposed schemes was accomplished separately after data collection, in practice, the proposed schemes will be part of the signal processing component of the instrumentation and an integral part of the antenna array. This cycle of interdependence highlights the contributions in the instrumentation and measurements aspect.

The rest of the paper is organized as follows. Section 2, shows how signal representation of the near-field sources work. Subsequently, the 2D MUSIC-WN and 2D MUSIC- SSA are introduced to address deficiencies caused by correlation among the sources and the color effect of the noise. Section 3 presents details of the hardware setup. Section 4 presents localization results for single, multiple correlated and uncorrelated sources with estimation of the DOA and distance between the sources and antenna array by evaluating the proposed schemes. In addition, the results with Smooth 2D MUSIC where the color effect of the noise is ignored are given for the sake of comparison. The discussion is finalized with conclusions in Section 5.

2. DATA MODEL AND PROBLEM FORMULATION

2.1 NEAR-FIELD SIGNAL MODEL AND BACKGROUND

Let us assume a uniform linear array (ULA), which consists of *L=2M+1* antenna elements with inter-element spacing being *d*. Consider the existence of a *K*-narrow band unintendedly emitting sources placed in the near-field region of the antenna array where each source has p_k multipath signals due to the obstacles in the environment. Assume there are a total of K_T signals including the sources and the multipath; therefore, the received signal with the array is represented as

$$\mathbf{x}(t) = \sum_{k=1}^{K} \sum_{i=1}^{p_i} \mathbf{a}(\theta_{k,i}, r_{k,i}) s_k(t - \gamma_{k,i}) + \mathbf{n}(t), \tag{2.1}$$

where $t=1,\ldots,N$ represents the number of samples and $\mathbf{n}(t) = [n_{-M}(t), \ldots n_M(t)]^T \in \Re^L$ depicts noise output of the array. $s_k(t-\gamma_{k,i}) \in \Re$ is the received signal power from the i^{th} path of k^{th} source, $\gamma_{k,i}$, $\forall k = 1,...,K$, $\forall i = 1,..., p_k$ is the transmission delay for path *i* of k^{th} passive source, and *T* is the transpose operator. $\mathbf{a}(\theta_{k,i}, r_{k,i}) \in \Re^L$ is the phase response of the antenna array to the k^{th} signal and i^{th} path, which is defined as

$$\mathbf{a}(r_{k,i}, \theta_{k,i}) = [e^{-j\tau_{-M}(\theta_{k,i}, r_{k,i})} \ldots e^{-j\tau_M(\theta_{k,i}, r_{k,i})}]^T \tag{2.2}$$

where $\theta_{k,i}$ and $r_{k,i}$ represents DOA of the signal from i^{th} path of the k^{th} source and distance between signal and the array reference, respectively. $\tau_m(\theta_{k,i}, r_{k,i})$ is the phase difference between the reference antenna and the m^{th} antenna. This phase difference depends only upon the DOA information in the far-field region, but in the near-field region, it is also a function of distance between the source and the array. With the Fresnel approximation [7], the phase difference is expressed as

$$\tau_m(\theta_{k,i}, r_{k,i}) \approx \frac{2\pi}{\lambda}\left(md\sin\theta_{k,i} - \frac{m^2 d^2 \cos\theta_{k,i}}{2r_{k,i}} \right), \quad m = -M, \ldots, M, \tag{2.3}$$

where λ is the wavelength of the received signal, *d* is the distance between adjacent antennas, and *m* is the m^{th} antenna element. The array steering vector for each source and path is given by [7]

$$\mathbf{a}(r_{k,i}, \theta_{k,i}) = \begin{bmatrix} a_{k,i,-M} \\ \vdots \\ a_{k,i,M} \end{bmatrix} = \begin{bmatrix} e^{j\left(-\frac{2\pi d}{\lambda}\sin\theta_{k,i}\right)M + j\left(-\frac{\pi d^2}{\lambda r_{k,i}}\cos^2\theta_{k,i}\right)M^2} \\ \vdots \\ e^{-j\left(-\frac{2\pi d}{\lambda}\sin\theta_{k,i}\right)M + j\left(-\frac{\pi d^2}{\lambda r_{k,i}}\cos^2\theta_{k,i}\right)M^2} \end{bmatrix} \quad k = 1, \ldots K. \tag{2.4}$$

Then, the received signal at m^{th} antenna for K sources can be written as [7]

$$x_m(t) = \sum_{k=1}^{K}\sum_{i=1}^{p_k} e^{j\left(-\frac{2\pi d}{\lambda}\sin\theta_{k,i}\right)m + j\left(-\frac{\pi d^2}{\lambda r_{k,i}}\cos^2\theta_{k,i}\right)m^2} s_k(t - \gamma_{k,i}) + n(t), \tag{2.5}$$

where *m=-M,…M.* The received signal at the ULA is represented in matrix form as

$$\mathbf{x}(t) = \mathbf{A}\mathbf{s}(t) + \mathbf{n}(t) \quad t = 1, \ldots N, \tag{2.6}$$

$\mathbf{x}(t) = \left[x_{-M}(t), \ldots\ldots, x_M(t)\right]^T \in \Re^L$ is the vector of antenna outputs, $\mathbf{n}(t) = [n_{-M}(t), \ldots, n_M(t)]^T \in \Re^L$ is the noise vector. $\mathbf{A} \in \Re^{L \times K_T}$ is the array manifold, which is

$$\mathbf{A} = \left[\underbrace{\mathbf{a}(r_{1,1}, \theta_{1,1}), \cdots \mathbf{a}(r_{1,p_1}, \theta_{1,p_1})}_{1^{st}\ Source}, \cdots, \underbrace{\mathbf{a}(r_{K,1}, \theta_{K,1}), \cdots, \mathbf{a}(r_{K,p_K}, \theta_{K,p_K})}_{k^{th}\ Source} \right] \tag{2.7}$$

and $\mathbf{s}(t) \in \Re^{K_T}$ is the vector of signal powers represented by

$$\mathbf{s}(t) = \left[\underbrace{s_1(t - \gamma_{1,1}) \cdots s(t - \gamma_{1,p_1})}_{1^{st}\ Source} \cdots \underbrace{s(t - \gamma_{k,p_1}) \cdots s(t - \gamma_{k,p_k})}_{k^{th}\ Source} \right]^T. \tag{2.8}$$

If *K* sources are uncorrelated and no multipath fading exists, the subspace based estimation schemes use the orthogonality between signal and noise subspaces which are determined with second order statistics of received signal as

$$\mathbf{R} = E[\mathbf{x}\mathbf{x}^H] = \mathbf{R}_s + \mathbf{R}_n = E[\mathbf{A}\mathbf{s}\mathbf{s}^H\mathbf{A}^H] + E[\mathbf{n}\mathbf{n}^H] = \mathbf{E}_s\mathbf{\Lambda}_s\mathbf{E}_s^H + \mathbf{E}_n\mathbf{\Lambda}_n\mathbf{E}_n^H, \quad (2.9)$$

where $\mathbf{R} \in \Re^{L\times L}$ is the covariance matrix of the received signal at ULA, $\boldsymbol{R}_s \in \Re^{L\times L}$ is the signal covariance matrix with rank *K*, and *H* denotes the conjugate transpose. $\mathbf{R}_n \in \Re^{L\times L}$ is the noise covariance, $\mathbf{E}_s \in \Re^{L\times K}$ and $\mathbf{E}_n \in \Re^{L\times K}$ are eigenvector matrices of the signal and noise covariance matrix, respectively; $\mathbf{\Lambda}_s \in \Re^{K\times K}$ and $\mathbf{\Lambda}_n \in \Re^{L-K\times L-K}$ are the diagonal eigenvalue matrices of signal and noise outputs. When the noise is assumed to be white, the covariance matrix is written as

$$\mathbf{R} = \mathbf{A}\mathbf{S}\mathbf{A}^H + \sigma^2\mathbf{I} = = \mathbf{R}_s + \sigma^2\mathbf{I}, \quad (2.10)$$

where $\mathbf{I} \in \Re^{L\times L}$ is the identity matrix and σ^2 is the power of additive white Gaussian noise. When the *K* sources are uncorrelated, **R** has *L*-*K* zero eigenvectors due to noise eigenvalues. If $\mathbf{e}_l \in \Re^L$ is such an eigenvector when $l = K+1,\ldots,L$, with the orthogonality between the signal and noise subspaces, it can be written as

$$\mathbf{R}_s\mathbf{e}_l = \mathbf{A}\mathbf{S}\mathbf{A}^H\mathbf{e}_l = 0, \quad (2.11)$$

where $\mathbf{A}^H\mathbf{e}_l = 0.$ Then 2D MUSIC [23] defines the pseudo spectrum for near- field localization as

$$P_{MUSIC}(\theta, r) = \frac{1}{\mathbf{a}^H(\theta, r)\mathbf{E}_n\mathbf{E}_n^H\mathbf{a}(\theta, r)}, \quad (2.12)$$

where $\mathbf{E}_n \in \Re^{L\times(L-K)}$ is the matrix of noise eigenvectors $\mathbf{e}_l, l = K+1,\ldots,L$.

Remark 1: The term (θ_k, r_k), makes the denominator of (2.12) minimal since the signal and noise subspaces [4] are orthogonal with $k = 1, 2, ..., K$ being the location of K near-field sources.

2.2 2D MUSIC-WHITENED NOISE

In the traditional MUSIC [4], the noise covariance matrix is assumed to be white as in (10). However, this assumption is not valid especially for practical applications. Due to the correlation between noise components of the antenna elements, the noise covariance matrix is not an identity matrix or even diagonal [12]. Therefore, the separation of signal and noise subspaces will be unsatisfactory, which degrades the performance of subspace-based estimation schemes such as MUSIC as reported in [12]. For this reason, the noise covariance matrix should be whitened before DOA estimation.

In this study, the signal was generated with stimulation; therefore, without stimulation signal-free samples can be collected. A whitening filter, given by

$$\mathbf{Z} = \mathbf{R}_n^{-1/2} = (\mathbf{E}_n \mathbf{\Lambda}_n \mathbf{E}_n)^{-1/2} = \mathbf{E}_n \mathbf{\Lambda}_n^{-1/2}, \tag{2.13}$$

is constructed with second order statistics of these noise-only samples [21] where $\mathbf{R}_n \in \Re^{L \times L}$ is the covariance matrix of signal-free samples collected before stimulation. Later, the stimulation signal is turned on and the new measurements contain unintended emissions from the RC devices. If the received signal by the ULA is filtered with this whitening filter, the new covariance matrix after filtering is expressed as [21]

$$\hat{\mathbf{R}} = \mathbf{ZRZ} = \hat{\mathbf{R}}_s + \hat{\mathbf{R}}_n = \hat{\mathbf{E}}_s \mathbf{\Lambda}_s \hat{\mathbf{E}}_s^H + \hat{\mathbf{E}}_n \mathbf{\Lambda}_n \hat{\mathbf{E}}_n^H, \tag{2.14}$$

where $\hat{\mathbf{R}} \in \Re^{L \times L}$ is the array covariance matrix and $\hat{\mathbf{R}}_s \in \Re^{L \times L}$ is the signal covariance matrix after insertion of the whitening filter. $\hat{\mathbf{E}}_s \in \Re^{L \times K_T}$ and $\hat{\mathbf{E}}_n \in \Re^{L \times L - K_T}$ are new

eigenvector matrices after the whitening process, $\mathbf{\Lambda}_s$ and $\mathbf{\Lambda}_n$ are the diagonal eigen value matrices of the signal and the noise, respectively. After insertion of the whitening filter, the noise covariance matrix, $\hat{\mathbf{R}}_n = \hat{\mathbf{E}}_n \mathbf{\Lambda}_n \hat{\mathbf{E}}_n^H$, becomes an identity matrix; therefore, the correlation among the noise is removed. Signal and noise subspaces become orthogonal, which enables the use of subspace-based estimation methods.

Remark 2: With the noise-only samples, the effect of colored noise is removed, and the new noise covariance matrix becomes an identity matrix. Therefore, the noise and signal subspaces are orthogonal, and they can be separated.

Next, the location estimation is performed with this new covariance matrix. When the *K* sources are assumed to be uncorrelated and no multipath fading occurs, the covariance matrix $\hat{\mathbf{R}}$ has *L-K* zero eigenvectors corresponding to noise eigenvalues. However, the correlation between the sources or multipath fading can result in a reduced rank $\hat{\mathbf{R}}_s$. Then, these correlated sources cannot be located. To overcome this challenge, a spatial smoothing procedure is included. For smoothing, *L* element antenna array is divided into multiple overlapping subarrays, each of which contains its own Q antennas. The new covariance matrix is given by

$$\hat{\mathbf{R}}_{Smooth} = \frac{1}{B} \sum_{i=1}^{B} \hat{\mathbf{R}}_i, \tag{2.15}$$

where $\hat{\mathbf{R}}_i \in \Re^{Q \times Q}$ is the covariance matrix of i^{th} subarray after whitening filter. $\hat{\mathbf{R}}_{Smooth} \in \Re^{Q \times Q}$ is the average value of subarray covariance matrices when the correlation among the sources are removed, and *B* denotes the number of subarrays which is *L-Q+1*. Next the following theorem is stated.

Theorem 1: Consider the passive RC sources operating under multipath fading and color noise environment. Given the received signal $\mathbf{x}(n)$ as (1), let the whitening filter be designed as in (2.13). Then, the DOA and distance between passive RC sources to antenna array can be obtained as

$$(\hat{\boldsymbol{\theta}}, \hat{\mathbf{r}}) = \arg\max_{\theta,r} \left[P_{MUSIC}(\theta, r) \right] = \arg\max_{\theta,r} \left[\frac{1}{\mathbf{a}^H(\theta, r)\hat{\mathbf{E}}_n \hat{\mathbf{E}}_n^H \mathbf{a}(\theta, r)} \right], \qquad (2.16)$$

where $\hat{\mathbf{E}}_n$ is the eigenvector matrix corresponding to Q-K_T eigenvalues of $\hat{\mathbf{R}}_{Smooth} \in \Re^{L \times L}$.

Proof: See Appendix A.

Remark 3: With the smoothing procedure, the Smooth 2D MUSIC-WN scheme is able to locate correlated sources in the presence of colored noise with the new covariance matrix defined in (2.15).

2.3 2D MUSIC-SMOOTH SPARSE ARRAYS

The whitening filter in (2.13) is constructed with second order statistics of the signal free samples, and its accuracy depends upon the number of samples [19], [20]. As the number of samples goes to infinity, the whitening filter will converge to its correct value. However, the number of signal-free samples will be limited in practical application and then estimation errors in the whitening filter will affect the location accuracy. Hence, the proposed 2D MUSIC-SSA is introduced in this subsection in order to efficiently estimate the signal and noise subspaces for location estimation.

Assume that K_T correlated narrowband sources and multipath signals are impinging on two well-separated antenna arrays. The arrays should be separated by a distance of at least three wavelengths in order to have uncorrelated noise outputs [22]. Received data by each array is represented as

$$\mathbf{x}_1(t) = \mathbf{A}_1(\boldsymbol{\theta}_1, \mathbf{r}_1)\mathbf{s}_1(t) + \mathbf{n}_1(t), \tag{2.17}$$

$$\mathbf{x}_2(t) = \mathbf{A}_2(\boldsymbol{\theta}_2, \mathbf{r}_2)\mathbf{s}_2(t) + \mathbf{n}_2(t), \quad t = 1, \ldots, N,$$

where $\mathbf{x}_i(t) \in \Re^{M_i}$ is the array output with $i = 1, 2$. $\mathbf{A}_i(\boldsymbol{\theta}_i, \mathbf{r}_i) \in \Re^{M_i \times K_T}$ is the array manifold with $\boldsymbol{\theta}_i \in \Re^{K_T}$ representing the DOAs from K_T near-field signals. $\mathbf{r}_i \in \Re^{K_T}$ is the distance vector between sources and the arrays, while $\mathbf{n}_i \in \Re^{M_i}$ is the noise output for each array, N is the number of snapshots and $\mathbf{s}_i \in \Re^{K_T}$ is the signal power vector for K_T sources received by the two separated arrays. If there is no distortion in the received signals between two arrays, $\mathbf{s}_2(t)$ is the delayed version of $\mathbf{s}_1(t)$.

In this experiment, the narrow band signals can be modeled and the delay between two arrays can be included in the directional matrices. Noise components for each array is assumed to be uncorrelated; hence, joint covariance matrix of noise is represented as

$$E\left\{\begin{bmatrix}\mathbf{n}_1 \\ \mathbf{n}_2\end{bmatrix}\begin{bmatrix}\mathbf{n}^H{}_1 & \mathbf{n}^H{}_2\end{bmatrix}\right\} = \begin{bmatrix}\mathbf{R}_{1n} & \mathbf{0} \\ \mathbf{0} & \mathbf{R}_{2n}\end{bmatrix} \tag{2.18}$$

where $\mathbf{R}_{1n} \in \Re^{M_1 \times M_1}$ and $\mathbf{R}_{2n} \in \Re^{M_2 \times M_2}$ denote auto covariance matrices of noise in well separated arrays. Assume that M_1 and M_2 antennas work in each array, respectively; hence, the joint covariance matrix of received data with two arrays is represented as

$$\mathbf{R} = E\left\{\begin{bmatrix}\mathbf{x}_1 \\ \mathbf{x}_2\end{bmatrix}\begin{bmatrix}\mathbf{x}^H{}_1 & \mathbf{x}^H{}_2\end{bmatrix}\right\} = \begin{bmatrix}\mathbf{R}_{11} & \mathbf{R}_{12} \\ \mathbf{R}_{21} & \mathbf{R}_{22}\end{bmatrix} \tag{2.19}$$

where

$$\mathbf{R}_{ii} = \mathbf{A}_i(\boldsymbol{\theta}_i, \mathbf{r}_i)\mathbf{R}_{is}\mathbf{A}^H{}_i(\boldsymbol{\theta}_i, \mathbf{r}_i) + \mathbf{R}_{in}, \quad i = 1, 2 \tag{2.20}$$

$$\mathbf{R}_{12} = \mathbf{R}^H{}_{21} = \mathbf{A}_1(\boldsymbol{\theta}_1, \mathbf{r}_1)\mathbf{R}_{s12}\mathbf{A}^H{}_2(\boldsymbol{\theta}_2, \mathbf{r}_1)$$

$\mathbf{R}_{ii} \in \Re^{M_i \times M_i}$ and $\mathbf{R}_{12} \in \Re^{M_1 \times M_2}$ are the auto and cross covariance matrices of the arrays where $\mathbf{R}_{is} \in \Re^{M_i \times M_i}$ and $\mathbf{R}_{s12} \in \Re^{M_1 \times M_2}$ represent the auto and cross covariance matrices of the signals. As mentioned in (2.20), $\mathbf{R}_{12} \in \Re^{M_1 \times M_2}$ contains only signal information. The locations can be estimated from this matrix by using singular value decomposition (SVD).

Before performing estimation, a spatial smoothing is needed due to the correlation between sources and multipath fading. Spatial smoothing yields a random phase modulation, which in turn aims to decorrelate the signals causing the rank drop [24]. If the arrays are divided into B overlapping subarrays, as demonstrated in Figure 2.1, the new joint covariance matrix is written as

$$\tilde{\mathbf{R}} = \frac{1}{B}\sum_{i=1}^{B}\begin{bmatrix}\mathbf{x}_{1b}\\ \mathbf{x}_{2b}\end{bmatrix}\begin{bmatrix}\mathbf{x}_{1b}^H & \mathbf{x}_{2b}^H\end{bmatrix} \qquad b = 1,\ldots,B \tag{2.21}$$

$$\tilde{\mathbf{R}}_{ii} = \mathbf{A}_i(\boldsymbol{\theta}_i, \mathbf{r}_i)\tilde{\mathbf{R}}_{is}\mathbf{A}^H{}_i(\boldsymbol{\theta}_i, \mathbf{r}_i) + \tilde{\mathbf{R}}_{in}, \qquad i = 1,2$$

and

$$\tilde{\mathbf{R}}_{12} = \tilde{\mathbf{R}}_{21}^T = \mathbf{A}_1(\boldsymbol{\theta}_1, \mathbf{r}_1)\tilde{\mathbf{R}}_{s12}\mathbf{A}^H{}_2(\boldsymbol{\theta}_2, \mathbf{r}_1)$$

where $\tilde{\mathbf{R}}$ is the joint covariance matrix of the arrays after spatial smoothing, B is the number of subarrays with $\mathbf{x}_{ib}$ representing the array output of the b^{th} subarray of the i^{th} array, $\tilde{\mathbf{R}}_{ii} \in \Re^{Q_i \times Q_i}$ and $\tilde{\mathbf{R}}_{12} \in \Re^{Q_1 \times Q_2}$ denote the auto and cross covariance matrices of the arrays after smoothing respectively, $\tilde{\mathbf{R}}_{is} \in \Re^{Q_i \times Q_i}$ and $\tilde{\mathbf{R}}_{s12} \in \Re^{Q_1 \times Q_2}$ represent the auto and cross covariance matrix of the signal components, and $\tilde{\mathbf{R}}_{in} \in \Re^{Q_i \times Q_i}$ is the auto covariance matrix of the noise in each antenna array. In order to estimate the signal subspace and its

complement from the cross covariance matrices $\tilde{\mathbf{R}}_{12} \in \Re^{Q_1 \times Q_2}$ and $\tilde{\mathbf{R}}_{21} \in \Re^{Q_2 \times Q_1}$, the generalized correlation decomposition [22] technique is given next.

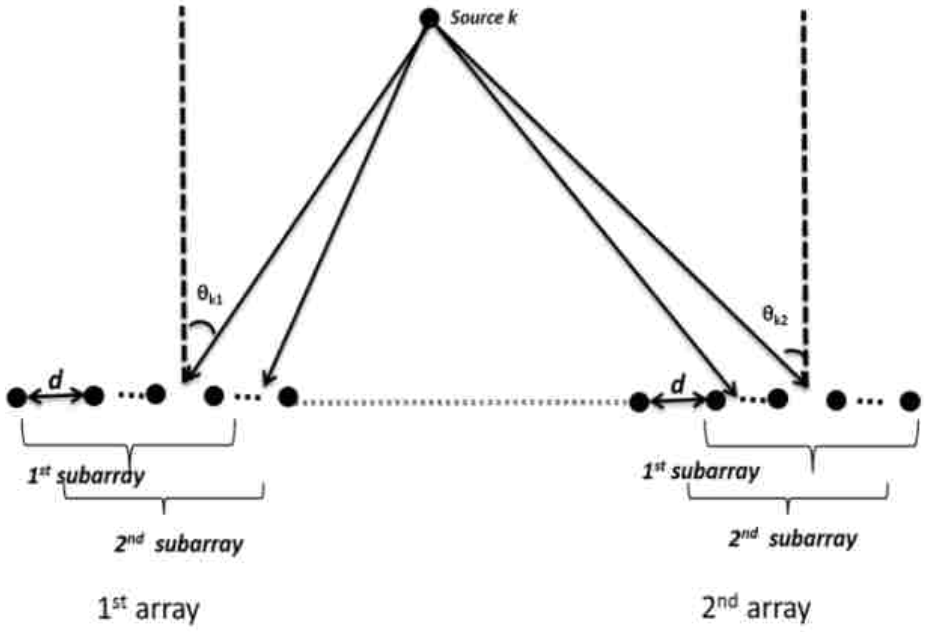

Figure 2.1. Sparse arrays with consisting overlapping subarrays.

2.3.1 Generalized Correlation Decomposition (GCD*)*. Let $\mathbf{\Pi}_1$ and $\mathbf{\Pi}_2$ be positive definite Hermitian matrices with dimensions $M_1 \times M_1$ and $M_2 \times M_2$. Then there exists two unitary matrices, $\mathbf{U}_1$ and $\mathbf{U}_2$, such that

$$\mathbf{\Pi}_1^{-1/2} \tilde{\mathbf{R}}_{12} \mathbf{\Pi}_2^{-1/2} = \mathbf{U}_1 \mathbf{\Gamma}_0 \mathbf{U}_2 \tag{2.22}$$

where $\tilde{\mathbf{R}}_{12}$ is the cross covariance matrix of the two arrays, which is defined as in (2.22) after spatial smoothing. $\mathbf{U}_1 \in \Re^{M_1 \times K_T}$ and $\mathbf{U}_2 \in \Re^{K_T \times M_2}$ are obtained from SVD of $\mathbf{\Pi}_1^{-1/2} \tilde{\mathbf{R}}_{12} \mathbf{\Pi}_2^{-1/2}, \mathbf{\Gamma}_0$, which is a $M_1 \times M_2$ matrix given by

$$\mathbf{\Gamma}_0 = \begin{bmatrix} \mathbf{\Gamma} & \mathbf{0} \\ \mathbf{0} & \mathbf{0} \end{bmatrix} \tag{2.23}$$

where $\mathbf{\Gamma} = diag\{\gamma_1, \ldots, \gamma_{K_T}\} \in \Re^{K_T \times K_T}$ being the diagonal matrix of generalized correlation coefficients. However, this matrix will not be diagonal if the sources are correlated. Therefore, a spatial smoothing procedure is applied to each array in order to decorrelate the sources as in (2.21) and

$$\mathbf{L}_1 = \mathbf{\Pi}_1^{-1/2}\mathbf{U}_1, \quad \mathbf{L}_2 = \mathbf{\Pi}_2^{-1/2}\mathbf{U}_2 \tag{2.24}$$

$$\mathbf{G}_1 = \mathbf{\Pi}_1^{1/2}\mathbf{U}_1, \quad \mathbf{G}_2 = \mathbf{\Pi}_2^{1/2}\mathbf{U}_2$$

$\mathbf{L}_1 \in \Re^{Q_1 \times Q_1}$ and $\mathbf{L}_2 \in \Re^{Q_2 \times Q_2}$ are the generalized correlation vector matrices of $\tilde{\mathbf{R}}_{12}$ and $\tilde{\mathbf{R}}_{21}$, respectively. Similarly, $\mathbf{G}_1 \in \Re^{Q_1 \times Q_1}$ and $\mathbf{G}_2 \in \Re^{Q_2 \times Q_2}$ are the reciprocal generalized correlation vector matrices of $\tilde{\mathbf{R}}_{12}$ and $\tilde{\mathbf{R}}_{21}$, respectively. Different choices of $\mathbf{\Pi}_i, i = 1, 2$ in GCD lead to different decompositions [22]. When $\mathbf{\Pi}_i = \tilde{\mathbf{R}}_{ii}$, the decomposition is referred to as canonical correlation decomposition (CCD) [25], which has been proven to be the optimal selection for eigen decomposition [22]. Eigen projectors are defined next in order to project the generalized correlation matrices onto orthogonal subspaces in order to use orthogonality of the subspace for location estimation.

2.3.2 Eigen Projectors of a General Hermitian Matrix. Define a generalized Hermitian matrix $\Psi_i = \mathbf{\Pi}_i^{-1}\tilde{\mathbf{R}}_{i\bar{i}}\mathbf{\Pi}_{\bar{i}}^{-1}\tilde{\mathbf{R}}_{\bar{i}i} \in \Re^{M_i \times M_i}$, where $\bar{i}$ denotes the complement of the index *i*. It can be proven that $\mathbf{L}_i \in \Re^{M_i \times K_T}$ defined in (2.24) contains the generalized eigenvectors of Ψ_i [22]. Then, the eigen projections of Ψ_i can be used for general eigen analysis, which is employed in subspace based estimation schemes. The eigen projector of Ψ_i, associated with the eigenvalue γ_m^2 is defined as a projector onto the subspace

spanned by the corresponding eigenvector $\mathbf{l}_{im} \in \Re^{M_i}$ in the metric of $\mathbf{\Pi}_i$ where $\mathbf{l}_{im}$ is the m^{th} column of $\mathbf{L}_i$ [25].

Such an eigen projector is formulated as $\mathbf{l}_{im}\mathbf{l}_{im}^H\mathbf{\Pi}_i$. An eigen projector $\mathbf{Y}_{in} \in \Re^{M_i \times M_i}$ associated with $Q_i - K_T$ are zero eigenvalues of Ψ_i which projects onto the subspace spanned by $\{\mathbf{l}_{im}\}$, $m = K_T + 1, \ldots, Q_i$, and is defined as

$$\mathbf{Y}_{in} = \sum_{m=K_T+1}^{Q_i} \mathbf{l}_{im}\mathbf{l}_{im}^H\mathbf{\Pi}_i = \mathbf{L}_{in}\mathbf{L}_{in}^H\mathbf{\Pi}_i = \mathbf{L}_{in}\mathbf{G}_{in}^H \tag{2.25}$$

where Q_i is the number of antennas in each subarray after smoothing. Similarly for the first K_T eigenvalues, the eigen projector for the signal subspace $\mathbf{Y}_{is} \in \Re^{M_i \times M_i}$ is given as

$$\mathbf{Y}_{is} = \sum_{k=1}^{K_T} \mathbf{l}_{ik}\mathbf{l}_{ik}^H\mathbf{\Pi}_i = \mathbf{L}_{is}\mathbf{L}_{is}^H\mathbf{\Pi}_i = \mathbf{L}_{is}\mathbf{G}_{is}^H. \tag{2.26}$$

Next the DOA and distance between the antennas are estimated as given in the following theorem.

Theorem 2: Assume that the unintended emissions from multiple RC sources are received at the ULA in the presence of colored noise. Given that the received signal is modeled as (2.1) and eigen projectors are generated with two sparse arrays as in (2.25), the DOA and distance between the antennas can be estimated as

$$\begin{aligned}(\hat{\boldsymbol{\theta}}_i, \hat{\mathbf{r}}_i) &= \arg\max_{\theta,r} \left[P_{MUSIC}(\theta, r)\right], \\ &= \arg\max_{\theta,r} \left[1/\left(\mathbf{a}_i^H(\theta, r)\mathbf{Y}_{in}\mathbf{Y}_{in}^H\mathbf{a}_i(\theta, r)\right)\right], \\ &= \arg\max_{\theta,r} \left[1/\left(\mathbf{a}_i^H(\theta, r)\mathbf{L}_{in}\mathbf{G}_{in}^H\mathbf{G}_{in}\mathbf{L}_{in}^H\mathbf{a}_i(\theta, r)\right)\right]\end{aligned} \tag{2.27}$$

where $\mathbf{L}_{in} \in \Re^{M_i \times Q_i - K_T}$ and $\mathbf{G}_{in} \in \Re^{M_i \times Q_i - K_T}$, $i = 1, 2$ represent the generalized correlation matrices of noise output for the two arrays.

Proof: See Appendix B.

Remark 4: The separation of noise and signal subspaces with conventional eigen-decomposition techniques is not efficient if the colored noise is present in the environment. The proposed 2D MUSIC-SSA introduced in this section extracted the noise and signal subspaces efficiently by using generalized correlation decomposition when the near-field sources were correlated. Therefore, it can be concluded that $\mathbf{Y}_{in}$ projects onto $\overline{span}(\mathbf{A}_i(\boldsymbol{\theta},\mathbf{r}))$, and the angle and distance components which make(2.27) to be a maximum represents the locations of the passive RC sources.

3. EXPERIMENTAL SETUP

Two walkie-talkies and a doorbell were employed for the experiment. The stimulating signal with -40 dBm power and 467.5625 MHz frequency was generated with an Agilent MXG-N5182A signal generator. The continuous stimulating signal kept the walkie-talkies on [3]. The 7-element antenna arrays consisted of broadband, omnidirectional lightweight, wearable wide-band antennas with an operating bandwidth in the range of 225–2500 MHz. The 40 dB low noise amplifiers were connected to the antennas to amplify the weak emitting signal and to reduce the effect of noise. The 4-channel Agilent MSO6104A and Agilent MSO7104B oscilloscopes were connected to the arrays. The oscilloscopes were connected to the PC for data collection and storage with a LabVIEW interface. The hardware setup for the experiment is shown in Figure 3.1.

Figure 3.1. Hardware Setup.

Under active stimulation, besides the frequency generated by the quench oscillator of the super regenerative receiver in the doorbell, the harmonics of the emission, which are separated by integral multiples of the frequency, were generated by the quench oscillator. These harmonics also appeared in the spectrum. In this experiment, the stimulation signal was at 315 MHz, and the separation of the harmonics was 550 kHz [1]. The signal frequency from the walkie-talkie was taken as 445.862 MHz whereas the wavelength was obtained as

$$\lambda = c / f = \frac{3\times10^{8}\ \text{m/s}}{445.8625\times10^{6}\ 1/\text{s}} = 0.67\ \text{m} \tag{3.1}$$

where c is speed of light. The Fresnel region for a seven-element antenna array is given by $1.8\ \text{m} < r_k < 11\ \text{m}$. The passive devices were placed at different points within this region, and measurements were repeated five times at each position by collecting 200,000 data points each time. Signal free samples were collected before the continuous RF stimulation signal began for the noise characterizing and whitening filter. For 2D MUSIC-SSA, measurements were taken from two well separated arrays to establish the spatial diversity of the noise on the antenna arrays. Then the locations of unintended emitting passive devices were calculated with 2D MUSIC-SSA technique.

4. RESULTS AND DISCUSSION

Performance evaluation of the Smooth 2D MUSIC, 2D MUSIC-WN and 2D MUSIC-SSA was carried out and is described herein to verify the analytical results given in the previous section. Experimental results for single, multiple correlated and uncorrelated devices are provided in the following subsections.

4.1 CASE I-SINGLE RC DEVICE

A single walkie-talkie was stimulated and the location estimation was performed for multiple positions in a multipath fading environment. The experiment was held in a area. Figure 4.1 shows the localization performance of Smooth 2D MUSIC-SSA. The device was placed in the (x,y) coordinates as shown in Figure 4.1, and the root mean square (RMS) errors were calculated as shown by each 2D bar. The RMS error was found to be less than 0.02 m when the device was placed at (7.3 m, 3.6 m); however, the RMS error reached up to 0.37 m when it was located at (3.6 m, 7.3 m). The average error was found to be 0.13 m.

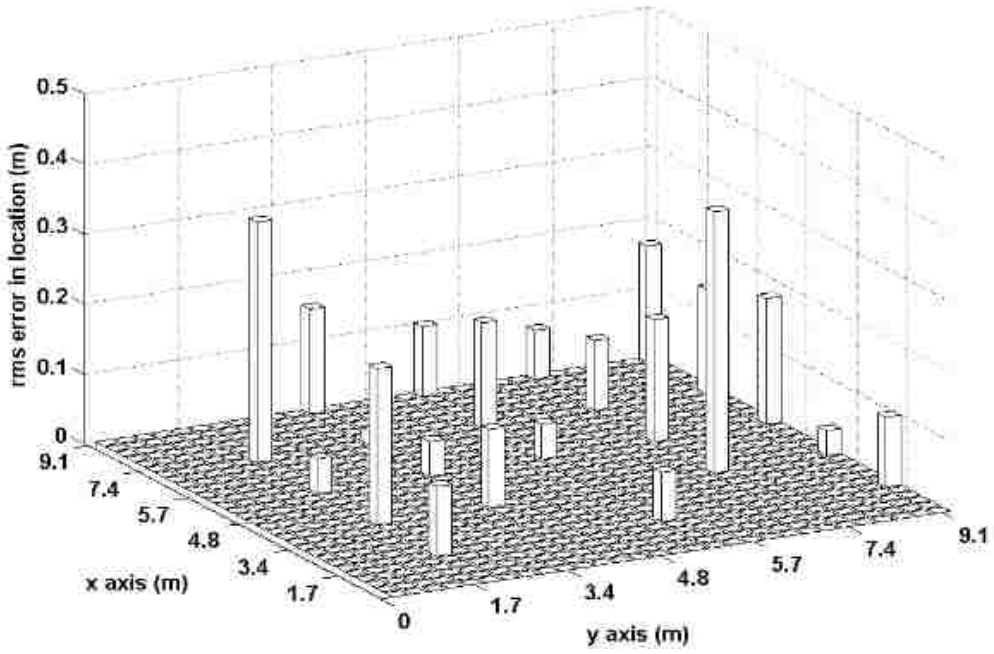

Figure 4.1. Localization errors of a single device with 2D MUSIC-SSA for different positions.

Localization errors of the single device after utilizing the 2D MUSIC-WN are demonstrated in Figure 4.2. The maximum error was found to be 0.41 m and the minimum error was 0.03 m while the average error was calculated as 0.18 m. There was a 27% increase in the average error when a whitening filter was used instead of two well separated arrays.

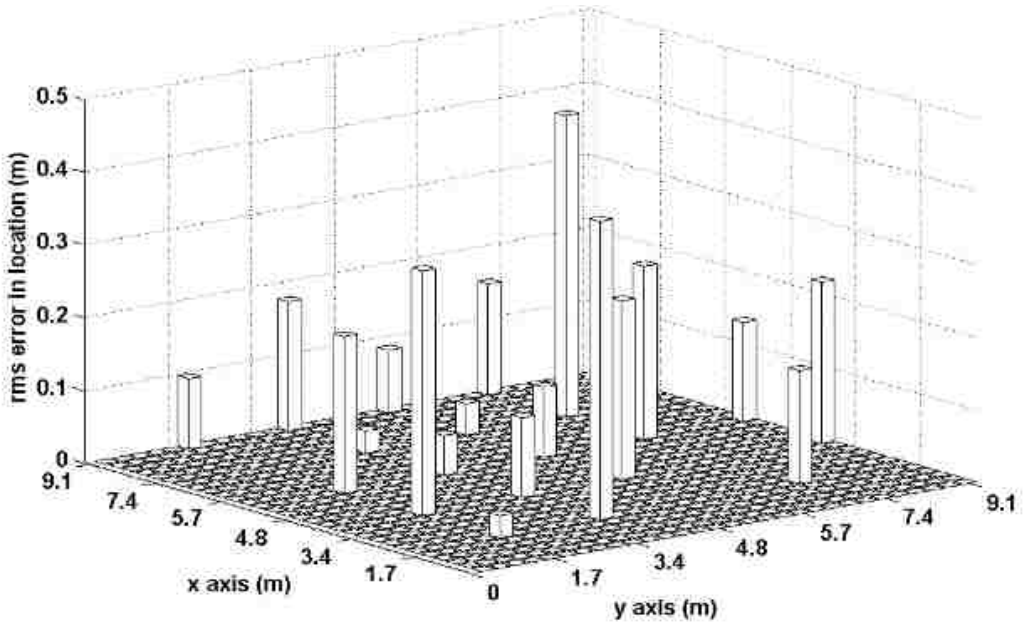

Figure 4.2. Localization errors of a single device with 2D MUSIC-WN for different positions.

In order to demonstrate the effect of colored noise, Smooth 2D MUSIC without a whitening filter is shown in Figure 4.3. Minimum error was 0.06 m when it was placed at (9.1 m, 5.5 m); however, it reached up to 0.54 m when placed at (1.7 m, 5.5 m). The average RMS error increased to 0.25 m when whitening filter was not used and the color of the noise was ignored. It is clear from the figures that the proposed schemes outperformed the performance of Smooth 2D MUSIC where a white noise was assumed in the estimation.

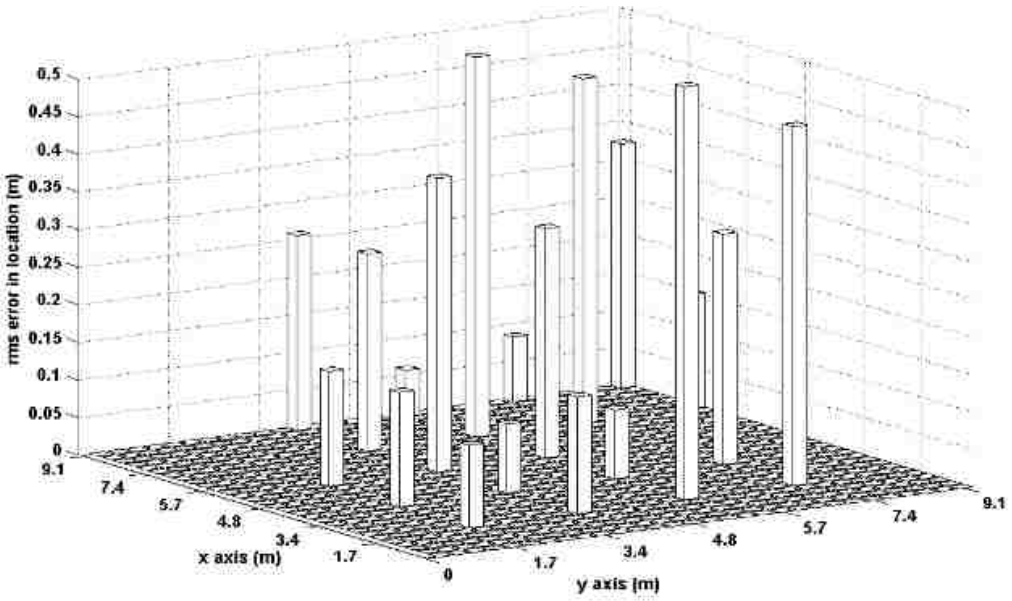

Figure 4.3. Localization errors of a single device with Smooth 2D MUSIC for different positions.

4.2 CASE II- MULTIPLE CORRELATED RC DEVICES

In this subsection, location performance of two correlated sources is demonstrated. The correlation between the sources required a smoothing procedure before finding the 2D MUSIC spectrum. However, there was a tradeoff between the antenna number in each subarray and the number of subarrays which affects the efficiency of the smooth MUSIC. A higher number of subarrays can locate more coherent sources since the decorrelation will be efficient despite the low resolution. However, when the number of antennas in each subarray is high, the decorrelation may be unsatisfactory even though more uncorrelated sources can be located. Calculating the optimum number of subarrays is given in [27]. After estimating the DOA and distance between the sources and the antenna array, Cartesian coordinates were calculated according to known antenna positions.

Localization results of 2D MUSIC-SSA are depicted in Figure 4.4. Maximum error was 1.51 m when the device was at (8 m, 7 m) and the average error was calculated as 1.04 m and 0.75 m for the two devices, respectively.

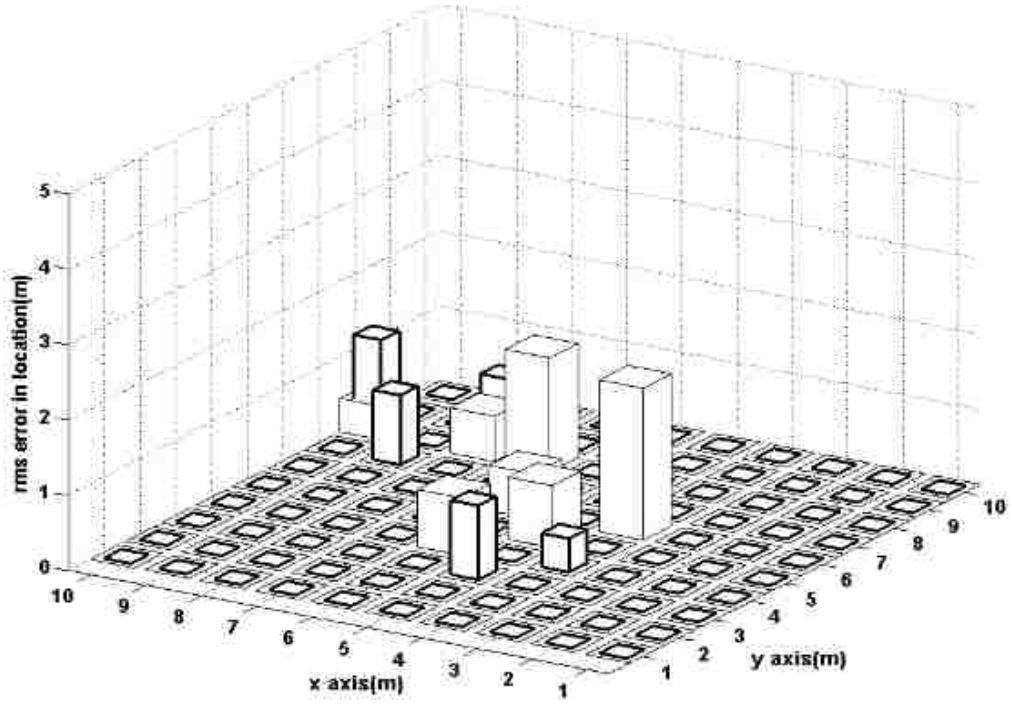

Figure 4.4. Localization errors of two correlated devices with 2D MUSIC-SSA for different positions.

Localization results for two correlated sources with 2D MUSIC-WN are depicted in Figure 4.5. The RMS error was less than 0.3 m when the source was placed at (8 m, 8 m); however, RMS error reached up to 3.1 m when placed at (10 m, 9 m). The average RMS error for two correlated sources was calculated as 1.2 m and 1.92 m for devices, respectively. Moreover, results with Smooth 2D MUSIC scheme are given in Figure 4.6 for comparison. Figures 4.4-4.6 show that the localization performance degrades when the spatial color noise effects are ignored.

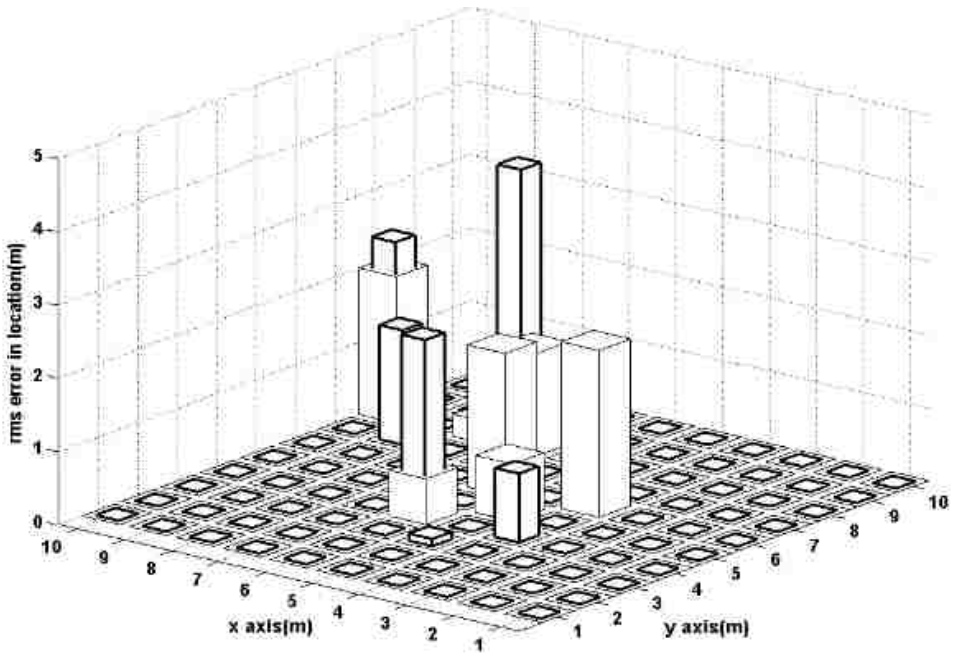

Figure 4.5. Localization errors of two correlated devices with 2D MUSIC-WN for different positions.

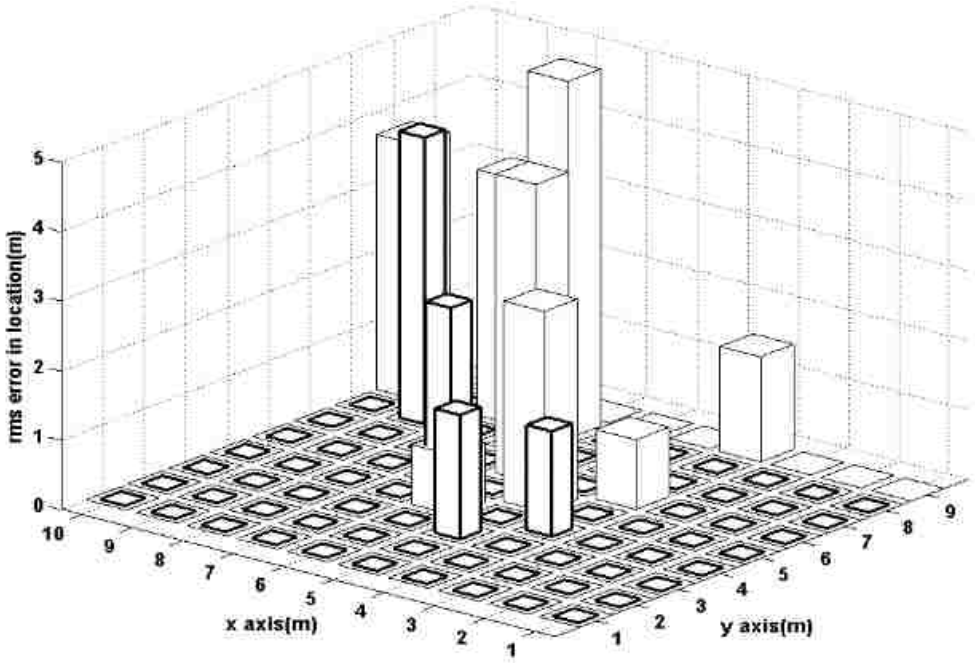

Figure 4.6. Localization errors of two correlated devices with Smooth 2D MUSIC for different positions.

4.3 CASE III- MULTIPLE UNCORRELATED RC DEVICES

The response of the doorbell to an active stimulation has harmonics around a center frequency [1]. Along with the doorbell, a single tone device placed at the center frequency of the doorbell response was employed for the experiment. Localization errors for 2D MUSIC-SSA are depicted in Figure 4.7. The maximum error was found to be 0.93 m when the device was placed at (4 m, 9 m), and the average errors for the two devices were 0.51 m and 0.6 m, respectively. Compared with the single device case, the RMS error was increased even when sources were uncorrelated. This is due to the limited number of antennas. Furthermore, device placement affected accuracy: when placed close, the error increased, but the error decreased when they were apart.

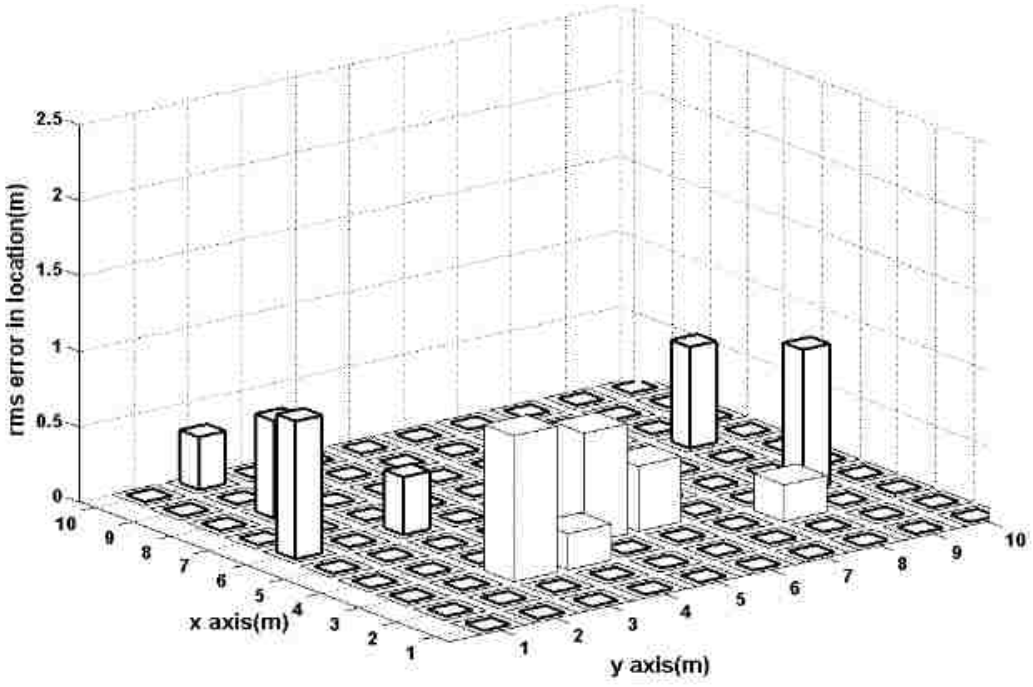

Figure 4.7. Localization errors of two uncorrelated devices with 2D MUSIC-SSA for different positions.

The RMS localization performance of the Smooth 2D MUSIC-WN for two uncorrelated sources is given in Figure 4.8 for different positions. Maximum error was 1.43 m when placed at (9 m, 4 m) and the lowest error was found to be 0.14 m when the device was placed at (3 m, 8 m). The average errors for the devices were 0.87 m and 0.75 m, respectively.

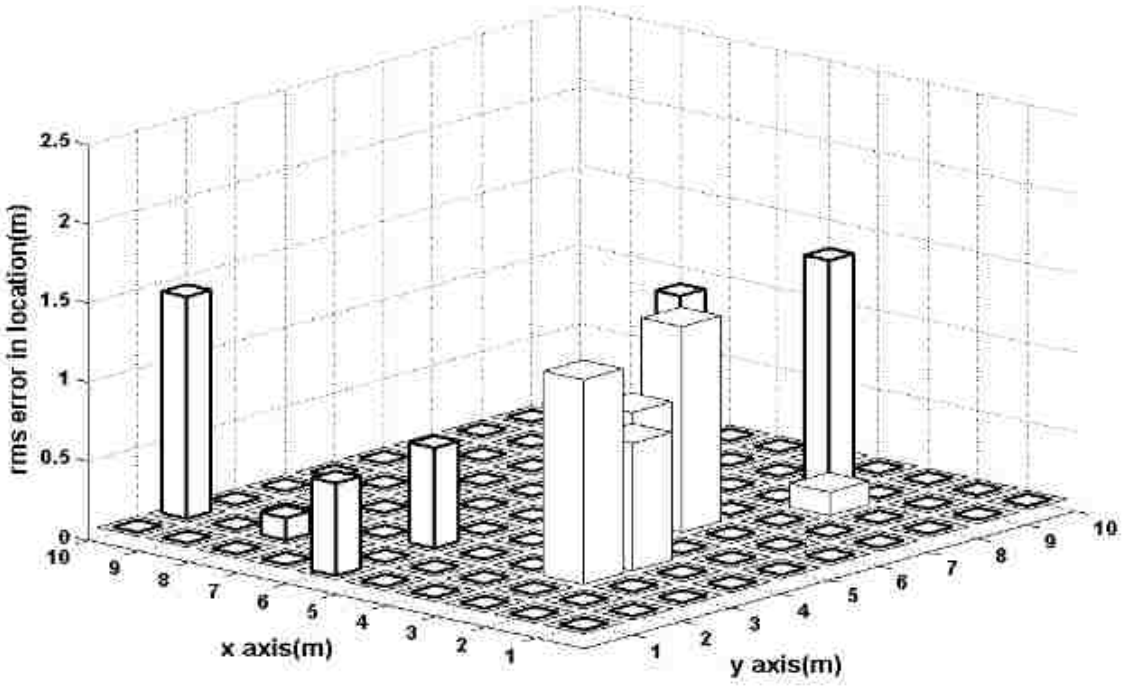

Figure 4.8. Localization errors of two uncorrelated devices with 2D MUSIC-WN for different positions.

The results for the localization errors when a whitening filter was not used are given in Figure 4.9. Measurements were evaluated with Smooth 2D MUSIC, and as can be seen from the figure, the RMS error was higher than the other schemes. Average RMS errors for this case were 1.2 m and 1.1 m.

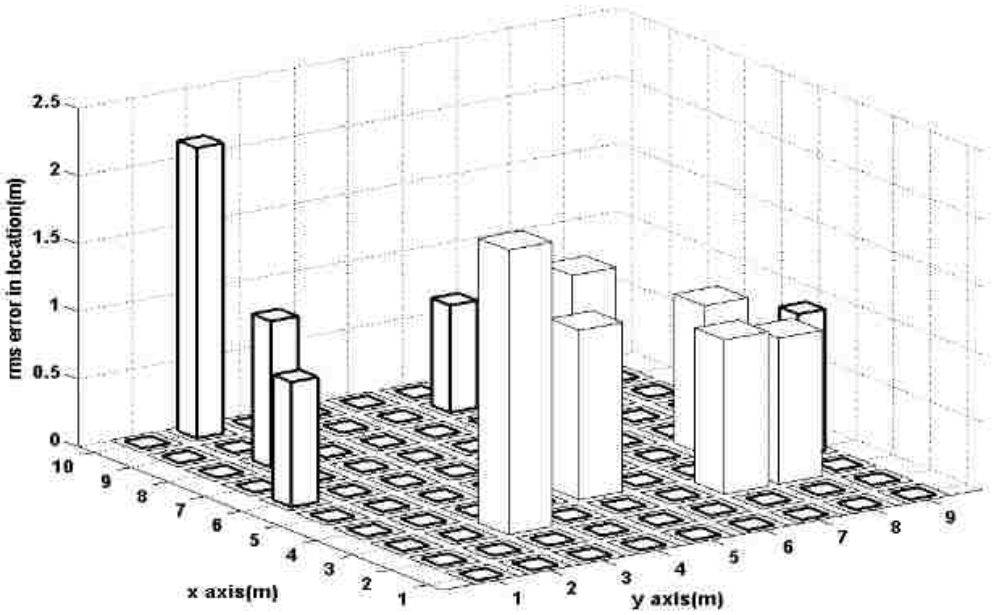

Figure 4.9. Localization errors of two uncorrelated devices with Smooth 2D MUSIC for different positions.

Table 4.1. Localization performance of two correlated sources.

Dev1 (m)	**Dev2 (m)**	**Dev1 RMSE Sparse Arrays (m)**	**Dev2 RMSE Sparse Arrays (m)**	**Dev1 RMSE Whitened Noise (m)**	**Dev2 RMSE Whitened Noise (m)**
(4,6)	(8,10)	2	1.27	0.62	2.41
(5,5)	(7,9)	0.82	0.92	0.77	1.56
(6,4)	(10,9)	0.76	0.41	2.28	3.16
(6,6)	(4,6)	0.6	0.5	1.94	2.46
(8,7)	(4,4)	1.51	0.44	1.4	0.94
(8,8)	(3,5)	0.6	0.98	0.3	1
Average error (m)		1.04	0.75	1.22	1.92

Table 4.2. Localization performance of two uncorrelated sources.

Dev1 (m)	**Dev2 (m)**	**Dev1 RMSE Sparse Arrays (m)**	**Dev2 RMSE Sparse Arrays (m)**	**Dev1 RMSE Whitened Noise (m)**	**Dev2 RMSE Whitened Noise (m)**
(6,4)	(3,6)	0.43	0.38	1.29	0.63
(4,3)	(9,7)	0.24	0.67	0.8	1
(3,3)	(2,10)	0.96	0.34	1.29	0.14
(5,4)	(9,4)	0.72	0.93	0.84	1.43
(8,3)	(1,6)	0.24	0.91	0.14	0.58
Average error (m)		0.51	0.64	0.87	0.75

When compared to the Smooth 2D MUSIC, hardware evaluation of the results demonstrated in Figures 4.1-4.9 indicate that 2D MUSIC-WN had a better performance for single, multiple correlated and uncorrelated sources in near field regions with colored noise. However, 2D MUSIC-SSA outperformed 2D MUSIC-WN since the limited number of noise free samples affected the accuracy of the whitening filter estimation. The experiment was held in the M Parking Lot of Missouri S&T campus, and hardware evaluation results are given in Tables 4.1-4.2. Figure 4.10 also indicates that the best estimation performance was obtained with the 2D MUSIC-SSA.

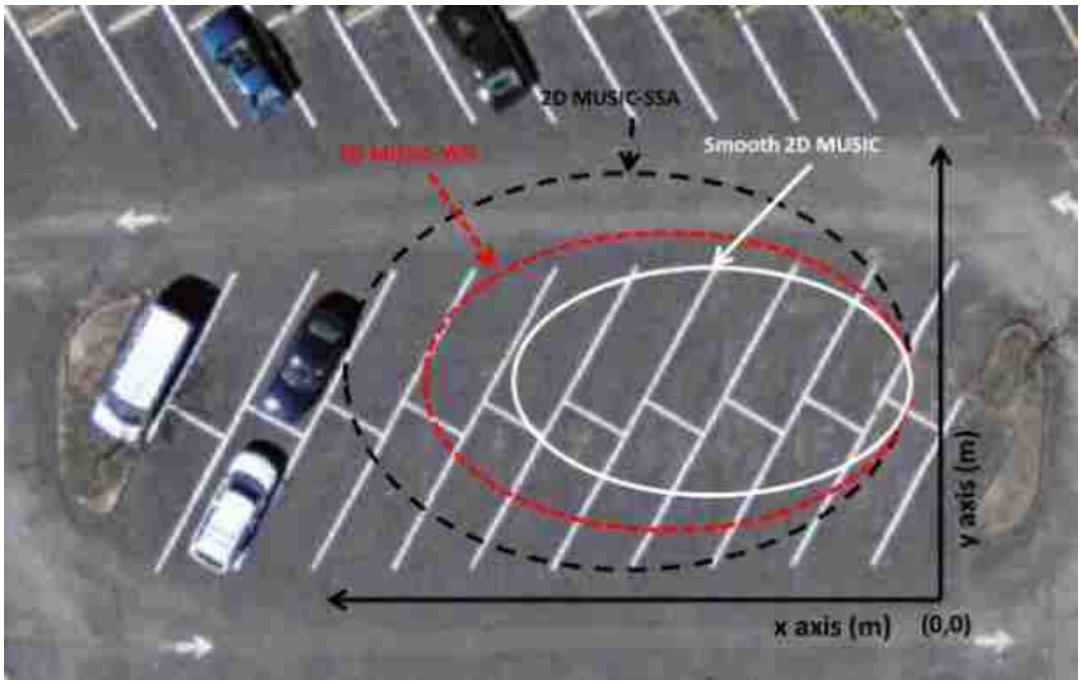

Figure 4.10. Performances of the proposed schemes and Smooth 2D MUSIC in the experiment area.

5. CONCLUSIONS

Development and hardware evaluation of two novel estimation schemes have been proposed for locating near-field unintended emitting RC sources in a colored noise environment. In Smooth 2D MUSIC-WN, signal free samples were collected to whiten the colored noise, and in 2D MUSIC-SSA the spatial diversity of two well separated arrays was used for locating a device in colored noise. Spatial smoothing eliminated the correlation among the sources and the multipath signals. The experimental results indicate that localization performance increases with application of the whitening filter when compared to Smooth 2D MUSIC. However, since the number of noise only samples was limited in practice, errors in the whitening filter estimation affected the localization accuracy. Therefore using spatial diversity of noise on two separate arrays yielded a better performance for near-field localization than Smooth 2D MUSIC-WN and the conventional Smooth 2D MUSIC. Furthermore, since the noise statistics were not used in the 2D MUSIC-SSA, the instrumentation became adaptive to locate the RC device in any environment.

6. REFERENCES

[1] V. Thotla, M. T. A. Ghasr, M. J. Zawodniok, S. Jagannathan and S. Agarwal, "Detection of Super-Regenerative Receivers Using Hurst Parameter," *IEEE Trans. Instrum. Meas*., vol.62, no.11, pp.3006-3014, Nov. 2013.

[2] V. Thotla, M. T. A. Ghasr, M. Zawodniok, S. Jagannathan and S. Agarwal, "Detection and localization of multiple R/C electronic devices using array detectors," *2012 IEEE International Instrumentation and Measurement Technology Conference (I2MTC)*, pp.1687-1691, 13-16 May 2012.

[3] Sarah Seguin, "Detection of low cost radio frequency receivers based on their unintended electromagnetic emissions and an active stimulation," Ph.D dissertation, Missouri S&T, Rolla, MO 2009.

[4] R. Schmidt, "Multiple emitter location and signal parameter estimation," *IEEE Trans. on Ant. and Prop.*, vol.34, no.3, pp. 276- 280, March 1986.

[5] R. Roy, A. Paulraj and T. Kailath, "Direction-of-arrival estimation by subspace rotation methods – ESPRIT," *IEEE International Conference on Acoustics, Speech, and Signal Proc.*, vol.11, pp.2495-2498, Apr 1986.

[6] M. Viberg and B. Ottersten, "Sensor array processing based on subspace fitting," *IEEE Trans. on Signal Proc.*, vol.39, no.5, pp.1110-1121, May 1991.

[7] W. Zhi and M. Y. W. Chia, "Near-Field Source Localization via Symmetric Subarrays," IEEE Signal Processing Letters, vol.14, no.6, pp.409-412, June 2007.

[8] N. Yuen and B. Friedlander, "Performance analysis of higher order ESPRIT for localization of near-field sources," *IEEE Transactions on Signal Processing*, vol.46, no.3, pp.709-719, Mar 1998.

[9] E. Cekli and H. A. Cirpan, "Unconditional maximum likelihood approach for near-field source localization," *8th IEEE International Conference on Electronics, Circuits and Systems*, vol.2, pp.753-756, Sep 2001.

[10] R. N. Challa and S. Shamsunder, "High-order subspace-based algorithms for passive localization of near-field sources," *Conference Record of the Twenty-Ninth Asilomar Conference on Signals, Systems and Computers*, vol.2, pp.777-781, Oct. 30 -Nov. 1 1995.

[11] N. Guzey, H. Xu and S. Jagannathan, "Localization of Near-Field Radio Controlled Unintended Emitting Sources in the Presence of Multipath Fading", *IEEE Transactions on Instrumentation and Measurement*, vol.63, no.11, pp.2696,2703, Nov. 2014.

[12] L. Fu and R. J. Vaccaro, "Performance degradation of DOA estimators due to unknown noise fields," *IEEE Transactions on Signal Processing*, vol.40, no.3, pp.686-690, Mar 1992.

[13] V. Nagesha and S. Kay, "Maximum likelihood estimation for array processing in colored noise," *IEEE International Conference on* Acoustics, *Speech, and Signal Processing*, vol.4, pp.240-243, 27-30 April 1993.

[14] H. Ye and R. D. DeGroat, "Maximum likelihood DOA estimation and asymptotic Cramer-Rao bounds for additive unknown colored noise," *IEEE Transactions on Signal Processing*, vol.43, no.4, pp.938-949, Apr 1995.

[15] B. Goransson and B. Ottersten, "Direction estimation in partially unknown noise fields," *IEEE Transactions on Signal Processing*, vol.47, no.9, pp.2375-2385, Sep 1999.

[16] B. Friedlander and A. J. Weiss, "Direction finding using noise covariance modeling," *IEEE Trans. on Signal Proc.*, vol.43, no.7, pp.1557-1567, Jul 1995.

[17] M. Viberg, P. Stoica and B. Ottersten, "Maximum likelihood array processing in spatially correlated noise fields using parameterized signals," *IEEE Trans. on Signal. Proc.*, vol.45, no.4, pp.996-1004, Apr 1997.

[18] K. Werner and M. Jansson, "Optimal Utilization of Signal-Free Samples for Array Processing in Unknown Colored Noise Fields," *IEEE Trans. on Signal Processing*, vol.54, no.10, pp.3861-3872, Oct. 2006.

[19] A. L. Swindlehurst and T. Kailath, "A performance analysis of subspace-based methods in the presence of model errors. I. The MUSIC algorithm," *IEEE Transactions on Signal Processing*, vol.40, no.7, pp.1758-1774, Jul 1992.

[20] A. L. Swindlehurst and T. Kailath, "A performance analysis of subspace-based methods in the presence of model error. II. Multidimensional algorithms," *IEEE Trans. on Signal Proc.*, vol.41, no.9, pp.2882-2890, Sep 1993.

[21] M. G. Christensen and A. Jakobsson, *Multi-pitch Estimation.* Morgan&Claypool, pp. 85-86, 2009.

[22] Q. Wu and K. M. Wong, "UN-MUSIC and UN-CLE: An application of generalized correlation analysis to the estimation of the directions of arrival of signals in unknown correlated noise," *IEEE Transaction on Signal Processing*, vol. 42, pp. 2331–2343, Sep. 1994.

[23] Y. D. Huang and M. Barkat, "Near-field multiple source localization by passive sensor array," *IEEE Transactions on Antennas and Propagation*, vol.39, no.7, pp.968-975, Jul 1991.

[24] T. Shan, M. Wax and T. Kailath, "On spatial smoothing for direction-of-arrival estimation of coherent signals,"*IEEE Transactions on Acoustics, Speech and Signal Processing*, vol.33, no.4, pp. 806-811, Aug 1985.

[25] A. Dogandˇzić and A. Nehorai, "Generalized multivariate analysis of variance: A unified framework for signal processing in correlated noise," *IEEE Signal Processing Magazine*, vol. 20, pp. 39–54, Sep. 2003.

[26] A. B. Gershman, P. Stoica, M. Pesavento, and E. G. Larsson, "Stochastic Cramér-Rao bound for direction estimation in unknown noise fields," Proc. Inst. Electr. Eng.—Radar Sonar Navig., vol. 149, pp. 2–8, Feb. 2002.

[27] A. B. Gershman and V. T. Ermolaev, "Optimal subarray size for spatial smoothing," *IEEE Signal Processing Letters*, vol.2, no.2, pp.28-30, Feb 1995.

APPENDIX

A: Proof of Theorem 1

After the whitening filter was applied as in (2.14), noise and signal subspaces became orthogonal; therefore, if $\hat{\mathbf{e}}_m \in \Re^L, m = Q - K_T, \ldots, Q$ is a noise eigenvector from the noise eigenvector matrix $\hat{\mathbf{E}}_n$, it results in

$$\hat{\mathbf{R}}_s \hat{\mathbf{e}}_m = 0 \tag{A.1}$$

which leads to $\mathbf{A}^H \hat{\mathbf{e}}_m = 0$, where $\hat{\mathbf{R}}_s$ is the signal covariance matrix after whitening filter application and smoothing, and $\mathbf{A}$ is the array steering matrix. Since the noise and signal subspaces are well separated now, and the new signal covariance matrix is of full rank, the correct angle in the steering vector will make (15) maximum. Therefore, the maximum of P_{MUSIC} spectrum represents the DOA and range.

B: Proof of Theorem 2

With the smoothing procedure introduced in (2.21), the correlated sources and the multipath components are separated. Generalized correlation coefficient matrix, $\mathbf{\Gamma} = diag\{\gamma_1, \ldots, \gamma_{K_T}\}$, became diagonal and the generalized correlation matrices were calculated with the smoothed covariance matrix. Further, as given in [22], $\mathbf{Y}_{in}$ defined in (25) projects onto the subspace spanned by the vectors $\{\mathbf{l}_{im}\}$, $m = K_T + 1, \ldots, Q_i$, but these vectors span the orthogonal complements of the signal subspace spanned by $\mathbf{A}_i(\boldsymbol{\theta}, \mathbf{r})$. Therefore, it can be concluded that $\mathbf{Y}_{in}$ projects onto $\overline{span}(\mathbf{A}_i(\boldsymbol{\theta}, \mathbf{r}))$, and the angle and distance components which make (2.27) maximum represent the locations of the passive RC sources.

III. TRACKING OF RADIO-CONTROLLED SOURCES USING UNINTENDED EMISSIONS

ABSTRACT

This paper presents the tracking of unintended emissions from radio-controlled (RC) sources in a multipath fading environment by using uniform linear array (ULA) antennas. Existing methods [12]-[18] use the direction of arrival (DOA) information from the moving target to track objects by computing covariance matrix of the array output, whereas if the target is moving in the near-field region of the antenna array, the tracking performance will degrade. In addition, estimation of covariance matrix of the array output at every instant of time is tedious. Therefore, a novel method is proposed to track multiple targets in both near and far-field regions of the antenna array even if multipath fading is present. The proposed method uses the array output directly instead of computing the covariance matrix in order to estimate the angle and distance between the source and the array. Experimental evaluation of the proposed method for single and multiple devices are provided; moreover, the hardware evaluation of Park's method [17] is included to compare and demonstrate the effectiveness of the proposed work.

1. INTRODUCTION

The devices which contain super heterodyne or regenerative receivers are sensitive to stimulation, which leads them to emit unintended and very low power emissions [1]-[3]. By using these emissions, location of these devices can be provided by using the high resolution direction of arrival (DOA) methods such as MUSIC [4], ESPRIT [5] and WSF [6]. These methods [4]-[6] are efficient if the DOA to each antenna is assumed to be equal. However, this assumption is not valid if a source is located in the near-field region of the antenna array since the phase difference between the antenna elements are nonlinear functions of DOA, and the distance between the array and the source complicates the location estimation. To eliminate these complexities, Fresnel approximation [7] is used by the near-field localization methods [7]-[11] to approximate the nonlinear phase difference with a second order Taylor series expansion. The near field localization techniques [8]-[9] use higher order statistics resulting in a high computational burden.

A maximum likelihood estimator, on the other hand, is presented in [10] to locate the near-field sources. Another method [7] uses symmetric arrays for near field localization. The location estimation with the near field methods [7]-[10] degrades when the sources are either correlated or multipath fading is present in the environment. The smooth 2D MUSIC method in [11] deals with these issues and provides an inexpensive solution to the problem of near field localization.

The unintentional emitting sources may not always be stationary; therefore, it can be critical to track these targets especially for security reasons. Angle tracking algorithms from [12] and [13] can be used to track a mobile target where the array

processing techniques are used under an assumption [12]-[13] that the targets are stationary during a limited integration time. For each time interval, a high resolution method such as MUSIC is applied and the target is tracked.

However these algorithms [12]-[13] do not perform well in the presence of multiple targets due to the data association problem of the DOA estimates obtained from two successive time intervals. The recursive tracking technique proposed by Sward et al. [14] uses the DOA estimates from the most recent array output to update the predicted DOA which in turn solves the data association problem in an efficient way. In [15], the distance between components of the true and estimated covariance matrix of array output is minimized to help associate multiple targets with their corresponding DOA estimates; however, it assumes that the signal powers of all the targets are different, which is difficult to achieve in practice.

A Kalman filter is used in [15]-[18] to decrease the estimation errors and solve the data association issue. In these techniques [15]-[18], during the prediction step of the filter, the previous state vector is used to estimate the current state vector, and subsequently in the correction step, the current measurements are utilized to refine the estimated state vector. In [17], authors proposed an algorithm that uses the predicted angles provided from Sward's method and constrained least-squares to restrain the dynamic range of the angles. However, this method is inefficient at low signal-to-noise ratios and at moving speeds. Park's method [17] is improved in [18] by estimating the angle variations of the targets from the signal subspace rather than the array output covariance matrix.

These methods [12]-[18] are dependent upon the covariance matrix of the array output or signal subspace. The covariance matrix is estimated with multiple snapshots of output of the antenna array at every time interval. However, in practice multiple snapshot measurement within each time increment may not be feasible for real-time tracking. Therefore the available methods [12]-[18] will not provide satisfactory results in the presence of a single snapshot. Instead of a sample covariance matrix, the array output is directly used in the extended Kalman filter (EFK) in [20]. However, distance effect on the phase difference between the antenna elements is not considered.

Aother drawback of the proposed schemes [12]-[18] is that they use a linear measurement model. However, the received signal with the ULA is a nonlinear function of the DOA information. The nonlinear measurement model is utilized in [19] with the extended Kalman filter (EKF) and array output covariance matrix to increase the tracking performance. Even so, none of the schemes [12]-[20] do consider the distance effect to the phase difference when the target is moving in the near-field region of the antenna array.

Therefore, a new near-field tracking method which is an extension of Park's [17] scheme is proposed in this paper to predict the angle and the distance between source and the array of maneuvering targets by using a single snapshot of the array output instead of computing the covariance matrix. The EFK is preferred, since it does not require an extra data association algorithm and the signal or noise statistics are not needed as in [21] and [22], therefore it is more convenient for the practical applications. The angle and the distance between the array and the source are considered as states of the system to be estimated. Later the estimates are smoothed by using Kalman gain. The initial estimates

of angle and range are provided by the Smooth 2D MUSIC [11] in order to separate the multipath and coherent sources. Evaluation of the proposed scheme is performed by collecting data.

Therefore, the contributions of this study include the: 1) development of a scheme in order to track multiple non-stationary targets both in a near and far-field multipath fading environment by using a single snapshot of array output for practical viability, 2) hardware evaluation of the proposed method with single and multiple devices and single and multiple antenna arrays via data collection, 3) hardware evaluation of the Park's method for both near- and far-field regions and comparing the results with the proposed method. Although the measured data was processed after its collection, the proposed method can be implemented in real time since it requires a single snapshot of array output at any instant of time thus enhancing the instrumentation and measurement aspect of tracking mobile objects.

The rest of the paper is organized as follows. Section 2, introduces the signal representation of the near-field sources. Subsequently, dynamic model for location tracking is given. In Section 3, the proposed method for tracking unintended emitting RC devices is introduced by using a single snapshot of array output. Section 4 presents the experimental setup for hardware evaluation. Section 5 introduces results with the proposed scheme in the presence of single and multiple sources by estimating DOA and distance between sources and antenna array. In addition, the tracking results of Park's model [17] are given for the sake of comparison. The discussion is finalized with conclusions in Section 6.

2. DATA MODEL AND PROBLEM FORMULATION

In this section, the problem of tracking maneuvering targets in both near and far-field multipath fading environment is formulated by using low power unintended emissions. First the received signal model of sources in the near-field region of an antenna array is given. Next the deterministic dynamic model of location trajectory is demonstrated.

2.1 NEAR-FIELD SIGNAL MODEL

Let us assume a uniform linear array (ULA), which consists of L antenna elements with inter-element spacing being d. Consider the existence of Ms narrow band unintentionally emitting sources placed in the near-field region of the antenna array; therefore, the received signal from the array, y(k), is represented as

$$\mathbf{y}(k) = \sum_{m=1}^{M_S} \mathbf{a}(\theta_m, r_m) s_m(k) + \mathbf{n}(k), \tag{2.1}$$

where k=1,…,Ks is the number of samples, $\mathbf{y}(k) = \left[y_1(k), \ldots\ldots, y_L(k)\right]^T \in \Re^L$ is the vector of antenna outputs, and $\mathbf{n}(k) = [n_1(k), \ldots n_L(k)]^T \in \Re^L$ represents noise output of the array. Additionally, $s_m(k) \in \Re$ is the received signal power from the m^{th} source, $m = 1, \ldots, M_s$, T is the transpose operator, and $\mathbf{a}(\theta_m, r_m) \in \Re^L$ is the phase response of the antenna array to the m^{th} source which is also referred as array steering vector defined as

$$\mathbf{a}(r_m, \theta_m) = [e^{-j\tau_1(\theta_m, r_m)} \ldots e^{-j\tau_L(\theta_m, r_m)}]^T \tag{2.2}$$

where θ_m and r_m represent the DOA of the signal from the m^{th} source and distance between source and the array reference, respectively, $\tau_l(\theta_m, r_m)$ is the phase difference between the reference antenna and the l^{th} antenna. This phase difference is a function of DOA information in the far-field region, but in the near-field region, it also depends upon distance between the source and the array. With Fresnel approximation as given by in [7], the phase difference, $\tau_l(\theta_m, r_m)$ is expressed as

$$\tau_l(\theta_m, r_m) \approx \frac{2\pi}{\lambda}\left((l-1)d\sin\theta_m - \frac{(l-1)^2 d^2 \cos\theta_m}{2r_m}\right), \quad l = 1,\ldots,L, \tag{2.3}$$

where λ is the wavelength of the received signal, d is the distance between adjacent antennas, and l is the l^{th} antenna element. The array steering vector, $\mathbf{a}(r_m, \theta_m)$, for each source is given by [7]

$$\mathbf{a}(r_m,\theta_m) = \begin{bmatrix} a_{m,0} \\ \vdots \\ a_{m,L-1} \end{bmatrix} = \begin{bmatrix} 1 \\ e^{-j\left(-\frac{2\pi d}{\lambda}\sin\theta_m\right)1 + j\left(-\frac{\pi d^2}{\lambda r_m}\cos^2\theta_m\right)1^2} \\ \vdots \\ e^{-j\left(-\frac{2\pi d}{\lambda}\sin\theta_m\right)(L-1) + j\left(-\frac{\pi d^2}{\lambda r_m}\cos^2\theta_m\right)(L-1)^2} \end{bmatrix} \quad m = 1,\ldots M_s. \tag{2.4}$$

Then, the received signal, $y_l(k)$, at l^{th} antenna for M_s sources can be written as [7]

$$y_l(k) = \sum_{m=1}^{M_s} e^{j\left(-\frac{2\pi d}{\lambda}\sin\theta_m\right)(l-1) + j\left(-\frac{\pi d^2}{\lambda r_m}\cos^2\theta_m\right)(l-1)^2} s_m(k) + n(k), \tag{2.5}$$

where $l = 1,\ldots,L$ being the number of antenna elements. The received signal at the ULA is represented in matrix form such as

$$\mathbf{y}(k) = \mathbf{A}\mathbf{s}(k) + \mathbf{n}(k) \quad \mathrm{k} = 1,\ldots K_s, \tag{2.6}$$

where $\mathbf{s}(k) \in \Re^{M_s}$ is the vector of signal powers, and $\mathbf{A} \in \Re^{L \times M_s}$ is the array manifold composed with the array response to all sources. This array manifold is represented as

$$\mathbf{A}(\theta, r) = [\mathbf{a}(\theta_1, r_1), \mathbf{a}(\theta_2, r_2), \ldots, \mathbf{a}(\theta_{M_s}, r_{M_s})] \tag{2.7}$$

If we define

$$\gamma_{lm}(k) = e^{-j\tau_{lm}(k)} \tag{2.8}$$

which is the response of each antenna element to each source, the array manifold can be rewritten as

$$\mathbf{A} = \begin{bmatrix} 1 & 1 & \cdots & 1 \\ \gamma_{21} & \gamma_{22} & \cdots & \gamma_{2M_s} \\ \vdots & \vdots & \ddots & \vdots \\ \gamma_{(L-1)1} & \gamma_{(L-1)2} & \cdots & \gamma_{(L-1)M_s} \end{bmatrix}. \tag{2.9}$$

The localization and tracking of a moving object with a uniform antenna array is represented in Figure 2.1. As observed from the figure, the location of the device depends upon the DOA and the distance between the antenna array and the source for different time instants. Next the deterministic trajectory model is represented for multiple mobile targets.

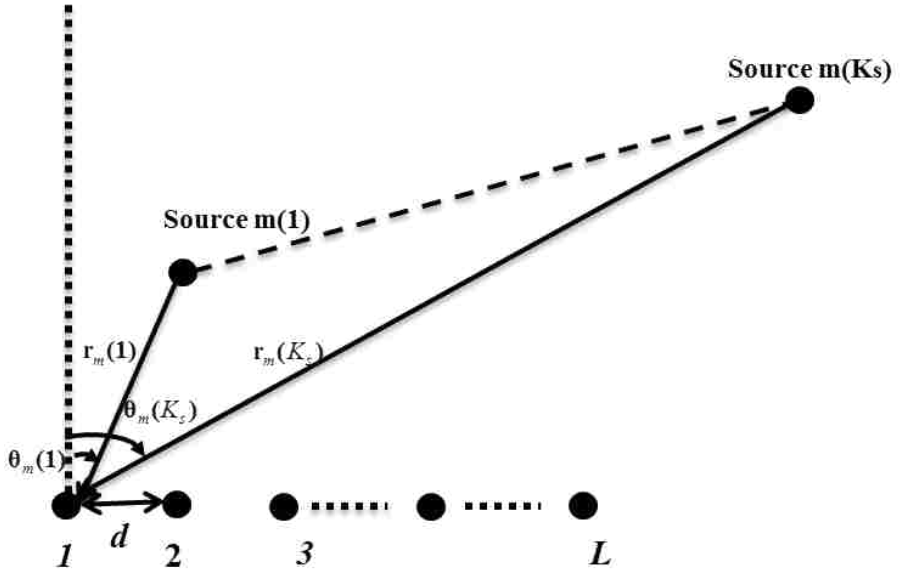

Figure 2.1. Near-field tracking process of a moving source

2.2 DETERMINISTIC DYNAMIC MODEL OF LOCATION TRAJECTORY

The state vector for the m^{th} target is defined as [15] $\mathbf{x}_m(k) = [\theta_m(k), \dot{\theta}_m(k), \ddot{\theta}_m(k), \mathrm{r}_m(k), \dot{\mathrm{r}}_m(k), \ddot{\mathrm{r}}_m(k)]^T \in \Re^6$, which consists of DOA, angular velocity, angular acceleration, distance between antennas, and source and change, and acceleration in the distance. The m^{th} target motion $\mathbf{x}_m(k)$ follows the rule [17]

$$\mathbf{x}_m(k+1) = \mathbf{F}_m \mathbf{x}_m(k) + \mathbf{w}_m(k), \quad k=1,\ldots K_s, \tag{2.10}$$

where

$$\mathbf{F}_k = \begin{bmatrix} 1 & T_p & \frac{1}{2}T_p^{\,2} & 0 & 0 & 0 \\ 0 & 1 & T_p & 0 & 0 & 0 \\ 0 & 0 & 1 & 0 & 0 & 0 \\ 0 & 0 & 0 & 1 & T_p & \frac{1}{2}T_p^{\,2} \\ 0 & 0 & 0 & 0 & 1 & T_p \\ 0 & 0 & 0 & 0 & 0 & 1 \end{bmatrix} \in \Re^{6x6} \tag{2.11}$$

represents the state transition matrix of the m^{th} source, $m=1,\ldots M_s$ being the number of sources, T_p is the sampling period between successive samples, and $\mathbf{w}_m(k)$ is the process noise which is assumed to be Gaussian with zero mean and covariance $\boldsymbol{Q_m}$. The composite state vector, $\mathbf{x}(k)$, for the total M_s sources is written as $\mathbf{x}(k)=\left[\mathbf{x}_1^T(k),\ldots,\mathbf{x}_{M_s}^T(k)\right]$. Then the dynamics for the M_s sources is represented as

$$\mathbf{x}(k+1)=\mathbf{F}\mathbf{x}(k)+\mathbf{w}(k), \tag{2.12}$$

where $\mathbf{F}=diag(\mathbf{F}_1,\ldots,\mathbf{F}_{M_s})$ is a block diagonal matrix and $\mathbf{w}(k)=[\mathbf{w}_1(k),\ldots\mathbf{w}_{M_s}(k)]$ is the process noise vector of M_s sources. The measurement model, $\mathbf{z}_m(k)$, for the Kalman filter is given in [17] as

$$\mathbf{z}_m(k)=\mathbf{H}_m\mathbf{x}_m(k), \tag{2.13}$$

where the measurement matrix is given by $\mathbf{H}_m=[1\ 0]\in\Re^{1x2}$ which is deterministic and same for all sources, and the state vector is defined as $\mathbf{x}_m=[\theta\ \dot{\theta}]\in\Re^2$ [17]. The tracking model is defined in far-field region of the antenna array and only DOA is obtained. In the near-field, the phase difference between two antenna elements is also a function of distance between the sources. Therefore, the range information should be added as a state variable. Further, the measurement model (2.5) is a nonlinear function of the state variables; therefore, instead of (2.13) a nonlinear model should be used. In [19], a nonlinear measurement model and its derivative are used in EKF, however they ignored the distance effect on the phase difference when the target is in the near-field region.

Although the presented scheme in [17] tracks the DOA without a data association problem and using the predicted angles in order to restrain the dynamic range of the DOAs, it requires the multiple snapshots of the array output at every time instant to form

the covariance matrix. Instead of multiple snapshots, the array output is directly used in [20], however, the near-field and multipath fading is not considered.

In order to eliminate the drawbacks of the Park's method [17] which are described in this section, a new scheme is introduced next in detail to track both DOA and the distance between the antenna array and the source in a multipath fading near-field environment by using a single snapshot of the array output. Furthermore, the new method uses a nonlinear measurement model and its first order derivative as given in [19] to perform a more efficient tracking performance.

3. 2D TRACKING METHOD OF MANEUVERING TARGETS

To track the multiple maneuvering targets in near-field, EKF is utilized in this paper to estimate the DOA and the distance between the array and the source. To estimate the initial values for EKF, Smooth 2D MUSIC [11] is employed where it is also able to locate multiple correlated sources in a multipath environment. After spatial smoothing, the targets become independent and the data association problem can be solved by using the EFK. Since the process is a nonlinear function of the DOA and distance between the source and antenna array, the array output, **y**(k), can be rewritten as [19]

$$\mathbf{y}(k) = \mathbf{h}(\mathbf{x}(k), \mathbf{s}(k))\mathbf{x}(k) + \mathbf{v}(k) = \mathbf{A}(\mathbf{x}(k))\mathbf{s}(k) + \mathbf{n}(k), \tag{3.1}$$

where **v**(k) is the measurement noise with zero mean and σ_v^2 is the variance. Thus for linearization, the partial derivative matrix of the measurement model is given by [19]

$$\mathbf{H}(k) = \frac{\partial \mathbf{h}}{\partial \mathbf{x}} = \left[\mathbf{H}_1(k), \ldots, \mathbf{H}_{M_s}(k) \right]. \tag{3.2}$$

By augmenting real and imaginary parts of $\mathbf{H}(k)$, the composite real matrix becomes

$$\bar{\mathbf{H}}(k) = \begin{bmatrix} \mathrm{Re}(\mathbf{H}_1(k), \ldots, \mathbf{H}_{M_s}(k)) \\ \mathrm{Im}(\mathbf{H}_1(k), \ldots, \mathbf{H}_{M_s}(k)) \end{bmatrix}$$

$$= \begin{bmatrix} 0 & 0 & 0 & 0 & 0 & 0 & 0 & 0 & 0 & 0 \\ g_{21}\dfrac{\partial \tau_{21}}{\partial \theta_1} & 0 & 0 & g_{21}\dfrac{\partial \tau_{21}}{\partial r_1} & 0 & 0 & \cdots & g_{2K}\dfrac{\partial \tau_{2M_s}}{\partial r_{M_s}} & 0 & 0 \\ \vdots & \vdots & \vdots & \vdots & \vdots & \vdots & \ddots & \vdots & \vdots & \vdots \\ g_{L1}\dfrac{\partial \tau_{L1}}{\partial \theta_1} & 0 & 0 & g_{L1}\dfrac{\partial \tau_{L1}}{\partial r_1} & 0 & 0 & \cdots & g_{LK}\dfrac{\partial \tau_{LM_s}}{\partial r_{M_s}} & 0 & 0 \\ 0 & 0 & 0 & 0 & 0 & 0 & \cdots & 0 & 0 & 0 \\ c_{21}\dfrac{\partial \tau_{21}}{\partial \theta_1} & 0 & 0 & c_{21}\dfrac{\partial \tau_{21}}{\partial r_1} & 0 & 0 & \cdots & c_{2K}\dfrac{\partial \tau_{2M_s}}{\partial r_{M_s}} & 0 & 0 \\ \vdots & \vdots & \vdots & \vdots & \vdots & \vdots & \ddots & \vdots & \vdots & \vdots \\ c_{L1}\dfrac{\partial \tau_{L1}}{\partial \theta_1} & 0 & 0 & c_{L1}\dfrac{\partial \tau_{L1}}{\partial r_1} & 0 & 0 & \cdots & c_{LK}\dfrac{\partial \tau_{LM_s}}{\partial r_{M_s}} & 0 & 0 \end{bmatrix}, \tag{3.3}$$

L is the number of antenna elements. Since $\gamma_{lm}(k) = e^{-j\tau_{lm}(k)}$ per (8), then

$$g_{lm} = -\sin(\tau_{lm}) s_m(k) \text{ and } c_{lm} = -\cos(\tau_{lm}) s_m(k). \tag{3.4}$$

The derivatives are then calculated as

$$\frac{\partial \tau_{lm}}{\partial \theta_m} = \frac{2\pi d}{\lambda}(l-1)\cos(\theta_m) + \frac{\pi d^2}{\lambda r_m}(l-1)^2 \sin(2\theta_m), \tag{3.5}$$

and

$$\frac{\partial \tau_{lm}}{\partial r_m} = \frac{\pi d^2 (l-1)^2 \cos^2(\theta_m)}{\lambda r_m^2}. \tag{3.6}$$

The derivatives (3.5) and (3.6) are different from the ones in [19] since the array output is a function of not only DOA but also distance between the array and the source in the near field. Thus more states are being tracked in the near-field, which makes the tracking and the data association more challenging.

Initially, the target angles and range parameters at two successive time instants $\{\theta_m(-1), \theta_m(0), r_m(-1)\ r_m(0)\}$ are estimated with Smooth 2D MUSIC [11]. Therefore, the initial state vector, $\mathbf{x}_m(0|0)$, for the m^{th} source can be defined as

$$\mathbf{x}_m(0|0) = \left[\hat{\theta}_m(0), (\hat{\theta}_m(0) - \hat{\theta}_m(-1))/T_p\ ,0\ \hat{r}_m,(0),(\hat{r}_m(0) - \hat{r}_m(-1))/T_p,\ 0\right]^T, \tag{3.7}$$

and the initial state vector for the total M_s emitting sources is represented as

$$\mathbf{x}(0|0) = [\hat{\theta}_1(0), (\hat{\theta}_1(0) - \hat{\theta}_1(-1))/T_p, 0, \hat{r}_1(0), (\hat{r}_1(0) - \hat{r}_1(-1))/T_p, 0\ldots \tag{3.8}$$

$$\ldots\hat{\theta}_{M_s}(0), (\hat{\theta}_{M_s}(0) - \hat{\theta}_{M_s}(-1))/T_p, 0, \hat{r}_{M_s}(0), (\hat{r}_{M_s}(0) - \hat{r}_{M_s}(-1))/T_p, 0]^T.$$

According to the initial state vector for the m^{th} source as given in (3.20), the initial covariance matrix of the state vector for the m^{th} source, $\mathbf{P}_m(0|0) = \mathbf{X}_m(0|0) \times \mathbf{X}_m^T(0|0)$, can be written as

$$\mathbf{P}_m(0|0) = \sigma_v^2 \begin{bmatrix} 1 & \frac{1}{T_p} & 0 & 0 & 0 & 0 \\ \frac{1}{T_p} & \frac{2}{T_p^{\,2}} & 0 & 0 & 0 & 0 \\ 0 & 0 & 0 & 0 & 0 & 0 \\ 0 & 0 & 0 & 1 & \frac{1}{T_p} & 0 \\ 0 & 0 & 0 & \frac{1}{T_p} & \frac{2}{T_p^{\,2}} & 0 \\ 0 & 0 & 0 & 0 & 0 & 0 \end{bmatrix}, \tag{3.9}$$

where T_p is the time period between two successive sample and σ_v^2 is the variance of measurement noise. The complete state covariance matrix for the total M_s sources, $\mathbf{P}(0|0)$, will be given by

$$\mathbf{P}(0|0) = diag(\mathbf{P}_1(0|0), \ldots \mathbf{P}_{M_s}(0|0)), \tag{3.10}$$

where the m^{th} block of the diagonal matrix is the state covariance matrix of the m^{th} source, $m=1,...M_s$. Next the estimation procedure of the state variables with EKF is explained in four steps.

Step 1, Prediction

The prediction of the state vector and the covariance matrix of the state vector can be achieved from the existing estimates such as

$$\mathbf{x}_m(k|k-1) = \mathbf{F}\mathbf{x}_m(k-1|k-1) + \mathbf{w}_m(k), \tag{3.11}$$

$$\mathbf{P}(k|k-1) = \mathbf{F}\mathbf{P}(k-1|k-1)\mathbf{F}^{\mathbf{T}} + \mathbf{Q}, \tag{3.12}$$

where $\mathbf{x}_m(k|k-1)$ is the predicted states at time k with the estimated states, $\mathbf{x}_m(k-1|k-1)$, at time *k-1*, $\mathbf{w}_m(k)$ is the process noise with a covariance matrix **Q**. Additionally, $\mathbf{P}(k|k-1)$ is the predicted covariance matrix of the states at time *k*. The first and fourth elements of state vector $\mathbf{x}_m(k|k-1)$ are the predicted estimates, $\hat{\theta}_m(k|k-1)$, $\hat{r}_m(k|k-1)$ of $\theta_m(k)$ and $r_m(k)$, respectively. The predicted array matrix $\mathbf{A}(k|k-1)$ can be obtained using the predicted DOA and distance parameter. Then the predicted array output will be given by

$$\mathbf{y}(k|k-1) = \mathbf{A}(k|k-1)\hat{\mathbf{s}}(k). \tag{3.13}$$

The array output can be obtained when the source vector is estimated with maximum likelihood as

$$\hat{\mathbf{s}}(k) = [\mathbf{A}^H(k|k-1)\mathbf{A}(k|k-1)]^{-1}\mathbf{A}(k|k-1)\mathbf{y}(k). \tag{3.14}$$

Step 2, Calculation of the variations

After a time interval, T_p, the new array output is observed and the new array matrix is represented as

$$\mathbf{A}(k) = \mathbf{A}(k \mid k-1) + \delta\mathbf{A}(k), \tag{3.15}$$

where $\delta\mathbf{A}(k)$ is the change in the array matrix between two successive time instants, in the element wise given by

$$[\delta\mathbf{A}(k)]_{lm} = -j\gamma_{lm}(t)\left[\frac{\partial\tau_{lm}}{\partial\theta_m}\delta\theta_m + \frac{\partial\tau_{lm}}{\partial r_m}\delta r_m\right], \tag{3.16}$$

with

$$\frac{\partial\tau_{lm}}{\partial\theta_m} = \frac{2\pi d}{\lambda}(l-1)\cos(\theta_m) + \frac{\pi d^2}{\lambda r_m}(l-1)^2\sin(2\theta_m) \tag{3.17}$$

and

$$\frac{\partial\tau_{lm}}{\partial r_m} = \frac{\pi d^2(l-1)^2\cos^2(\theta_m)}{\lambda r_m^2}. \tag{3.18}$$

Again the change in the array manifold between two time instants depends on the change in the DOA and distance between the array and the source. Therefore the partial derivative of the phase difference with respect to DOA and distance information is needed for tracking in near-field. By using the array manifold in (3.28), the output residual of the array is represented as

$$\boldsymbol{\delta}\mathbf{y}(k) = \mathbf{y}(k) - \mathbf{y}(k \mid k-1) = \delta\mathbf{A}(k)\mathbf{s}(k) + \mathbf{n}(k). \tag{3.19}$$

The array residual can be written as a function of change in the angle and the distance between array and the device such as

$$\boldsymbol{\delta y}(k) = \mathbf{B}\begin{bmatrix}\boldsymbol{\delta\theta}(k)\\ \boldsymbol{\delta r}(k)\end{bmatrix} + \mathbf{n}(k), \tag{3.20}$$

where $\mathbf{B}$ is an Lx$2M_s$ matrix represented as

$$\mathbf{B} = -j\begin{bmatrix} 1 & \cdots & 1 & 1 & \cdots & 1 \\ \gamma_{21}\dfrac{\partial\tau_{21}}{\partial\theta_1} & \cdots & \gamma_{2m}\dfrac{\partial\tau_{2M_s}}{\partial\theta_{M_s}} & \gamma_{21}\dfrac{\partial\tau_{21}}{\partial r_1} & \cdots & \gamma_{2M_s}\dfrac{\partial\tau_{2M_s}}{\partial r_{M_s}} \\ \vdots & \vdots & \vdots & \vdots & \vdots & \vdots \\ \gamma_{(L-1)1}\dfrac{\partial\tau_{(L-1)1}}{\partial\theta_1} & \cdots & \gamma_{(L-1)M_s}\dfrac{\partial\tau_{(L-1)M_s}}{\partial\theta_{M_s}} & \gamma_{(L-1)1}\dfrac{\partial\tau_{(L-1)1}}{\partial r_1} & \cdots & \gamma_{(L-1)M_s}\dfrac{\partial\tau_{(L-1)M_s}}{\partial r_{M_s}} \end{bmatrix}. \tag{3.21}$$

Then with the least square method, the parameter innovations are calculated as follows

$$\begin{bmatrix}\boldsymbol{\delta\theta}(k)\\ \boldsymbol{\delta r}(k)\end{bmatrix} = (\mathbf{B}^H\mathbf{B} + \mathbf{L_w})^{-1}\mathbf{B}^H\boldsymbol{\delta y}(k), \tag{3.22}$$

where $\mathbf{L_w}$ is the weighting matrix and H represents the conjugate transpose operation .

Step 3, Updating the DOA and distance between the array and the source

The new estimates with the predicted states are calculated as

$$\hat{\theta}_m(k) = \hat{\theta}_m(k \mid k-1) + \delta\theta_m(k), \tag{3.23}$$

$$\hat{r}_m(k) = \hat{r}_m(k \mid k-1) + \delta r_m(k), \tag{3.24}$$

where $\delta\theta_m(k)$ and $\delta r_m(k)$ represent the calculated change in the angle and the distance for the m^{th} source between two successive time samples.

Step 4, Smoothing the estimates with the Extended Kalman Filter

The state estimate and its covariance matrix is updated with the estimated angle and the range innovations such as

$$\mathbf{x}(k \mid k) = \mathbf{x}(k \mid k-1) + \mathbf{G_K}(k)\boldsymbol{\delta\bar{y}}(k), \tag{3.25}$$

where $\boldsymbol{\delta}\bar{\mathbf{y}}(k) = [\mathrm{Re}(\boldsymbol{\delta}\mathbf{y}(k))\ \mathrm{Im}(\boldsymbol{\delta}\mathbf{y}(k))]$ and $\mathbf{G_K}(k)$ is the Kalman gain which is calculated as

$$\mathbf{G_K}(k) = \mathbf{P}(k \mid k-1)\bar{\mathbf{H}}^T(k)\left[\bar{\mathbf{H}}(k)\mathbf{P}(k \mid k-1)\bar{\mathbf{H}}^T(k) + \sigma_n^2\mathbf{I}\right]^{-1}, \tag{3.26}$$

$\mathbf{I}$ is the identity matrix and σ_n^2 is the variance of the noise present in the environment. The covariance matrix of $\mathbf{x}(k \mid k)$ is updated as

$$\mathbf{P}(k \mid k) = \left[\mathbf{I} - \mathbf{G_K}(k)\bar{\mathbf{H}}(k)\right]\mathbf{P}(k \mid k-1). \tag{3.27}$$

4. EXPERIMENTAL SETUP

Two walkie-talkies were used for the experiment. The -40 dBm continuous stimulating signal with 467.5625 MHz frequency was generated with an Agilent MXG-N5182A signal generator. The radio frequency (RF) stimulating signal kept the walkie-talkies on [3]. The 8-element antenna arrays contain broadband, omnidirectional lightweight, wearable antennas with an operating bandwidth in the range of 225–2500 MHz. In order to reduce the noise effects and to amplify the weak emitted signals from the targets, the antenna elements are connected to the 40 dB low noise amplifiers. The antennas were also connected to the 4-channel Agilent MSO6104A and Agilent MSO7104B oscilloscopes for data association and the oscilloscopes were connected to the PC for data storage with a LabVIEW interface. The hardware setup for the experiment is shown in Figure 4.1.

Figure 4.1. Hardware setup.

The signal frequency obtained from the walkie-talkie was 445.862 MHz. The Fresnel region for an eight-element antenna array is calculated as $1.8\ \text{m} < r_k < 17.8\ \text{m}$. The passive devices move at different speeds and initial position estimates for the extended Kalman filter are obtained by using Smooth 2D MUSIC [11]. Furthermore, to increase the tracking accuracy, the measurements are taken with 3 antenna arrays which are placed in different positions of the experimental area. A total of 200,000 data points are collected each time. Instead of array covariance matrix, the array output was used in the extended Kalman filter to predict the trajectories of the unintended emitting moving sources

5. RESULTS AND DISCUSSION

Performance evaluation of the proposed and Park's scheme [17] is carried out and compared with the proposed method in this section to verify the analytical results given in the previous section. Experimental results of tracking RC devices with different speeds are provided. Also, the performance evaluation of the proposed method is given with 3 antenna arrays instead of a single array.

5.1 CASE I- SINGLE ANTENNA ARRAY

In this subsection, the tracking performance of the proposed method for a single maneuvering device is given for different speeds. In theory, the time period between adjacent samples can be increased or decreased according to the optimal computational cost. If the time period is small, better tracking results can be achieved. However, in practice, increasing or decreasing the time period between adjacent samples may not be easy because it is also related with the number of data points collected at each sample. If we keep the time period small, there will be more samples collected in the experiment, however, the number of data points will decrease which will degrade the resolution. If the time period kept large, the data points collected at each sample will increase but this time the number of samples measured in the experiment will decrease which will weaken the tracking performance.

In this experiment, the number of data points collected at each sample was 200,000. So after every 200,000 data points, the hardware setup starts storing the next sample. Since the number of data points and the time period is fixed, the number of samples measured in the experiment depends upon the velocity of the moving target. If the device moves with a slower velocity, more samples are collected and since the

extended Kalman filter is updated often with more number of samples, a higher tracking accuracy is achieved as depicted in Figure 5.1. The 40 m path is completed in 2 min, 4 min and 6 min therefore with a speed of 0.33 m/s, 0.16 m/s and 0.11 m/s. The root mean square (RMS) error for different speeds is given in Table 5.1. As can be seen from the table and the figure, as the number of samples increase, the tracking error will decrease.

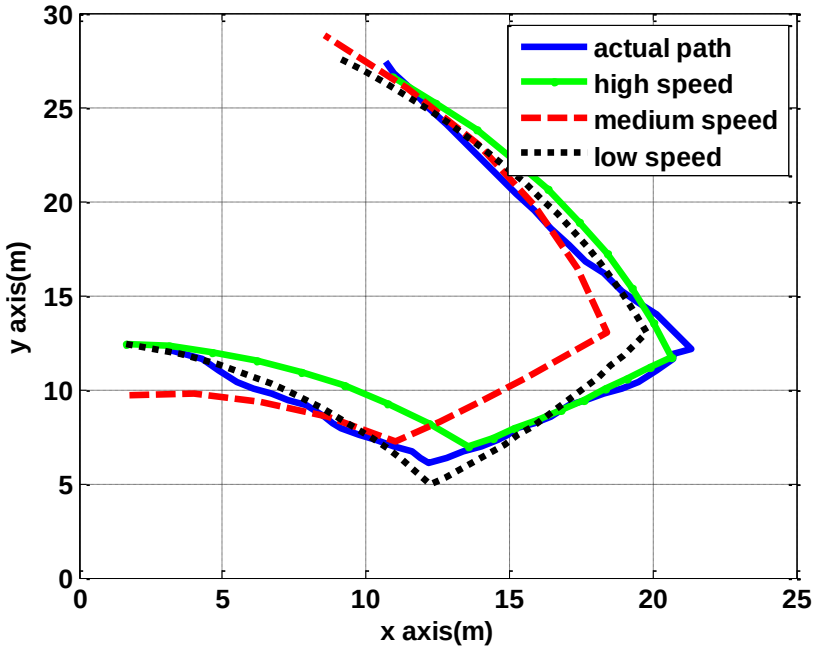

Figure 5.1. Trajectories of the device for different speeds.

Table 5.1. Tracking performance of a single device for different speeds.

	RMS Error (m)
High Speed	2.08
Medium Speed	1.32
Low Speed	1.17

5.2 CASE II-MULTIPLE ANTENNA ARRAYS

In this subsection in order to increase the accuracy of the tracking, three antenna arrays are placed at different positions in the experiment area. Mean of the results provided from three antenna arrays was considered as the location estimations for the moving target. As depicted in Figure 5.2, tracking accuracy is increased when three antenna arrays were employed instead of one. Also the mean error for the tracking is provided in Table 5.2.

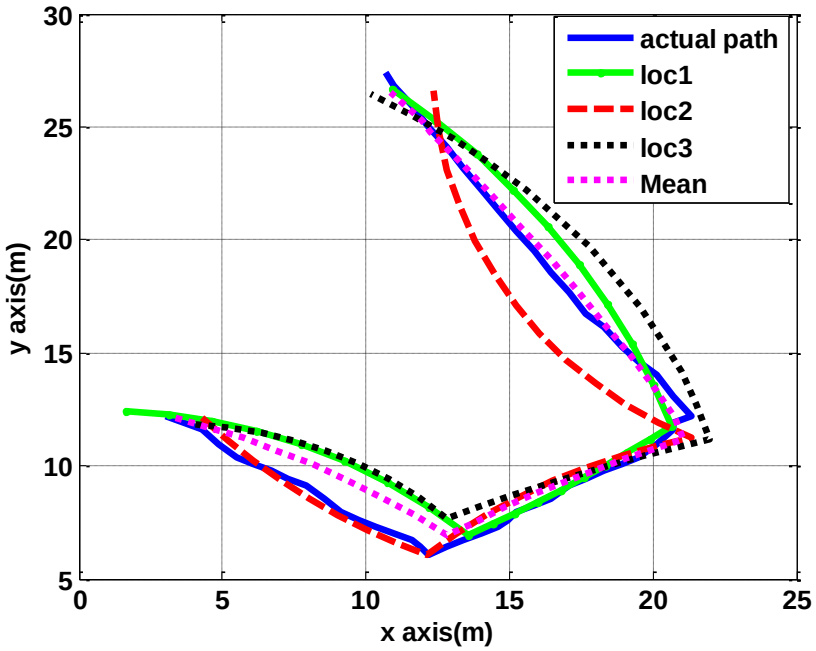

Figure 5.2. Trajectories of the device for different locations of ULA.

Table 5.2: Tracking performance of single and multiple ULAs.

	RMS Error (m)
Single array	1.17
Mean of 3 array	0.94

5.3 CASE III- COMPARISON WITH PARK'S METHOD

In this part, the proposed technique is compared with Park's method [17] where the predicted angles are used for the angle estimation with Kalman filter. However, in this method, the measurement model is assumed to be linear. On the other hand, as seen in (2.5), the measured array output is a nonlinear function of the DOA and the distance between array and the source. The proposed method uses a nonlinear measurement model and finds the first order derivative in order to linearize the measurement model. Furthermore, the proposed method uses the antenna array output directly instead of the array covariance matrix and this makes the proposed method more practical. The tracking performance of the proposed and Park's method is given in Figure 5.3. The calculated RMS errors are given in Table 5.3.

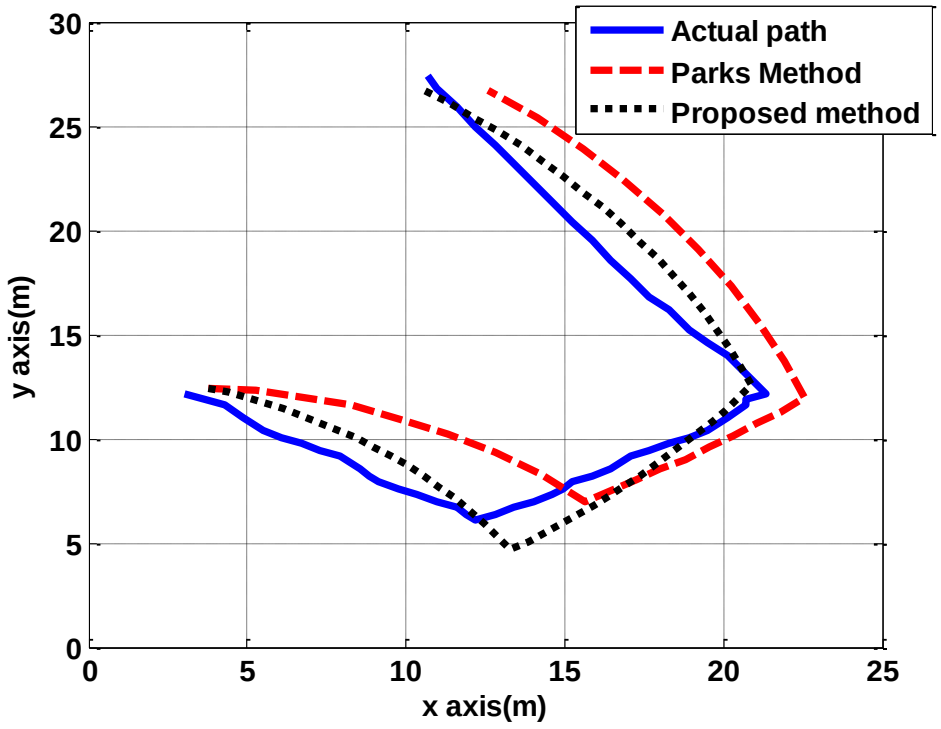

Figure 5.3. Trajectory estimations with the proposed and the Park's method.

Table 5.3. Tracking performance of proposed scheme and Park's method

	RMS Error (m)
Proposed Method	1.17
Park's Method	2.5

As can be seen from the figure and the table, the proposed method outperforms the Park's method when tracking a single maneuvering device with unintended emissions.

5.4 CASE IV- MULTIPLE MANEUVERING TARGETS

In this subsection tracking estimation of multiple maneuvering sources when they are moving with medium speed is given. The same kind of device was used for the experiment; therefore, the Smooth 2D MUSIC was able to separate the two devices if there was a correlation between them and also the multipath fading in the environment. After two devices are detected, the data association problem was solved by the extended Kalman filter. As can be seen from Figure 5.4, when devices approached to the crossover point, the tracking error was increased since it can be difficult to tune the extended Kalman filter especially when there are multiple targets and if they are crossing. Table 5.4 depicts the RMS errors for the unintended emitting RC sources when they exist together.

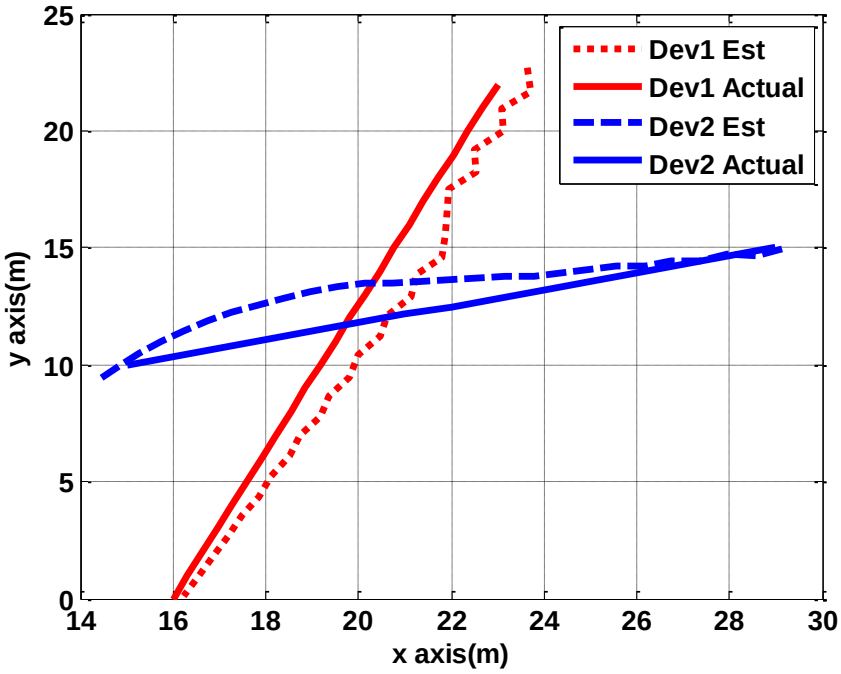

Figure 5.4. Trajectory estimations for multiple crossing targets.

Table 5.4. Tracking performance of proposed method for multiple devices

	RMS Error (m)
Device 1	3.72
Device 2	2.46

6. CONCLUSIONS

This research presents the development and hardware evaluation of a novel tracking algorithm for RC mobile sources in near and far-field regions of the antenna array, even the sources are correlated and multipath fading exist. Beside the DOA information estimated by many tracking algorithms, the distance between the source and the array is also estimated when using the near-field signal model for the unintended emissions. The EKF is preferred since an extra data association algorithm for multiple targets is not needed and it does not require the signal or noise statistics which makes it more appropriate for practical applications such as presented in this paper. Instead of assuming a linear model for the measurement equation, a first order derivative of the nonlinear near-field signal model was used to increase the tracking accuracy. Furthermore, instead of an array covariance matrix, the array output is directly used in the algorithm, which makes it more practical.

The experimental results indicate that the tracking performance increases if the target moves slower, since it provides more samples during a trajectory; therefore, the EFK is updated more in the given path. Besides, if more than one antenna array is used and their mean is considered as tracking result, the increase in the accuracy is observed clearly. Further, the results from Park's method show that the proposed method is more efficient when using a nonlinear measurement model and the array output instead of the covariance matrix.

7. REFERENCES

[1] V. Thotla, M. T. A. Ghasr, M. J. Zawodniok, S. Jagannathan and S. Agarwal, "Detection of Super-Regenerative Receivers Using Hurst Parameter," *IEEE Trans. Instrum. Meas*., vol.62, no.11, pp.3006-3014, Nov. 2013.

[2] V. Thotla, M. T. A. Ghasr, M. Zawodniok, S. Jagannathan and S. Agarwal, "Detection and localization of multiple R/C electronic devices using array detectors," 2012 IEEE International Instrumentation and Measurement Technology Conference (I2MTC), pp.1687-1691, 13-16 May 2012.

[3] Sarah Seguin, "Detection of low cost radio frequency receivers based on their unintended electromagnetic emissions and an active stimulation," Ph.D dissertation, Missouri S&T, Rolla, MO 2009.

[4] R. Schmidt, "Multiple emitter location and signal parameter estimation," IEEE Trans. on Ant. and Prop., vol.34, no.3, pp. 276- 280, March 1986.

[5] R. Roy, A. Paulraj and T. Kailath, "Direction-of-arrival estimation by subspace rotation methods – ESPRIT," IEEE International Conference on Acoustics, Speech, and Signal Proc., vol.11, pp.2495-2498, Apr 1986.

[6] M. Viberg and B. Ottersten, "Sensor array processing based on subspace fitting," IEEE Trans. on Signal Proc., vol.39, no.5, pp.1110-1121, May 1991.

[7] W. Zhi and M. Y. W. Chia, "Near-Field Source Localization via Symmetric Subarrays," IEEE Signal Processing Letters, vol.14, no.6, pp.409-412, June 2007.

[8] N. Yuen and B. Friedlander, "Performance analysis of higher order ESPRIT for localization of near-field sources," IEEE Transactions on Signal Processing, vol.46, no.3, pp.709-719, Mar 1998.

[9] R. N. Challa and S. Shamsunder, "High-order subspace-based algorithms for passive localization of near-field sources," Conference Record of the Twenty-Ninth Asilomar Conference on Signals, Systems and Computers, vol.2, pp.777-781, Oct. 30 -Nov. 1 1995.

[10] E. Cekli and H. A. Cirpan, "Unconditional maximum likelihood approach for near-field source localization," 8th IEEE International Conference on Electronics, Circuits and Systems, vol.2, pp.753-756, Sep 2001.

[11] N. Guzey, H. Xu and S. Jagannathan, "Localization of Near-Field Radio Controlled Unintended Emitting Sources in the Presence of Multipath Fading," IEEE Transactions on Instrumentation and Measurement, vol.63, no.11, pp.2696,2703, Nov. 2014.

[12] G. C. Carter, “Coherence and time delay estimation,” Proceedings of the IEEE, vol.75, no.2, pp.236- 255, Feb. 1987.

[13] J. F. Yang and M. Kaveh, “Adaptive eigen subspace algorithms for direction or frequency estimation and tracking,” IEEE Transactions on Acoustics, Speech and Signal Processing, vol.36, no.2, pp.241-251, Feb 1988.

[14] C. K. Sword, M. Simaan and E. W. Kamen, “Multiple target angle tracking using sensor array outputs,” IEEE Transactions on Aerospace and Electronic Systems , vol.26, no.2, pp.367- 373, Mar 1990.

[15] C. R. Rao, C. R. Sastry and B. Zhou, “Tracking the direction of arrival of multiple moving targets,” IEEE Transactions on Signal Processing, vol.42, no.5, pp.1133-1144, May 1994.

[16] J. Sanchez-Araujo and S. Marcos, “An efficient PASTd-algorithm implementation for multiple direction of arrival tracking,” IEEE Transactions on Signal Processing, vol.47, no.8, pp.2321-2324, Aug 1999.

[17] S. B. Park, C. S. Ryu and K. K. Lee, “Multiple target angle tracking algorithm using predicted angles,” IEEE Transactions on Aerospace and Electronic Systems, vol.30, no.2, pp.643- 648, Apr 1994.

[18] C. S. Ryu, S. H. Lee and K. K. Lee, “Multiple target angle tracking algorithm using angular innovations extracted from signal subspace,” IEEE Electronics Letters , vol.35, no.18, pp.1520-1522, 2 Sep 1999.

[19] D. Kong and J. Chun, “A fast DOA tracking algorithm based on the extended Kalman filter,” Proceedings of the IEEE National Aerospace and Electronics Conference, NAECON, pp.235-238, 2000.

[20] S. H. Chang, S. Y. Hou, S. C. Chang and H. S. Hung, “Novel algorithms for tracking multiple targets,” Journal of Marine Science and Technology, vol. 18, No. 2, pp. 259-267, March 2010.

[21] R.E. Zarnich, K.L. Bell and H.L. Van Trees, “A unified method for measurement and tracking of contacts from an array of sensors,” IEEE Transactions on Signal Processing, vol.49, no.12, pp.2950-2961, Dec 2001.

[22] J. F. Gu; S. C Chan, W. P. Zhu and M. N. S Swamy, “Joint DOA Estimation and Source Signal Tracking With Kalman Filtering and Regularized QRD RLS Algorithm,” IEEE Transactions on Circuits and Systems II: Express Briefs, vol.60, no.1, pp.46-50, Jan. 2013.

IV. ANALYSIS OF LOCALIZATION AND TRACKING METHODS FOR UNINTENDED EMITTING SOURCES

ABSTRACT

This paper presents an analysis of localization and tracking of unintended emissions from electronic devices using computer simulations. The available localization and tracking methods assume that the device is in the far-field region of the array. However, the received power of unintended emissions is very low and, therefore, requires near-field techniques. In the near-field, the performance of far-field schemes degrades since they ignore the effect of range on phase characteristics. Computer simulation results for localization and tracking methods developed by the authors are summarized to analyze the effects of near and far-field regions.

1. INTRODUCTION

Localization of electronic devices through their unintended emissions has many security and commercial applications. However, since the devices are not active and the emissions are generated with a stimulation signal, the signal power of the received emissions is very low [1]–[3], which makes the localization more challenging. In the literature, localization results are presented for active devices where they have a considerable output power and signal-to-noise ratio (SNR) [4]–[7] and also provide far-field localization [4]–[7]. However, the nature of unintended emissions requires near-field localization techniques. Most near-field localization techniques depend upon the higher order statistics of the received signal [8]–[10], which is not very convenient for practical applications.

To locate multiple correlated unintended emitting sources, an efficient method was proposed in [11]. The correlation problem among the sources was solved with spatial smoothing. In addition, localization methods [4]–[10] assume that noise in the environment has white Gaussian characteristics, but this may not be true—especially for practical applications. In [12], this assumption is relaxed using two well separated antenna arrays. Locations of devices are estimated with cross-covariance matrix of the separated arrays. Furthermore, for non-stationary sources, an extended Kalman filter-based tracking algorithm has been developed [13].

Most of the localization methods [4]–[12] neglect the effect of elevation and consider the azimuth angle as the direction of arrival (DOA). However applications such as an aerial vehicle locating ground-based sources require the estimation of elevation angles. In [14], it is shown that the L-shaped array is more efficient when compared to

other array configurations for 2D angle estimation. Both elevation and azimuth angles are estimated in [15], [16], but the source is assumed to be in the far-field of the array where the effect of distance between the array and the source is not considered.

The received signal power at the antenna array can also be expressed using the free space Green's function [17]. By using this function, phase of the received signal is written in terms of distance between the antenna and the source instead of DOA. With a 3D search, x, y and z coordinates of the device are provided directly without estimating DOA since a small error in DOA causes a significant location error in the far field region of the array. However, a 3D search is more computationally intensive.

In addition to the L-shaped array, a rectangular or circular array can be placed at a certain height for 3D localization by employing Green's function. For example, a rectangular array can be mounted to an unmanned aerial vehicle (UAV) or a UAV can construct an array to localize unintended emissions in an open terrain.

In our previous work [11]–[13], localization and tracking of unintended emitting devices were provided by experimental results. In this paper, analysis of localization and tracking methods is reported by considering different aspects such as the location of sources and number of antennas. This analysis is also utilized to verify the performance of our methods [11]–[13] via computer simulations and to observe whether or not the near-field approximation considered in our previous work is satisfactory.

In this paper, signals were generated similar to those generated in the experimental studies with unintended emissions, and the noise level was kept same as that of [1]. This setup provided opportunities to compare experimental and simulation results. Simulation results are helpful when conducting *'What if?'* analyses.

First, simulation results for 1D and 2D MUSIC are introduced to show the effect of far and near-fields on localization accuracy with and without noise in the environment. Then, tracking of unintended emissions using an extended Kalman filter (EKF) is analyzed with computer simulations. Also, estimation of range, azimuth and elevation angles for a 3D localization using an L-shaped array is provided. Further, simulation results for localization with Green's function for different array and source configurations are depicted.

The contributions of this paper include 1) the study of near and far-field effects on localization and tracking accuracy of unintended emitting sources, 2) computer simulation results for the given methods with different array and source configurations to analyze the effect of different aspects, such as SNR and antenna number.

The rest of the paper is organized as follows. Section 2, summarizes the methods for locating and tracking unintended emissions. Section 3 gives detailed computer simulation results by considering different aspects of localization and tracking. The discussion is finalized with conclusions in Section 4.

2. METHODOLOGY

2.1 LOCALIZATION

Consider M_s narrow-band sources that are emitting unintended radiation in the near-field region of a uniform linear array (ULA), which consists of L omnidirectional antennas. The received signal by the ULA is written as

$$\mathbf{y}(k) = \mathbf{A}\mathbf{s}(k) + \mathbf{n}(k) \quad \mathrm{k} = 1, \ldots K_s, \tag{2.1}$$

where K_s is number of samples, $\mathbf{s}(k) \in \Re^{M_s}$ being the vector of signal powers, and $\mathbf{n}(k) \in \Re^{L}$ is the additive noise vector; $\mathbf{A}(k) \in \Re^{L \times M_s}$ is the steering matrix, which consists of the steering vector of the array for each source. In the near-field of the array, $\mathbf{A}(k)$ is written as

$$\mathbf{A} = [\mathbf{a}(\theta_1, r_1), \mathbf{a}(\theta_2, r_2), \ldots, \mathbf{a}(\theta_{M_s}, r_{M_s})], \tag{2.2}$$

where

$$\mathbf{a}(\theta_m, r_m) = \left[e^{j\tau_1(\theta_m, r_m)}, e^{j\tau_2(\theta_m, r_m)}, \cdots, e^{j\tau_L(\theta_m, r_m)} \right]^T, m = 1, .., M_s. \tag{2.3}$$

θ_m is the DOA of the signal from the m^{th} source and r_m is the distance between the array and the m^{th} source. Steering vector $\mathbf{a}(\theta_m, r_m)$ contains the phase difference between antenna elements, which is approximated by Fresnel approximation [18] using delay elements as

$$\tau_l(\theta_m, r_m) \approx \frac{2\pi d}{\lambda} \left(kd \sin\theta_m - \frac{k^2 d^2 \cos\theta_m}{2r_m} \right), \ \mathrm{l} = 1, \ldots, L. \tag{2.4}$$

where λ is the wavelength of the signal and *d* is the space between the antenna elements. In the far field region, since the distance is higher, the second component can be neglected; then, the phase difference becomes a function of only DOA. Distance between the array and the source and DOA are estimated using 2D MUSIC such as

$$P(\theta, r) = \frac{1}{\mathbf{a}^H(\theta, r)\mathbf{U}_n\mathbf{U}_n^H\mathbf{a}\ (\theta, r)}, \tag{2.5}$$

where $\mathbf{U}_n \in \Re^{L\times(L-Ms)}$ consists of noise eigenvectors. When there are multiple correlated sources, spatial smoothing is needed as described in [11].

For 3D location estimation, an L-shaped array placed along the *x*-*z* plane can be employed. The signal-to-*x*-axis-array DOA consists of coupled elevation and azimuth angles; however, the phase difference between elements along the *z* axis array is independent of the azimuth angle. Elevation angle can be estimated using a *z* axis array and then the azimuth angle by the *x* axis array. This simplifies 3D localization by turning the coupled problem to two independent equations. The delay between the l^{th} antenna in the *z* axis array and the reference point for the m^{th} source can be written as

$$\tau_{l_z m} = \alpha_{zm} + \beta_{zm} = -2\pi\frac{d}{\lambda}\cos(\theta_m) + \pi\frac{d^2}{\lambda r_m}\sin^2(\theta_m), \tag{2.6}$$

and for the array in *x* plane

$$\tau_{l_x m} = \alpha_{xm} + \beta_{xm} = -2\pi\frac{d}{\lambda}\sin(\theta_m)\cos(\varphi_m) + \pi\frac{d^2}{\lambda r_m}(1-\sin^2(\theta_m)\cos^2(\varphi_m)). \tag{2.7}$$

Elevation angle and range is estimated using 2D MUSIC with a delay response as given in (2.5). Estimated values are placed in (2.6); then, with a 1D search with MUSIC, an azimuth angle is approximated.

2.2 LOCALIZATION WITH GREEN'S FUNCTION

Received signal from the m^{th} source by the l^{th} antenna of ULA using Green's function [17] is given as

$$x_l(k) = \sum_{m=1}^{Ms} \frac{\lambda}{(4\pi R_{lm}(k))^2} e^{(-j\frac{2\pi}{\lambda}R_{lm}(k))} + n(k) \qquad k=1,\ldots, K_s, \tag{2.8}$$

where $x_l(k)$ is the received power by the l^{th} antenna, and R_{lm} is the distance between l^{th} antenna and m^{th} source which is defined as

$$R_{lm} = \sqrt{(x_l - x_m)^2 + (y_l - y_m)^2 + (z_l - z_m)^2}, \tag{2.9}$$

where $(\mathrm{x}_l, \mathrm{y}_l, \mathrm{z}_l)$ is the position of the l^{th} antenna and $(\mathrm{x}_m, \mathrm{y}_m, \mathrm{z}_m)$ is the position of the m^{th} source. In matrix form, the received signal by the array is expressed as

$$\mathbf{x}(k) = \mathbf{A}\mathbf{s}(k) + \mathbf{n}(k) \tag{2.10}$$

where $\mathbf{A}(R) = [\mathbf{a}(R_1), \mathbf{a}(R_2), \ldots, \mathbf{a}(R_{M_s})]$ is the steering matrix of the array with

$$\mathbf{a}(R_m) = [e^{(-j\frac{2\pi}{\lambda}R_{1m})}, \ldots, e^{(-j\frac{2\pi}{\lambda}R_{Lm})}] \tag{2.11}$$

being the steering vector for the m^{th} source. If (10) is utilized in the MUSIC scheme, location of the devices can be calculated with a 3D search.

2.3 TRACKING

When the unintended emitting device is non-stationary, a tracking scheme is needed. An EKF with a nonlinear measurement model can be utilized to track the device in near-field. The array output,

$$\mathbf{y}(k) = \mathbf{h}(\mathbf{x}(k), \mathbf{s}(k))\mathbf{x}(k) + \mathbf{v}(k) = \mathbf{A}(\mathbf{x}(k))\mathbf{s}(k) + \mathbf{n}(k), \tag{2.12}$$

where $\mathbf{x}(k)$ consists of the system states, which are DOA and distance between array and the source, and $\mathbf{v}(k)$ is the measurement noise. By linearizing the measurement equation and using the least square technique, the states of the system can be estimated [19].

3. SIMULATION RESULTS AND DISCUSSION

Computer simulation results for the methods mentioned in Section 2 are presented to demonstrate the effect of near and far-field regions on estimation accuracy. Different array and source configurations were simulated for localization and tracking of unintended emissions using given methods.

3.1 1D MUSIC WITH UNIFORM LINEAR ARRAY

When a device is placed in the far-field region of the array, the DOA to each antenna is assumed to be equal. Therefore, the phase difference between the antenna elements is a function only of DOA. With a one dimensional search, the MUSIC spectrum provides DOA information. In antenna design theory, near-field is the part of the radiated field that is below Fraunhofer distance, $df = 2D2\lambda$, from the antenna with longitude or diameter D. Effects of near and far-field regions on the DOA estimation are given in this subsection with computer simulations.

Let us consider an eight-element ULA where the elements are spaced by λ /2, which is 0.3364 m (the wavelength of the unintended emissions), and the total size of the array is 2.35 m. Far-field region for this array is calculated as 16.3 m. The device is placed at the center of the array in x dimension and the effect of distance on the estimation is presented using a conventional MUSIC scheme [5].

- *Without noise*

If there is no noise in the environment (such as can be found in an anechoic chamber), as the device is placed further from the array, we can obtain a more reliable MUSIC spectrum as seen in Figures 3.1-3.6. Furthermore, the received signal from an unintended emitting device with respect to the distance is given in Figures 3.1, 3.3 and 3.5. Without

noise, the 1D MUSIC scheme is efficient if the device is further away, the DOA to each antenna is assumed to be the same. However, in the near field region, signal also depends on distance between the array and the source. Therefore, as can be seen from the figure that for near field detection, the 1D MUSIC spectrum does not provide a sharper peak.

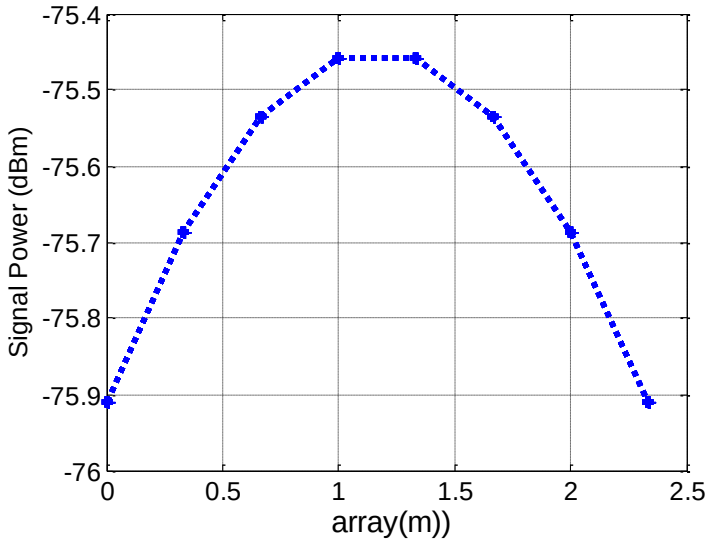

Figure 3.1. Received signal by ULA, y = 5 m

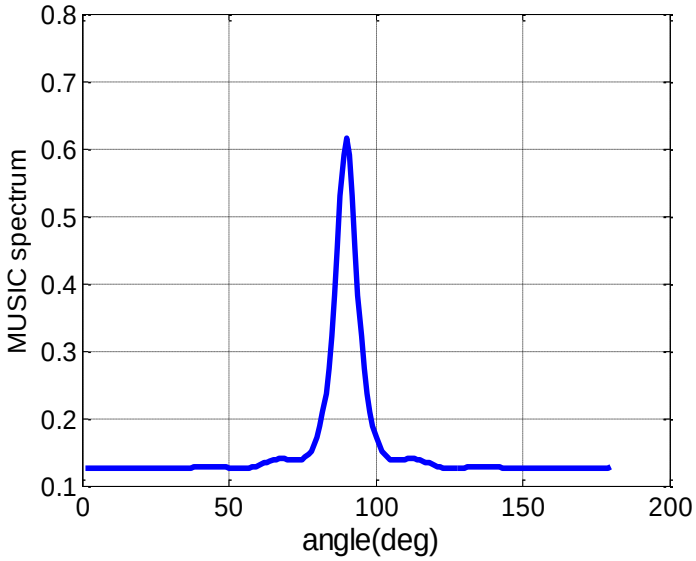

Figure 3.2. MUSIC Spectrum, y = 5 m.

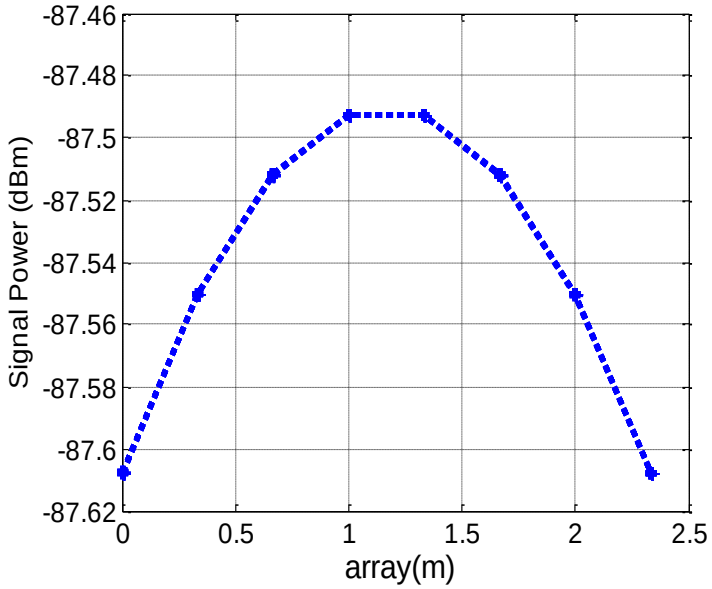

Figure 3.3. Received signal by ULA y = 10 m.

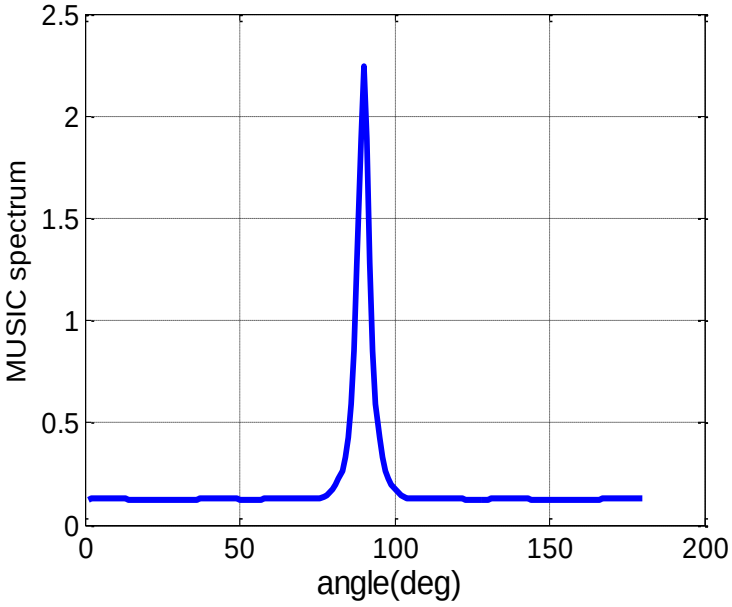

Figure 3.4. MUSIC Spectrum y = 10 m.

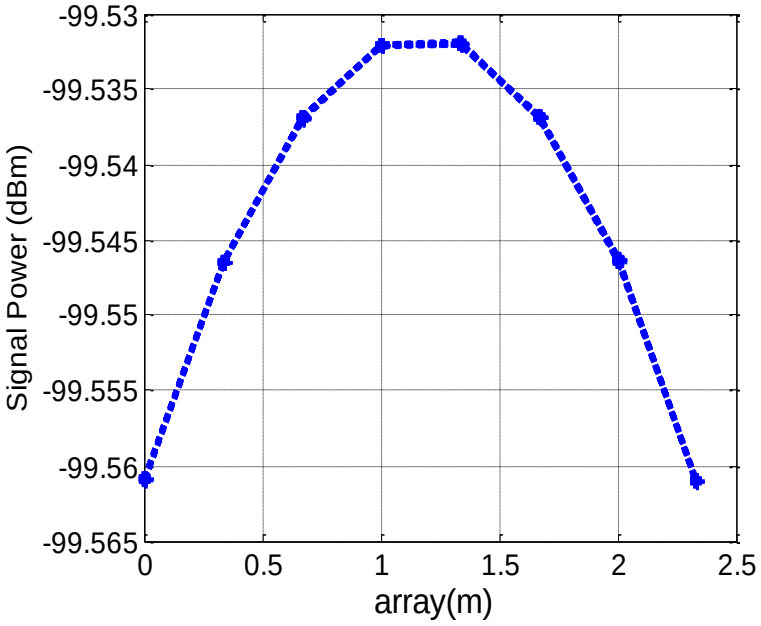

Figure 3.5. Received signal by ULA y = 20 m.

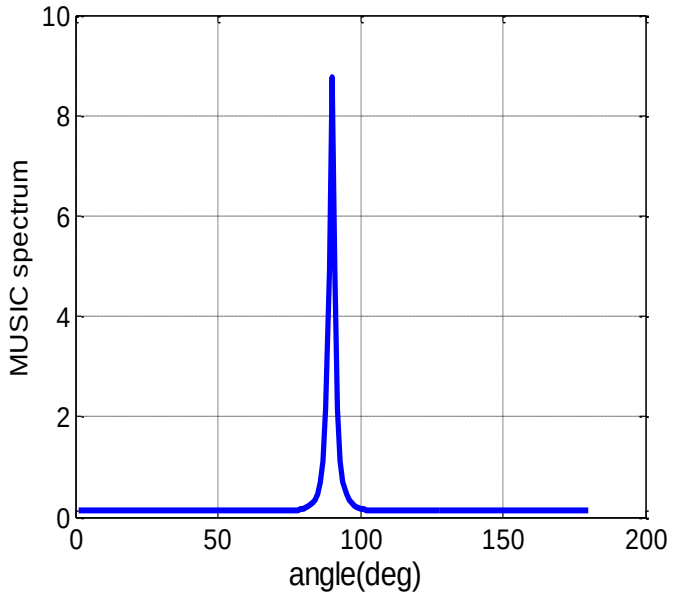

Figure 3.6. MUSIC Spectrum y = 20 m.

In addition, as indicated in Figures 3.1-3.6, signal power depends on the distance between the antenna array and the device. Also, noise level measured by the ULA is -95 dBm [1]; therefore, this will affect the estimation. Since the noise level is -95 dBm, after 15 m, the SNR level will be below zero. Simulation results with additive noise are given next.

- *With -95 dBm noise*

Since the power level of unintended emissions is very low, noise is a very important aspect to be considered. Figures 3.7-3.10 demonstrates that with a certain noise level, it is more appropriate to use near-field DOA techniques to locate unintended emissions.

Figure 3.11 depicts the DOA estimation by using the measured data. Similar to the simulation results, MUSIC spectrum is not very high due to low power emissions. In this experiment, the device was placed to 90^{o} and 15 m.

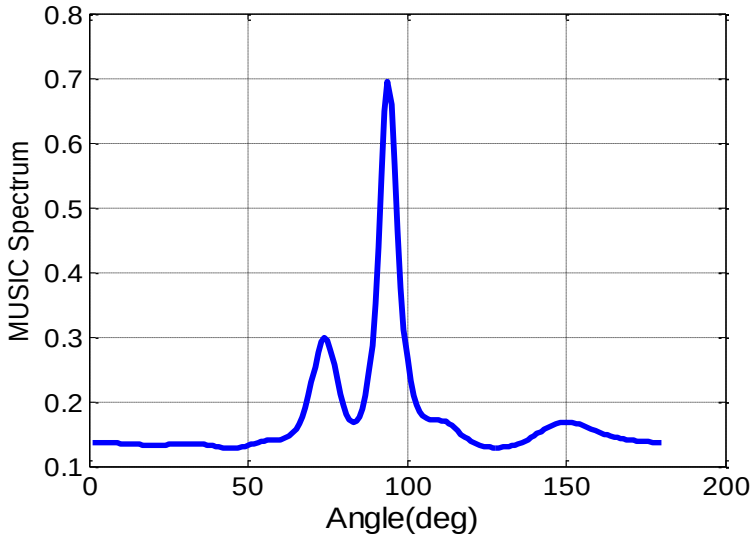

Figure 3.7. MUSIC spectrum, y = 5 m.

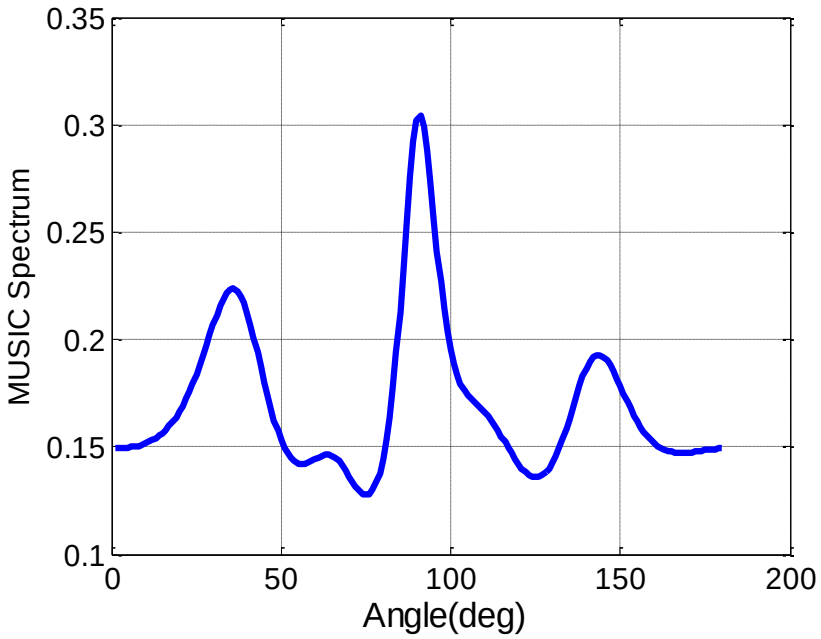

Figure 3.8. MUSIC spectrum, y = 10 m.

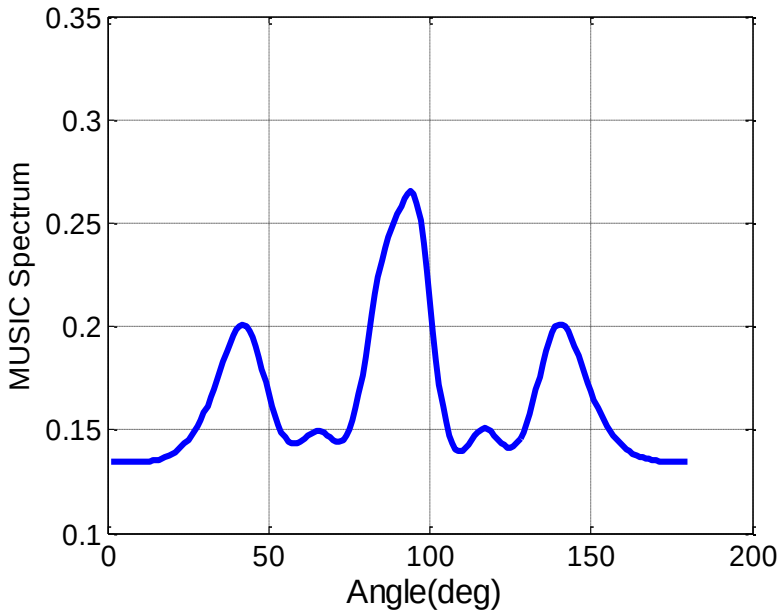

Figure 3.9. MUSIC spectrum, y = 15 m.

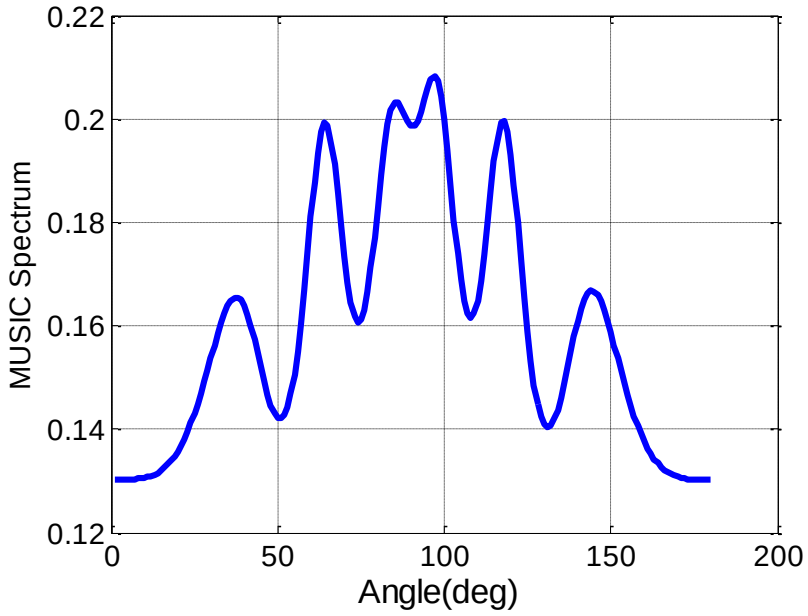

Figure 3.10. MUSIC spectrum, y = 20 m.

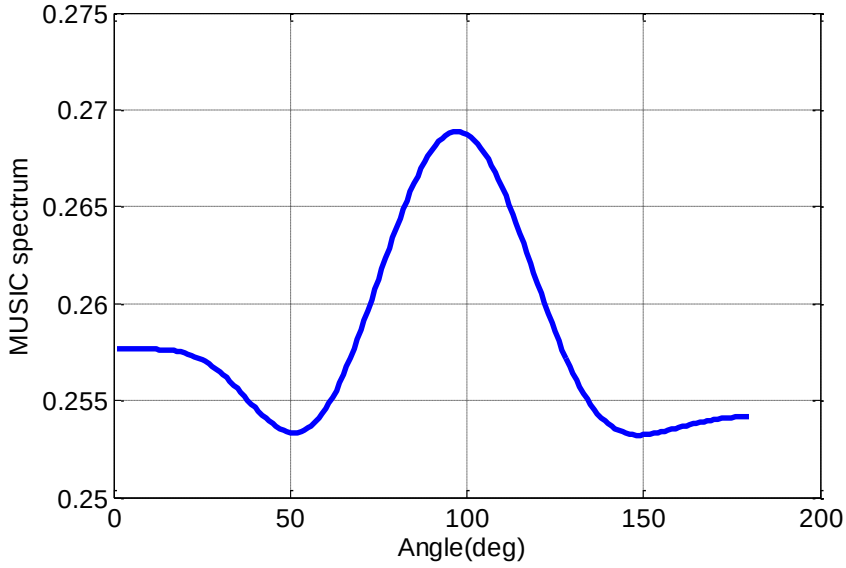

Figure 3.11. DOA estimation with experiment.

3.2 2D MUSIC WITH ULA

In near-field localization techniques, the phase difference between each antenna is a function of DOA and distance between the antenna array and the source. This makes it more challenging than far-field methods, since two parameters should be estimated for localization. Next the effects of near and far field are demonstrated in Figures 3.12-3.21.

- *Without noise*

Consider unintended emissions from a single, stimulated source are impinging on an eight-element ULA. As in1D MUSIC the 2D MUSIC spectrum becomes more reliable as the device is placed further away since the effect of range is reduced by distance. The 2D MUSIC spectrum in 3D plots is given next to show the near and far field effect without noise. Figures show that the peak becomes sharper with distance.

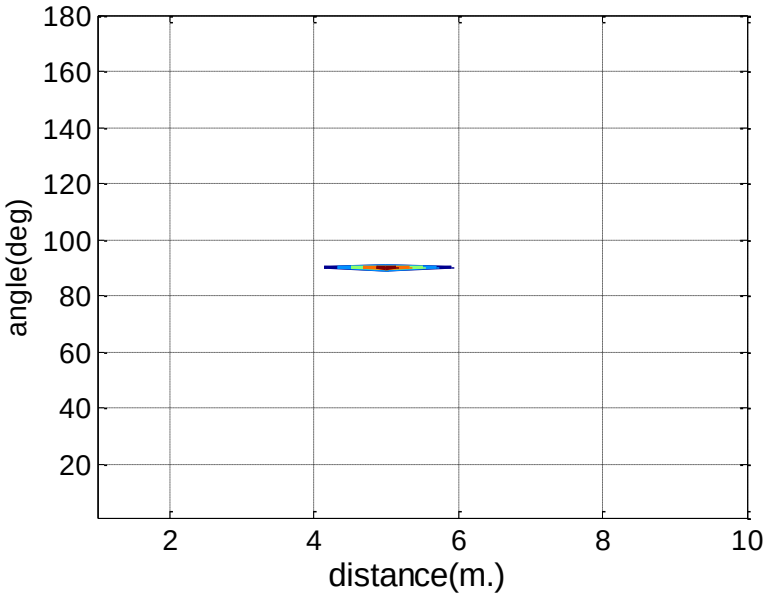

Figure 3.12. Angle and range estimation with 2D MUSIC, y = 5 m

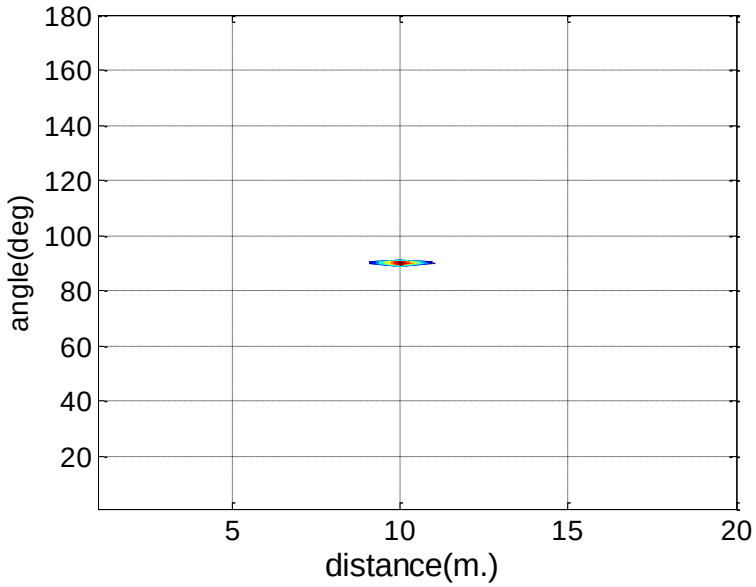

Figure 3.13. Angle and range estimation with 2D MUSIC, y = 10 m

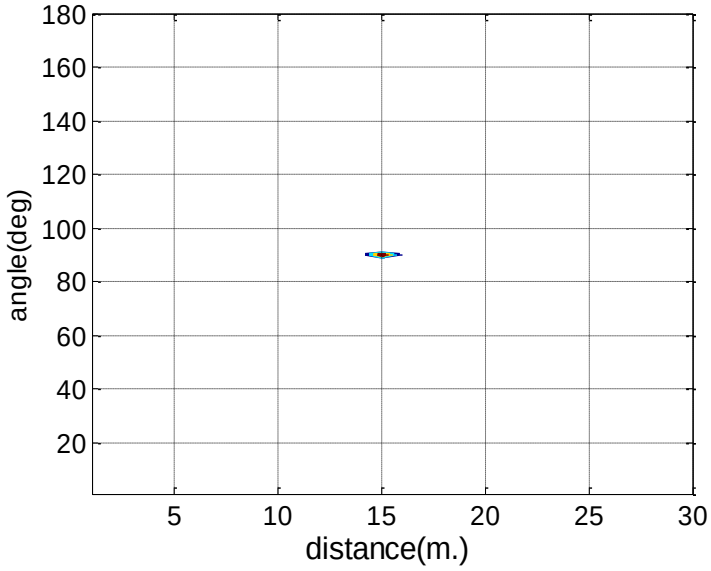

Figure 3.14. Angle and range estimation with 2D MUSIC, y = 15 m

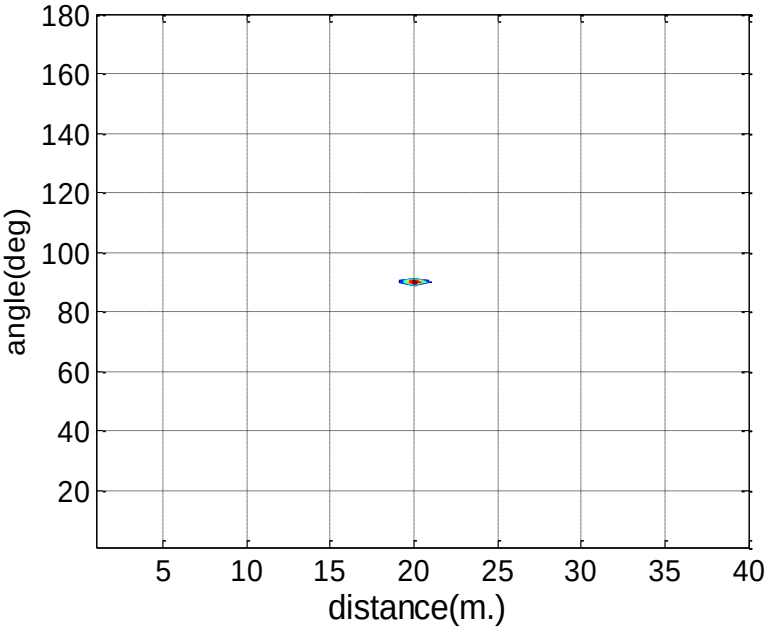

Figure 3.15. Angle and range estimation with 2D MUSIC, y=20m

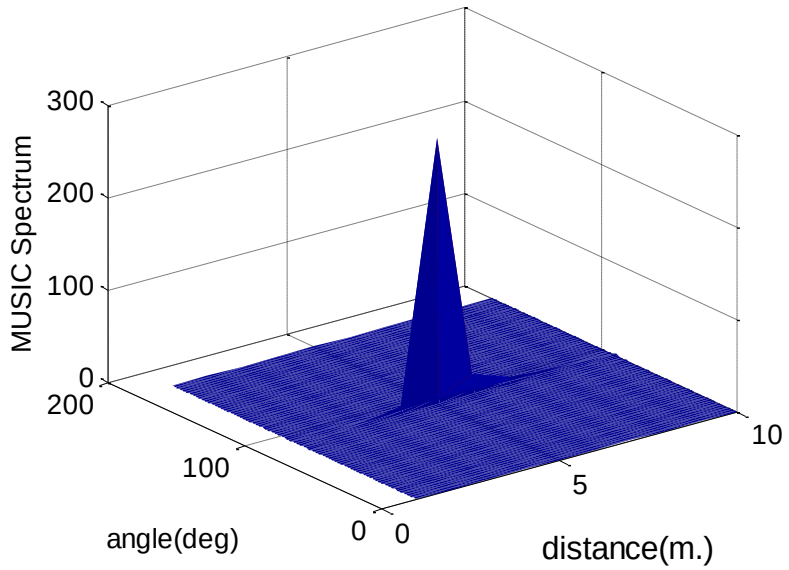

Figure 3.16. 2D MUSIC spectrum, y=5m.

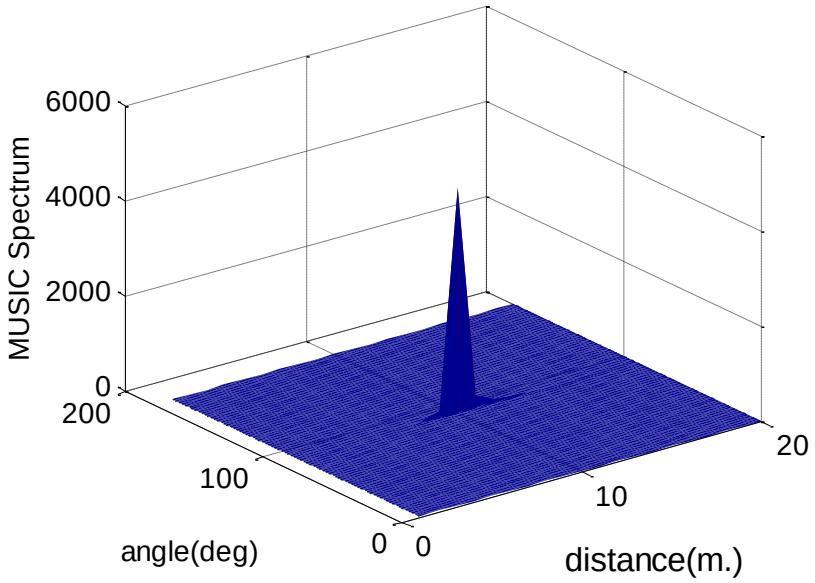

Figure 3.17. 2D MUSIC spectrum, y=10m.

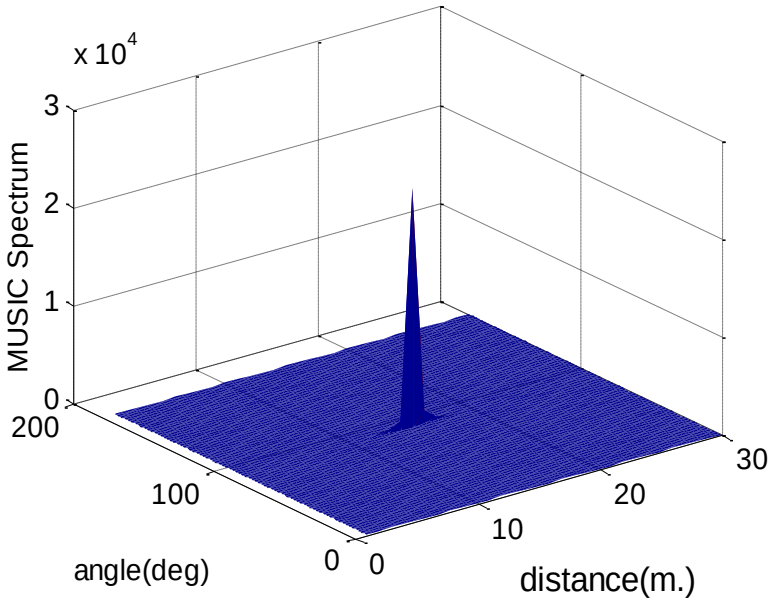

Figure 3.18. 2D MUSIC spectrum, y=15 m.

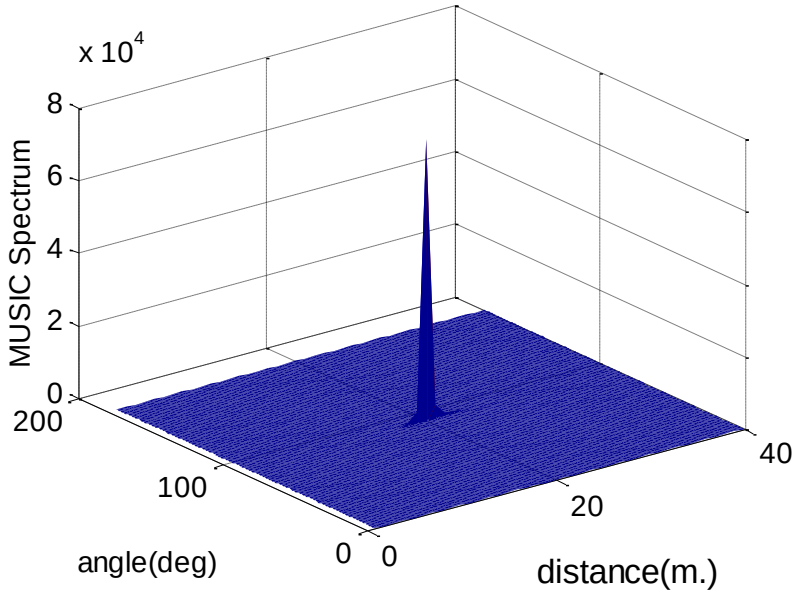

Figure 3.19. 2D MUSIC spectrum, y = 20 m.

- *With -95 dBm noise*

With noise, the location estimation of unintended emissions becomes more challenging. The 2D MUSIC spectrum for different positions shows the effect of noise and signal power with respect to distance in Figures 3.20-3.21. If the device is close to the array, the signal power is high and 2D MUSIC provides a better result compared to the case where the device is placed further away.

Next the experimental results for 2D localization are provided to compare it with the simulations. As can be seen from Figure 3.22, simulations and experiments show similar characteristics. This allows us to analyze different configurations by computer simulation instead of experiments which will save time and energy.

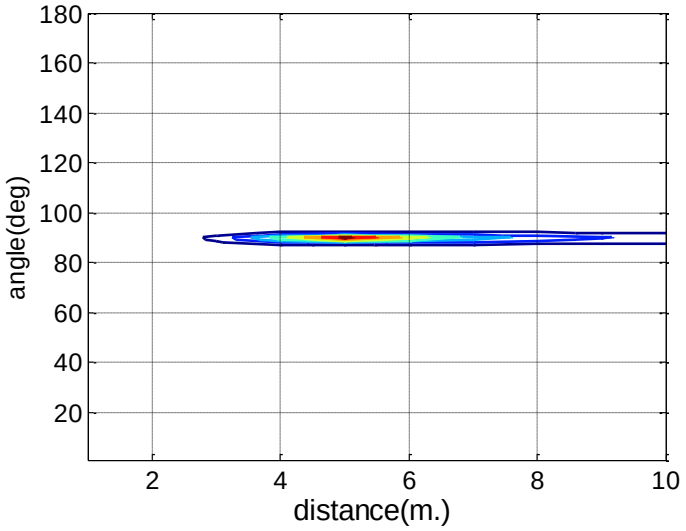

Figure 3.20. Angle and range estimation with 2D MUSIC, y = 5 m.

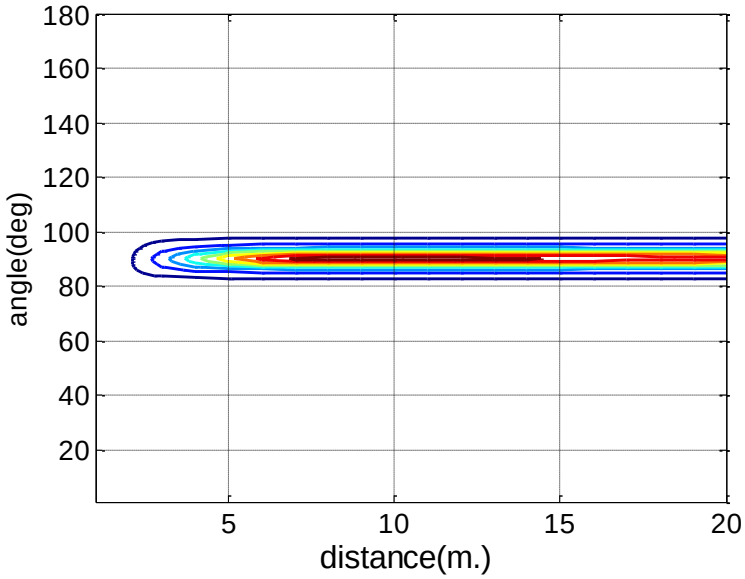

Figure 3.21. Angle and range estimation with 2D MUSIC, y = 10 m.

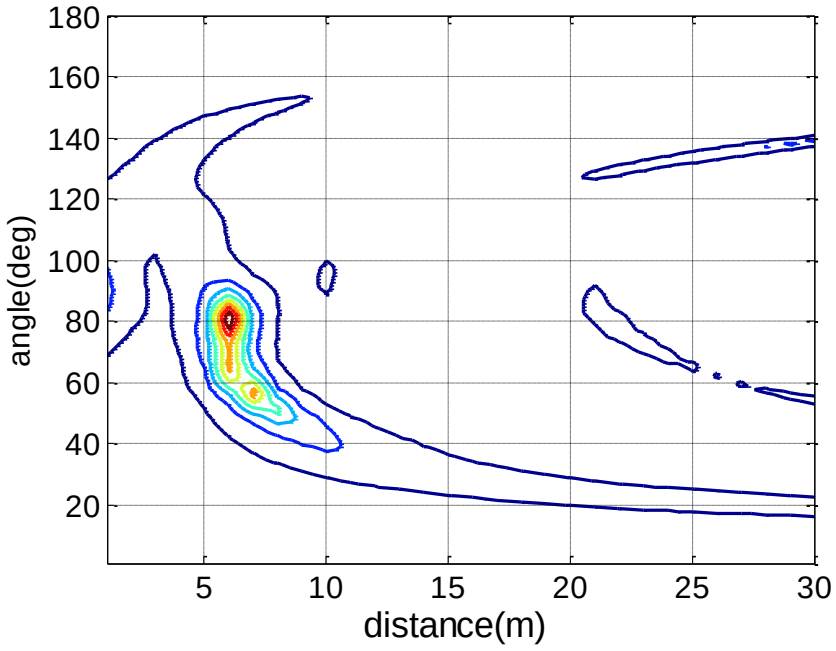

Figure 3.22. Experimental results for 2D localization.

The 3D MUSIC spectrum is also given for better understanding in Figures 3.23-3.24.

Root mean square (RMS) and mean errors with respect to SNR is given next. In these simulations, eight-element ULA, which is placed in *x* plane is employed. The device is placed at the center of the array in *x* dimension and the distance in *y* dimension is kept at 7 m.

As depicted in Figures 3.25-3.26, the estimation errors are very high in low SNR values compared to the higher SNR, which is a drawback of the MUSIC scheme. Another issue to consider for the location accuracy is the antenna number in the array. Resolution increases with the number of antenna elements providing better results as illustrated in Figure 3.27.

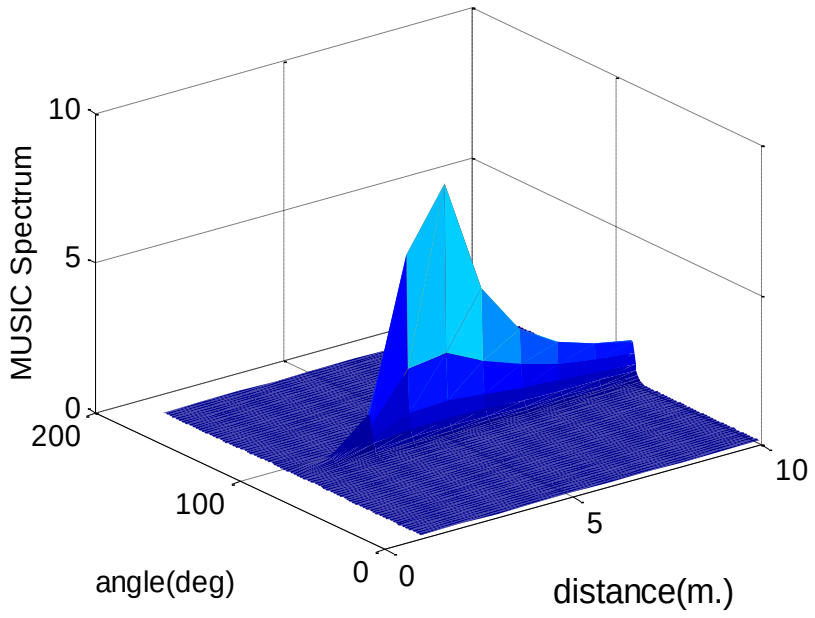

Figure 3.23. 2D MUSIC spectrum, y = 5 m.

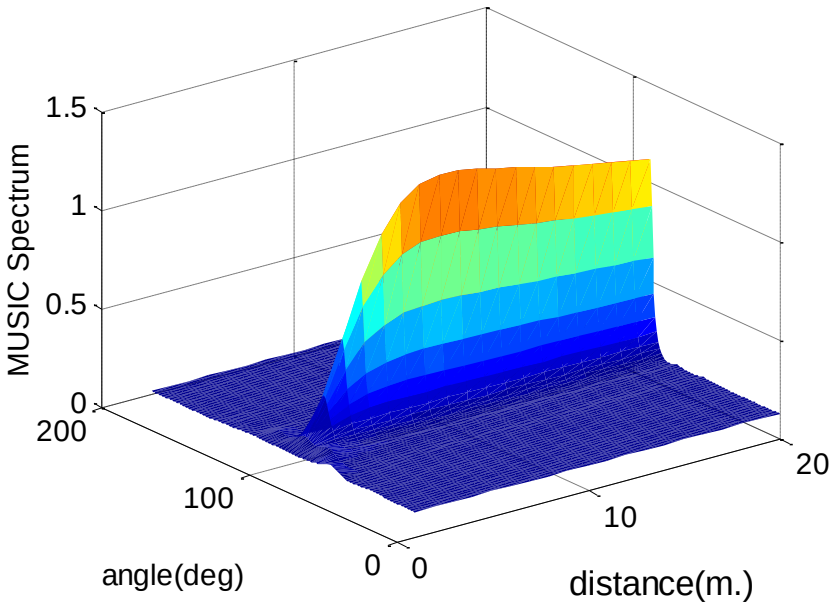

Figure 3.24. 2D MUSIC spectrum, y = 10 m.

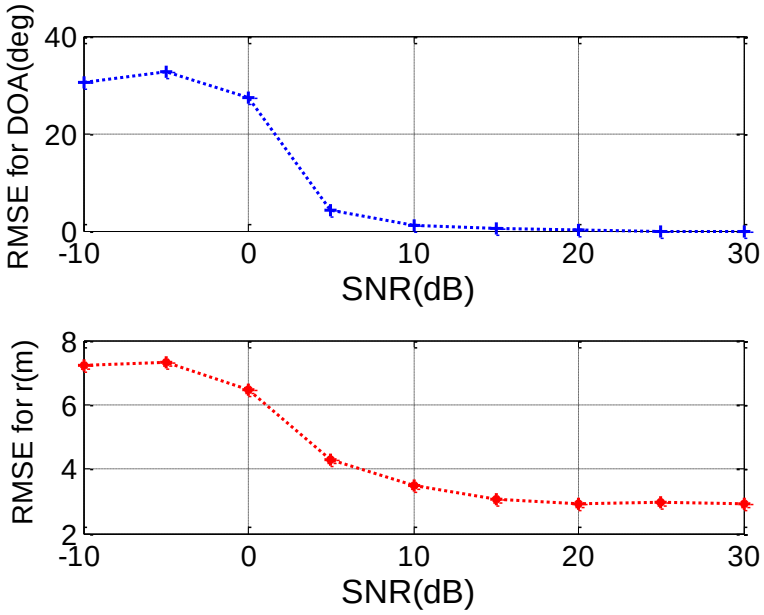

Figure 3.25. RMSE for location estimation with 2D MUSIC.

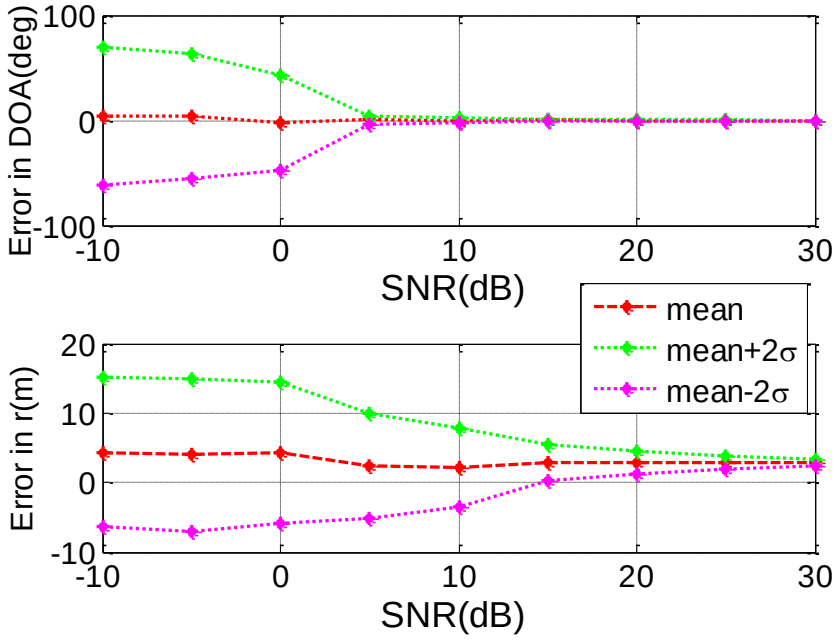

Figure 3.26. Mean error for location estimation with 2D MUSIC.

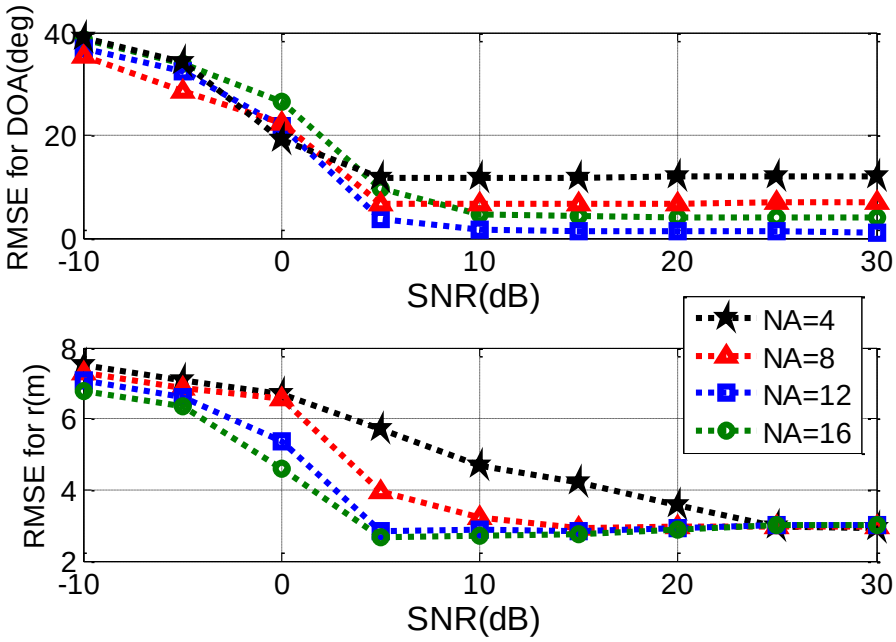

Figure 3.27. RMS estimation errors for different number of antennas.

For a linear array, when the antennas are the same kind, the best reception is obtained when the device is placed in front of the center of the array, and if the device is placed at the end points of the array, the DOA cannot be estimated properly. To show this placement effect on accuracy, the device is placed on two sides and the center. Distance to the array in the *y* direction is changed for each case and location is estimated with 2D MUSIC using a 12-element ULA. Noise level is kept as -95 dBm. The RMS error calculations for these estimations are given in Figure 3.28. Array center is at 2 m. As depicted in the figure, the angle estimation is best when the device is placed just across the center of the array. Figure 3.28 also shows how the error increases by distance due to a drop in received signal power.

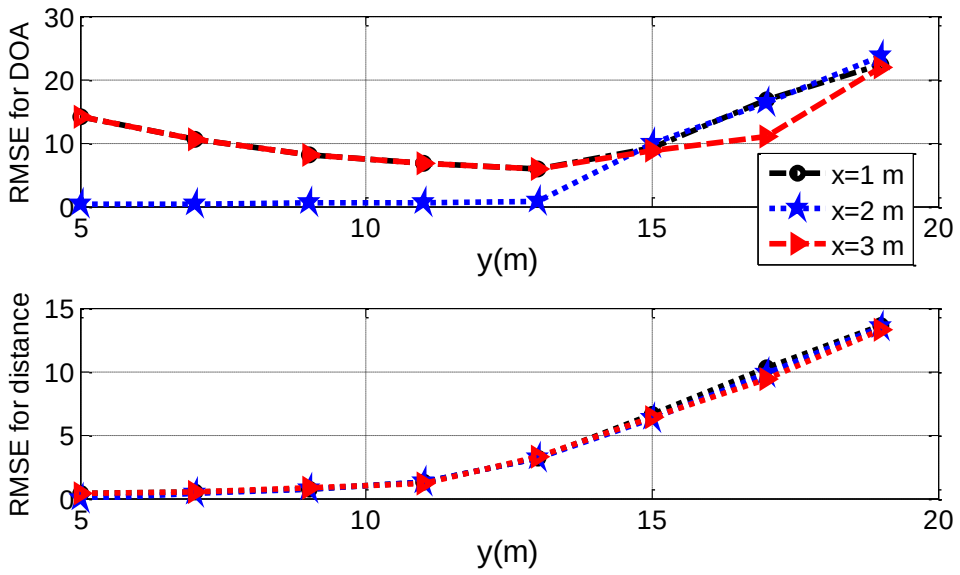

Figure 3.28. Localization error for different positions in x and y directions.

3.3 LOCALIZATION OF MULTIPLE DEVICES WITH ULA

It is also possible that there can be more than one source to be detected and located in the environment. However, the number of antennas in the array is generally limited; therefore, locating multiple devices is more difficult due to resolution as given in Figure 3.29. Moreover, if the sources are correlated, estimation becomes more challenging and a smoothing procedure is needed for source separation [11].

Also if the sources are placed closer, locating them becomes more challenging as depicted in Figure 3.30.

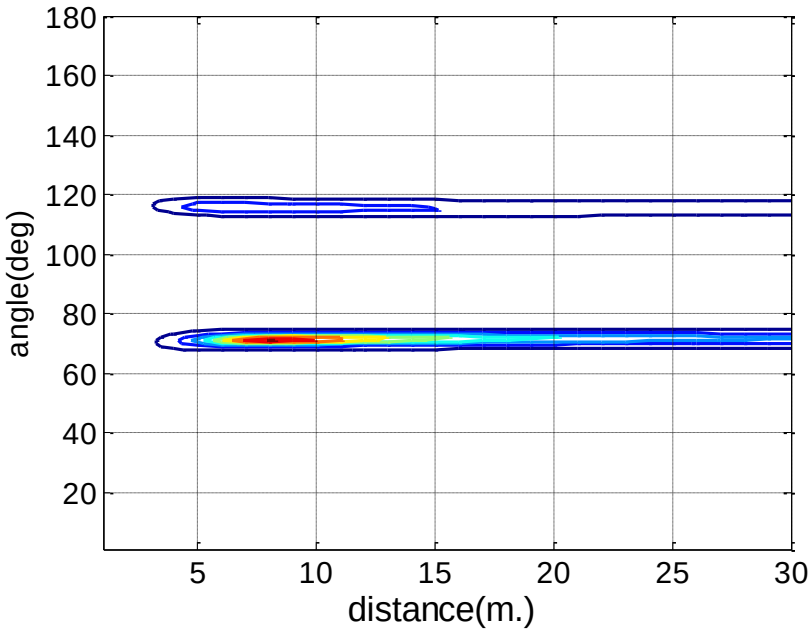

Figure 3.29. Estimation of elevation angles and distances between array and sources.

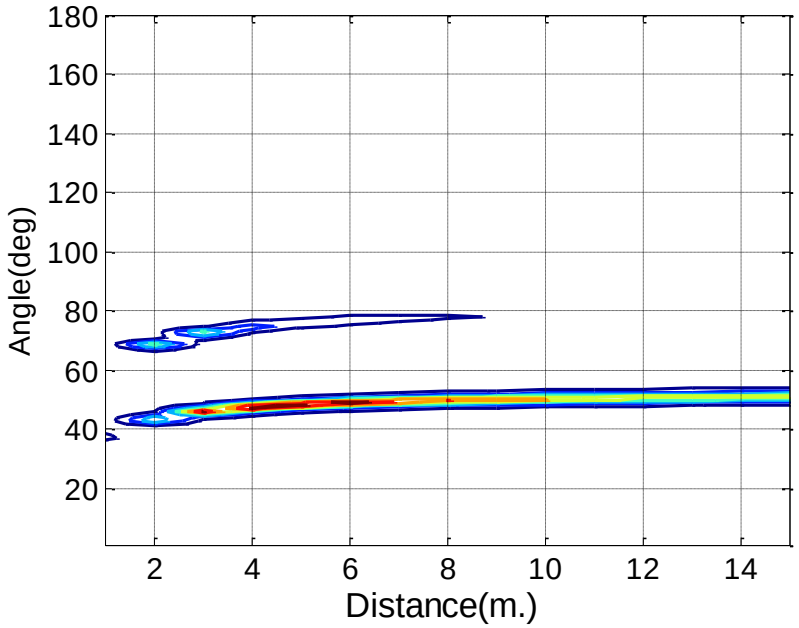

Figure 3.30. Estimation of elevation angles and distances between array and sources when they are closer.

3.4 TRACKING UNINTENDED EMISSIONS

When the unintended emitting device is not stationary, a tracking scheme is needed. In the next simulations, EKF is used with a nonlinear measurement model for more accurate tracking. Figure 3.31 gives the estimated and actual trajectory of a single unintended emitting target.

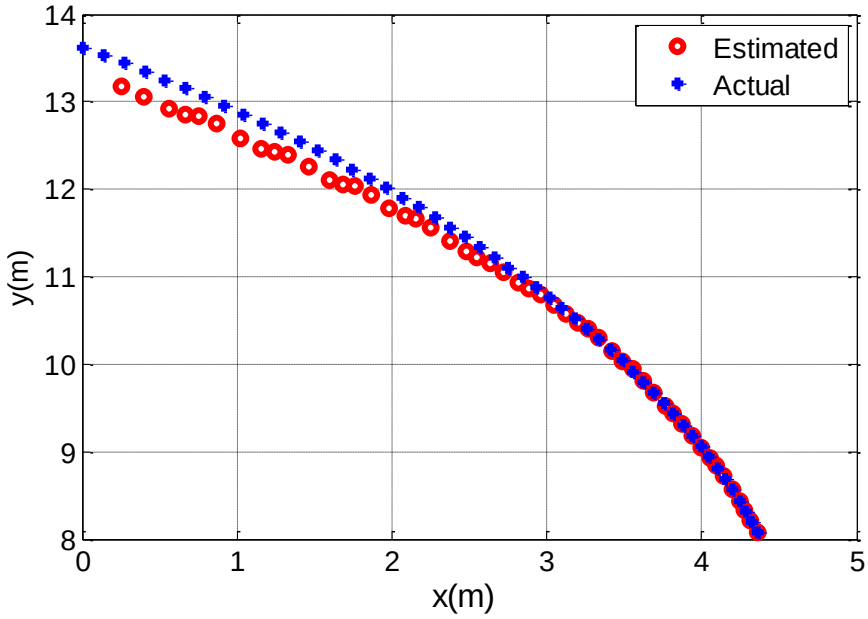

Figure 3.31. Trajectory estimation of single emitting device.

In the case of two unintended emitting devices, error increases around the crossing point as depicted in Figure 3.32. Since the number of elements in the array is limited, the resolution decreases with multiple targets.

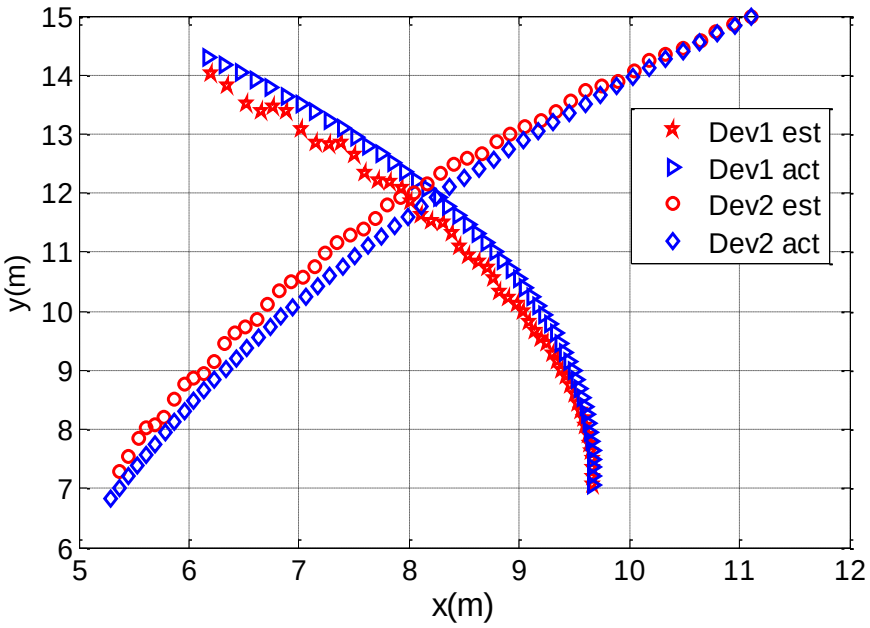

Figure 3.32. Trajectory estimations of two devices.

3.5 LOCALIZATION USING GREEN'S FUNCTION

Location estimations with MUSIC using Green's function for different positions are given in Figures 3.33-3.38. The device is placed at the center of the uniform linear array located in *x* plane and the distance in *y* plane is changed.

- *Without noise*

Results are similar to 2D MUSIC if there is no noise in the environment. The MUSIC scheme using Green's function gives more reliable results if the device is placed further away as depicted in Figures 3.33-3.36.

- *With -95 dBm noise*

Simulation results show similar performance with 2D MUSIC in noisy environment as given in Figures 3.37-3.38. The advantage of using Green's function is that it directly gives the location.

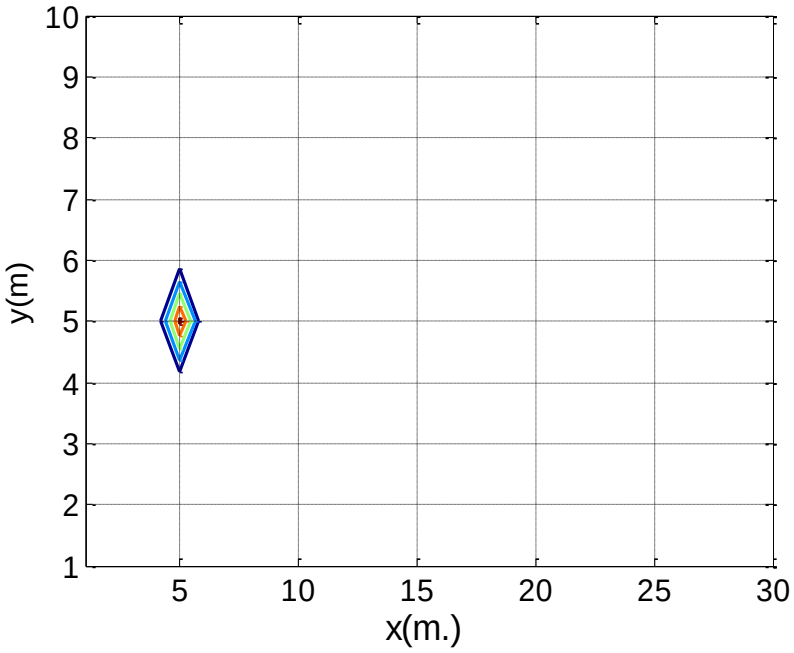

Figure 3.33. Location estimation, y=5m.

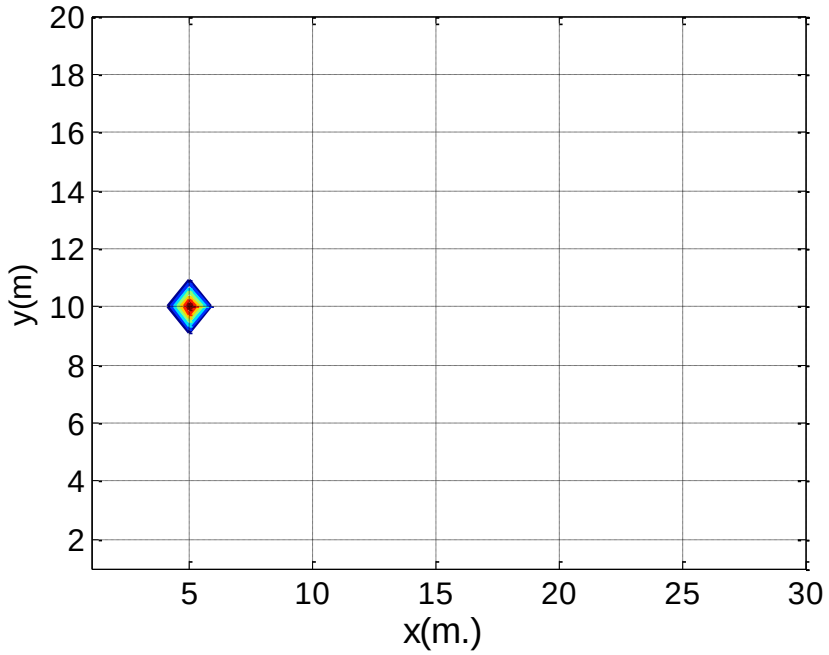

Figure 3.34. Location estimation, y=10m.

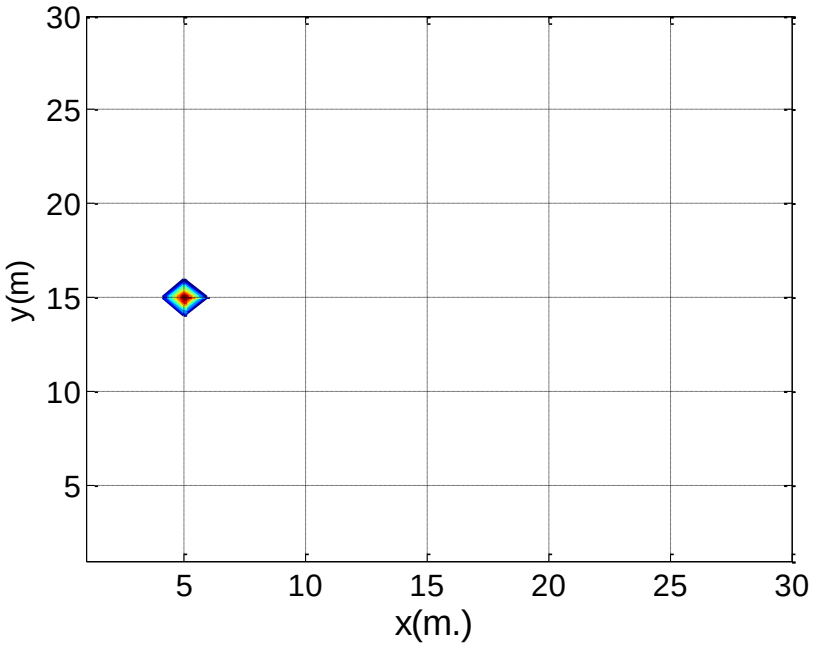

Figure 3.35. Location estimation, y=15m.

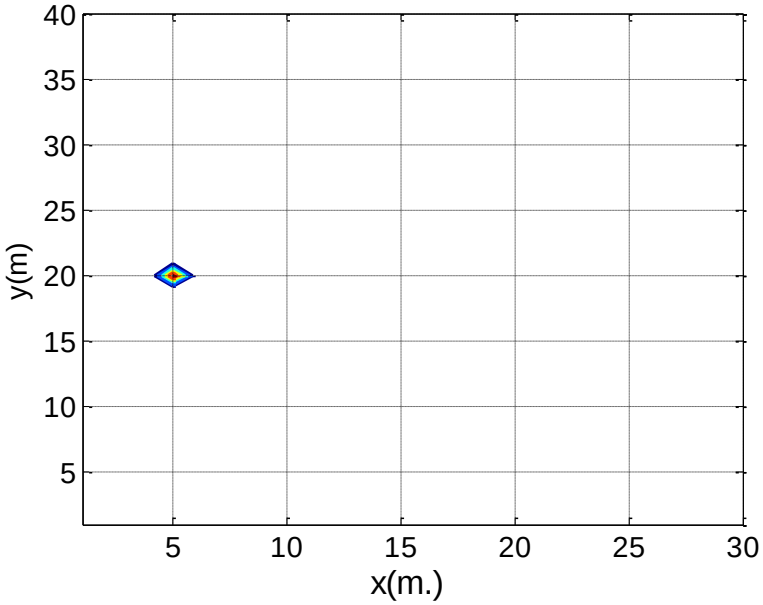

Figure 3.36. Location estimation, y=20m.

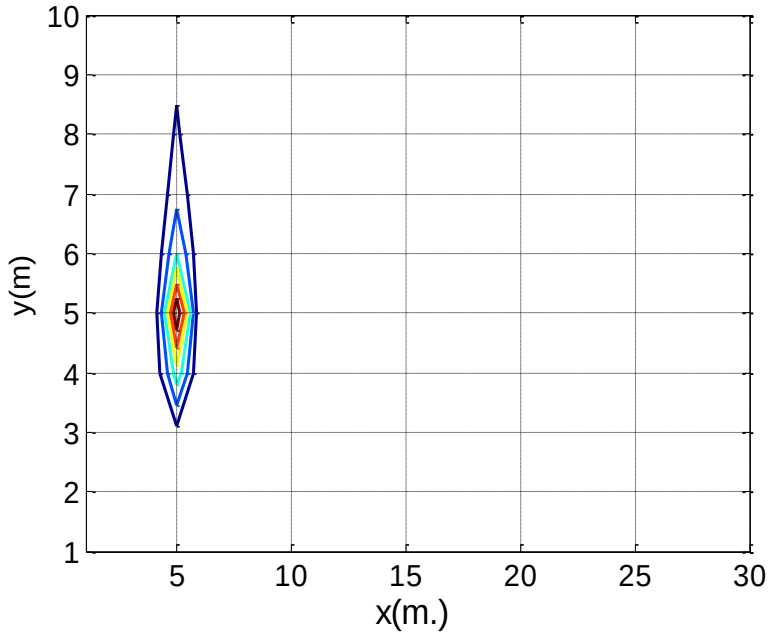

Figure 3.37. Location estimation, y=5m.

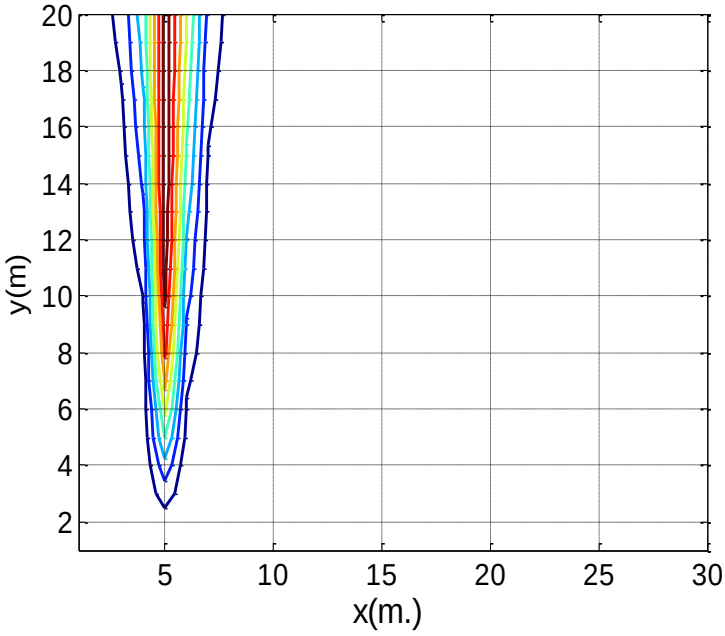

Figure 3.38. Location estimation, y=10m

RMS and mean errors for 2D localization with Green's function with respect to SNR are given in Figures 3.39-3.40. In these simulations, an eight-element ULA placed in the *x* plane was employed. The device placed at the center of the array in *x* dimension and the distance in *y* dimension is kept at 7 m. Since the array is located in *x* plane, the error in *x* dimension reaches zero before error in the *y* dimension. As depicted in the figures, the errors in the estimations are very high in low SNR values compared to the higher SNRs. Simulations show that results are similar to localization with 2D MUSIC.

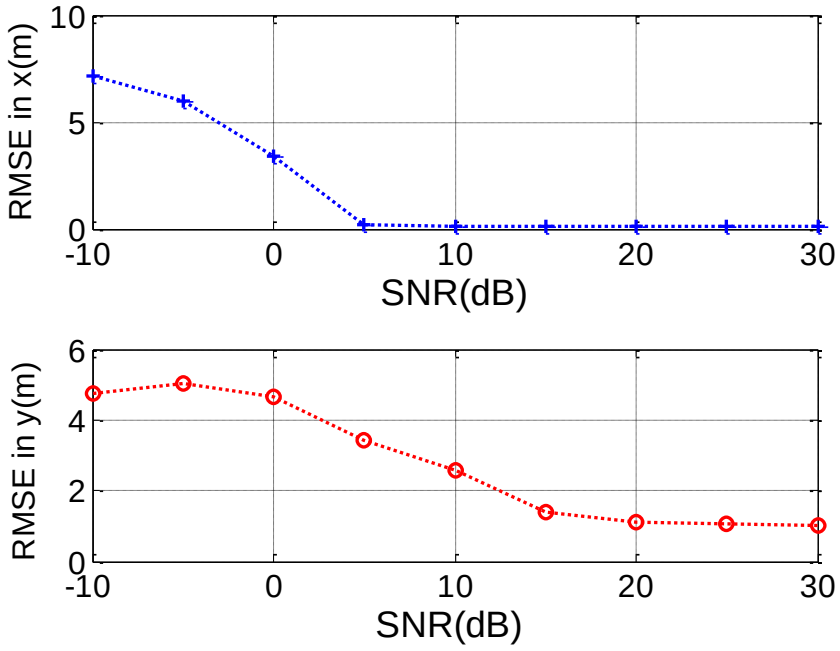

Figure 3.39. RMSE for location estimation with Green's function.

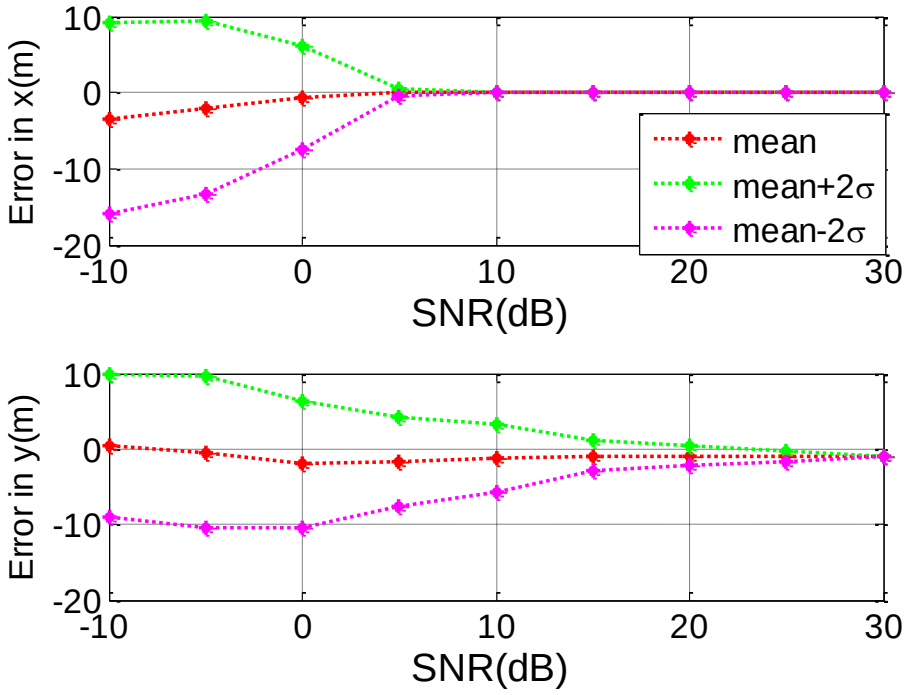

Figure 3.40. Mean error for location estimation with Green's function.

3.6 LOCALIZATION WITH L-SHAPED ARRAY

Localization using an L-shaped array, which is placed in *x*-*z* plane, is given in this subsection. Elevation angle and distance between the array and the source is estimated with the array in *z* axis as depicted in Figure 3.41 with a 2D search. These estimated values are then utilized by the array in *x* axis to find the azimuth angle as given in Figure 3.42. The array consists of eight antennas, and four of them are located in the *x* plane, and four are located in the *z* plane.

Then, device is fixed to y = 7 m and placement in the *x* plane is changed. As depicted in Figure 3.43, when the device is placed in the center, errors in *x* and *y* direction

decrease, but the error in *z* plane increases; this is because the effect of *z* direction increases when the device is placed at the center.

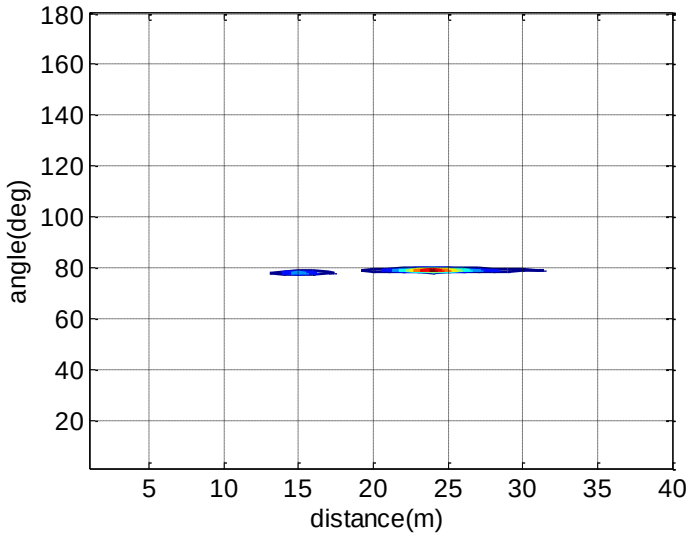

Figure 3.41. Estimation of elevation angle and distance.

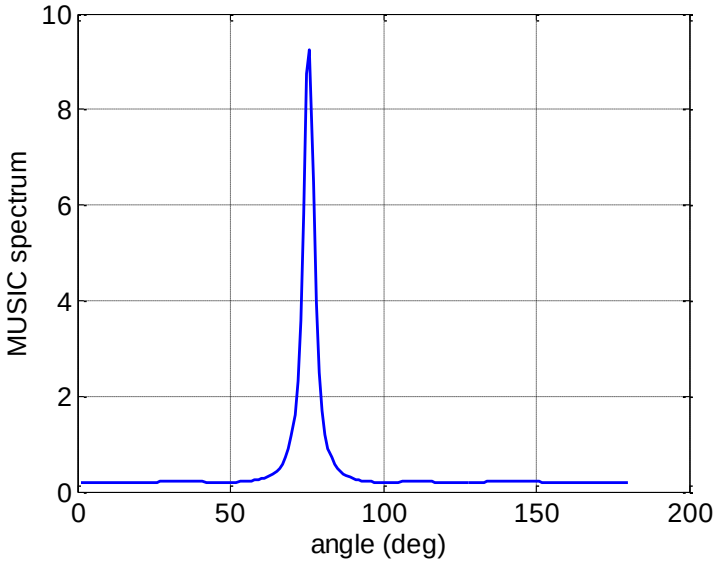

Figure 3.42. Estimation of azimuth angle.

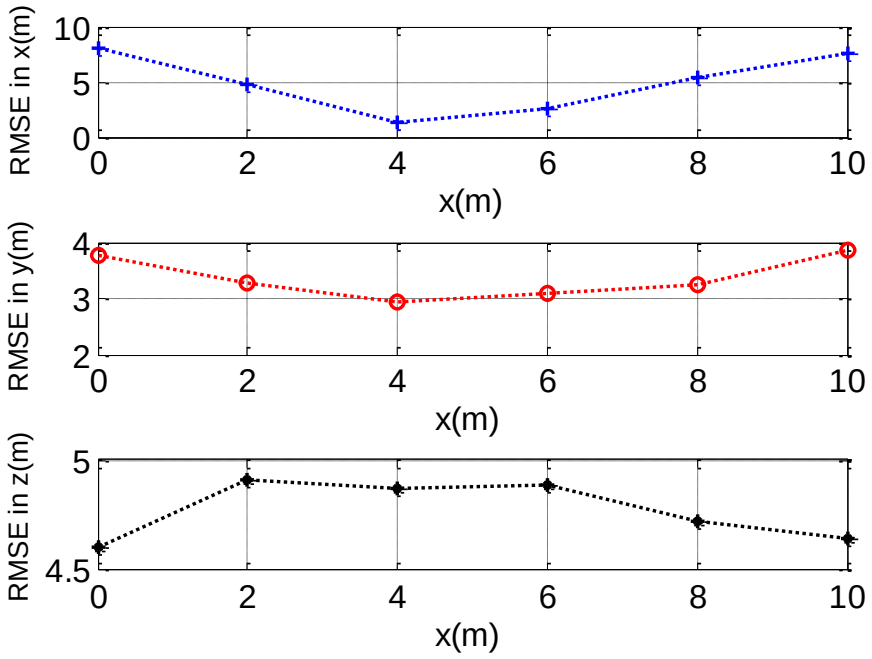

Figure 3.43. RMS error with respect to x position.

3.7 LOCATION ESTIMATION WITH RECTANGULAR ARRAY

In order to estimate location in 3D environment, we can also use a rectangular array which is placed to a certain height (exp: attached to a UAV). Simulation results for localization with different number of antenna elements and different positions are given in this subsection.

In these simulations, array size is kept as $10\lambda \times 10\lambda, (3m \times 3m)$ and the number of antennas is changed. First, the antenna elements are placed by λ/2 resulting in 82 antennas. The array is placed 4 m above ground level. The device is placed at the center of the array with a height of 1 m. Then, antenna spacing increased to λ, and 2λ consisting of 42 and 13 antennas, respectively. RMS errors are provided in Figure 3.44 for different spacing. As shown in the figure, error decreases with the antenna number especially for low SNR values.

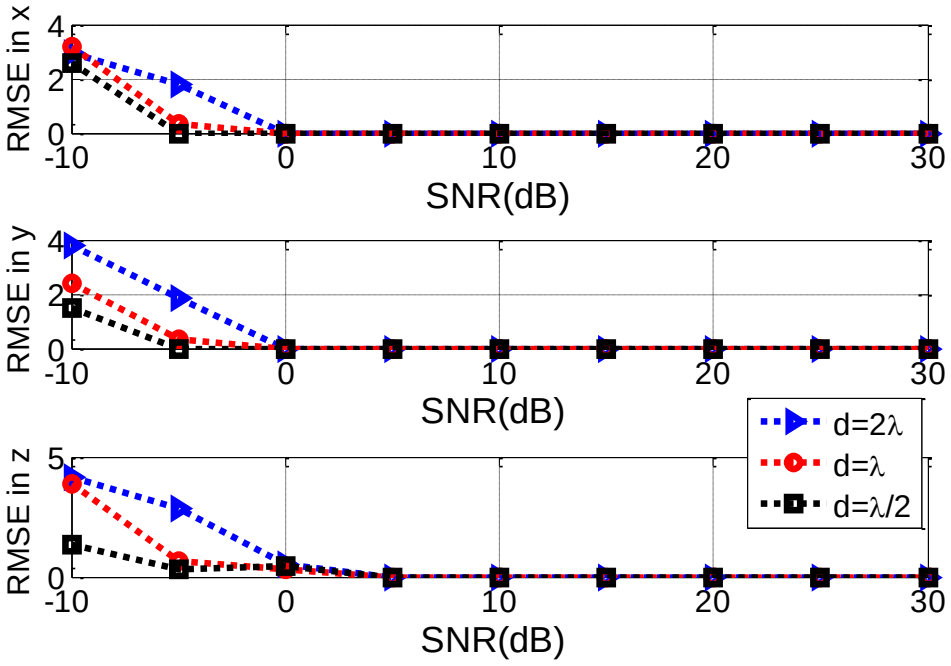

Figure 3.44. RMS error with respect to SNR for different spacing.

Next the effect of device position on the localization accuracy is represented in Figure 3.45. Antenna spacing is λ/2, the array is placed at 10 m height and the device position at *z* direction is changed. The error for *x* and *y* dimensions was not affected much, but the error in *z* dimension decreased by placing the device at a higher position. This was due to reduction of emissions when device was close to the ground [2].

In Figure 3.46, the distance between the array and the source changed, and the effect of the antenna number is demonstrated. A $10\lambda \times 10\lambda$ array was placed at a 10 m height. When the device was placed on the ground, the error reached the maximum value for all sampling sizes but when spacing was λ/2, the error was smaller compared to other sampling sizes.

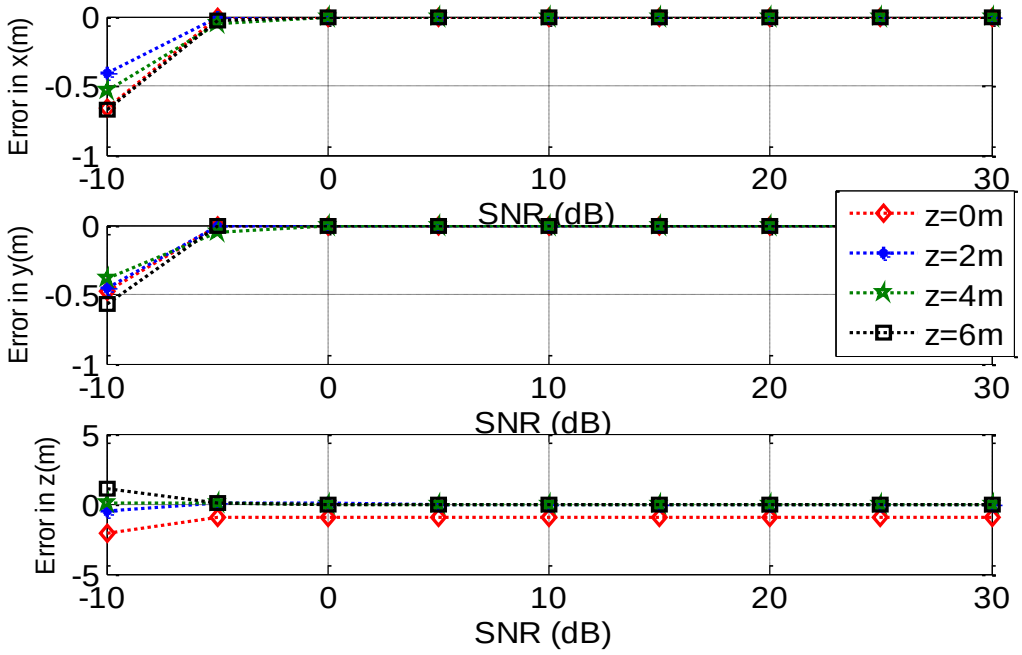

Figure 3.45. Mean error with respect to height for different antenna spacing.

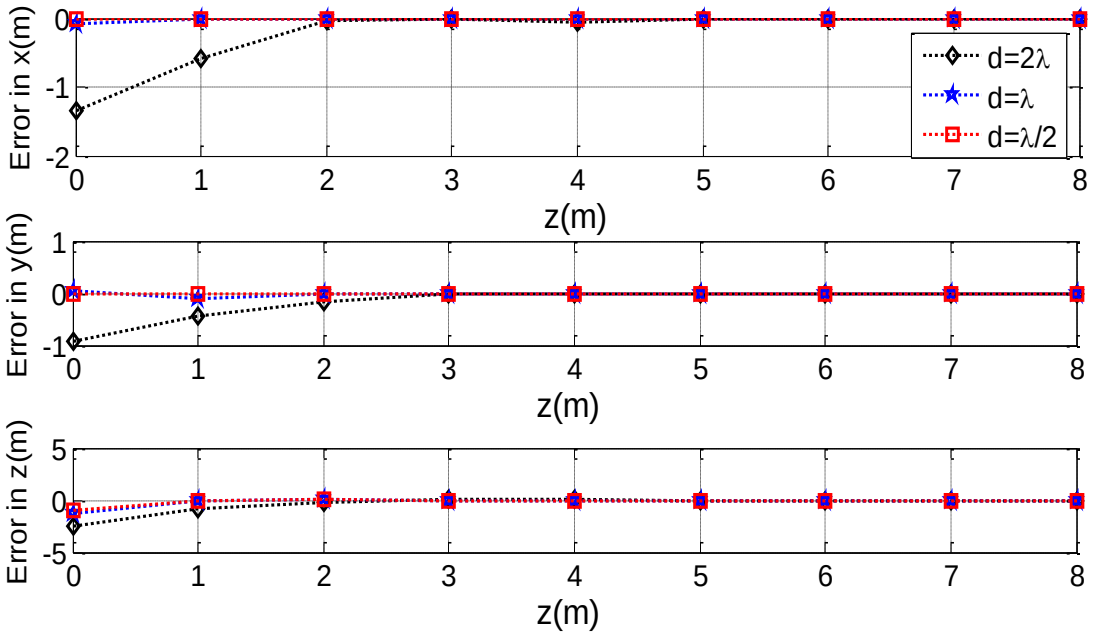

Figure 3.46. Mean error with respect to height for different antenna spacing.

4. CONCLUSIONS

To provide a broad perspective on localization and tracking of unintended emitting passive sources, computer simulation results are given in this paper. Signals are generated similar to unintended emissions; therefore, the simulations estimate the efficiency of localization techniques with different arrays and source configurations.

Simulations have shown that location estimation is more accurate when the device is farther from the array if the signal power is high and, therefore, the SNR level is high. However, since the power of the emissions was very low, and considering the noise in the environment, the results show that, it is more appropriate to use near-field localization techniques. Furthermore, results indicated that estimation accuracy increases with number of antennas due to an increase in resolution.

Results presented in this paper verify that the near-field approach in previous works is accurate and usable for localization and tracking of unintended emissions.

5. REFERENCES

[1] V. Thotla, M. T. A. Ghasr, M. J. Zawodniok, S. Jagannathan and S. Agarwal, "Detection of Super-Regenerative Receivers Using Hurst Parameter," *IEEE Trans. Instrum. Meas.*, vol.62, no.11, pp.3006-3014, Nov. 2013.

[2] V. Thotla, M. T. A. Ghasr, M. Zawodniok, S. Jagannathan and S. Agarwal, "Detection and localization of multiple R/C electronic devices using array detectors," *2012 IEEE International Instrumentation and Measurement Technology Conference (I2MTC)*, pp.1687-1691, 13-16 May 2012.

[3] Sarah Seguin, "Detection of low cost radio frequency receivers based on their unintended electromagnetic emissions and an active stimulation," Ph.D dissertation, Missouri S&T, Rolla, MO 2009.

[4] R. Roy, A. Paulraj and T. Kailath, "Direction-of-arrival estimation by subspace rotation methods – ESPRIT," *IEEE International Conference on Acoustics, Speech, and Signal Proc.*, vol.11, pp.2495-2498, Apr 1986.

[5] R. Schmidt, "Multiple emitter location and signal parameter estimation," *IEEE Trans. on Ant. and Prop.*, vol.34, no.3, pp. 276- 280, March 1986.

[6] M. Viberg and B. Ottersten, "Sensor array processing based on subspace fitting," *IEEE Trans. on Signal Proc.*, vol.39, no.5, pp.1110-1121, May 1991.

[7] W. Zhi and M. Y. W. Chia, "Near-Field Source Localization via Symmetric Subarrays," IEEE Signal Processing Letters, vol.14, no.6, pp.409-412, June 2007.

[8] N. Yuen and B. Friedlander, "Performance analysis of higher order ESPRIT for localization of near-field sources," *IEEE Transactions on Signal Processing*, vol.46, no.3, pp.709-719, Mar 1998.

[9] R. N. Challa and S. Shamsunder, "High-order subspace-based algorithms for passive localization of near-field sources," *Conference Record of the Twenty-Ninth Asilomar Conference on Signals, Systems and Computers*, vol.2, pp.777-781, Oct. 30 -Nov. 1 1995.

[10] E. Cekli and H. A. Cirpan, "Unconditional maximum likelihood approach for near-field source localization," *8th IEEE International Conference on Electronics, Circuits and Systems*, vol.2, pp.753-756, Sep 2001.

[11] N. Guzey, H. Xu and S. Jagannathan, "Localization of Near-Field Radio Controlled Unintended Emitting Sources in the Presence of Multipath Fading," *IEEE Transactions on Instrumentation and Measurement*, vol.63, no.11, pp.2696,2703, Nov. 2014.

[12] N. Guzey, H. Xu and S. Jagannathan, "Localization of Near-Field Sources in Spatially Colored Noise," in *IEEE Transactions on Instrumentation and Measurement, ,* vol.64, no.8, pp.2302-2311, Aug. 2015

[13] N. Guzey and S. Jagannathan, "Tracking of Radio-controlled Sources using Unintended Emissions," under review with *Measurement,* ISSN 0263-2241, 2015.

[14] Y.Hua, T.K. Sarkar and D.D. Weiner, "An L-shaped array for estimating 2-D directions of wave arrival," in *IEEE Transactions on Antennas and Propagation,* vol. 39, no. 2, pp.143-146, Feb. 1991.

[15] N. Tayem and H.M. Kwon, "L-shape 2-dimensional arrival angle estimation with propagator method," in *IEEE Transactions on Antennas and Propagation*, vol. 53, no. 5, pp.1622-1630, May 2005.

[16] L. Bai, C.-Y. Peng, and S. Biswas, "Association of DOA estimation from two ULAs," IEEE Trans. Instrum. Meas., vol. 57, no. 6, pp. 1094–1101, Jun. 2008.

[17] K. F. Warnick and D. V. Arnold, "Electromagnetic Green functions using differential forms," *Journal of Electromagnetic Waves and Applications*, vol.10, no.3, pp. 427-438, 1996.

[18] W. Zhi and M. Y. W. Chia, "Near-Field Source Localization via Symmetric Subarrays," IEEE Signal Processing Letters, vol.14, no.6, pp.409-412, June 2007.

[19] S. H. Chang, S. Y. Hou, S. C. Chang and H. S. Hung, "Novel algorithms for tracking multiple targets," *Journal of Marine Science and Technology,* vol. 18, No. 2, pp. 259-267, March 2010.

V. LOCALIZATION AND TRACKING OF UNINTENDED EMITTING SOURCES IN 3D ENVIRONMENTS

ABSTRACT

This paper presents 3D localization and tracking of electronic devices by measuring their unintended emissions in the near-field of a detector array. First, a 3D localization technique which uses an L-shaped array is presented. Existing localization methods which use L-shaped arrays estimate elevation and azimuth angles satisfactorily for direction of arrival (DOA) if the source is placed in the far-field region of the array. However, their performance degrades if the source is in the near-field. Therefore our new method aims to locate unintended emitting sources in the near-field of an L-shaped array using the difference in phase characteristics of the subarrays in the L-shaped array. Further, for moving sources, a 3D tracking scheme which uses the L-shaped array with extended Kalman filter (EKF) is also proposed. In addition, free space Green's function is used in conventional MUSIC algorithm to provide another perspective to array processing. By using this method, Cartesian coordinates of the device is estimated directly instead of DOA. Experimental evaluation and simulation results of the proposed localization and tracking schemes are provided to demonstrate the effectiveness of the proposed work.

1. INTRODUCTION

Electronic devices which have super heterodyne or super regenerative receivers emit unintended emissions. It may be critical to detect and identify these emissions for commercial and security applications [1]-[2]. Further, the received power from the emissions can be enhanced by using a stimulating signal which in turn enhances detection [3]. Besides detection, localization of these devices is very important. High resolution array processing methods such as ESPRIT [4], MUSIC [5] and WSF [6] can be employed for accurately locating unintended emissions. These DOA estimation methods are accurate if the source is in the far-field region of the array wherein the direction of arrival (DOA) to each antenna element is assumed to be equal and the phase difference between antenna elements is a function of DOA. However, this assumption is not valid if the source is in the near-field region of the array, since the phase is a nonlinear function of DOA and distance between the array and the source. This phase difference is approximated with Fresnel approximation [7] in the near-field localization methods [7]-[11]. Further, for both near and far-field localization, either if there are multiple correlated sources or multipath fading in the environment, a smoothing procedure [12] is needed to locate correlated sources [11].

Methods reported in [4]-[11] use the azimuth angle estimation for localization. However, for instance when an airborne array is employed to locate ground-based sources, besides azimuth angle, elevation angle should also be estimated. In [13], the authors found that using L-shaped array for elevation and azimuth angle estimation as the two dimensional direction of arrival (DOA) components is more advantageous than other array configuration. The L-shaped array has a simpler configuration compared to others,

and it provides better accuracy due to the fact that it has a larger array aperture, which can accommodate more distance among the sensors [13].

An efficient method is proposed by [14] where the 2D problem is decomposed into two independent 1D problems with an L-shaped array. However, two independent sets of angles have to be paired together properly by using an algorithm [15]. Unfortunately, the pair matching is inefficient when the difference in the corresponding azimuth and elevation angles is small and the signal-to-noise ratio (SNR) is low. In addition, these schemes [13]-[15] do not consider the near-field effect on the estimation.

DOA estimation reported in array processing methods from [4]-[15] is based on the phase difference between the antenna elements in the array whereas it is a function of DOA and range information in the near-field. On the other hand, received signals by an antenna can be modeled with the free space electromagnetic Green's function [16]. The phase of the received signal is a function of signal frequency and distance between the antenna and the source. This phase can be used in array processing to estimate the location of a device. By using this method [16], the Cartesian coordinates of the source is directly estimated instead of the DOA. This is advantageous over DOA estimation methods because a small error in DOA estimation leads to a large error in location when the device is placed far from the antenna array. Moreover, this method [16] is adaptive to any kind of array configurations since it uses the same phase expression for every configuration.

Unintended emissions may not always come from stationary sources; therefore, it may be crucial to track these sources. The extended Kalman filter (EKF) is preferred for tracking since it does not need an extra data association algorithm [17]. The signal and

noise statistics are not required as in [18] and [19]. However, the EKF method in [17] uses a linear measurement model, where in the near-field array processing, the measurements are a nonlinear function of the phase difference between the antenna elements.

Therefore, a suite of 3D localization methods are proposed with L-shaped array for near-field environment. An L-shaped array is placed in the *x*-*z* plane. Phase difference between the elements of array placed in the *z* plane is independent of the azimuth angle of arrival. Therefore, this property is used to construct an efficient 3D localization method for the near-field region which does not require a pair matching algorithm. In addition, the array is placed at a height to reduce reflections from the environment and subsequently multipath fading. The second scheme employs EKF, which is mostly used for tracking. By using EKF, the initial estimates are refined by subsequent measurements to provide more accurate localization results. The final localization method expresses the phase of the signal with free space Green's function. The performance of newly developed localization and tracking methods is also demonstrated with real measurements.

This paper presents a comprehensive study on utilizing an L-shaped array for localization and tracking of electronic devices. The efficacy of the proposed technique is validated using simulation results as well as using measurements. Thus, the contributions of the paper include 1) development of localizing and tracking schemes for unintended emissions in the 3D environment by using an L-shaped array, 2) introduction of an array processing technique by utilizing free space Green's function, 3) the experimental validation of the proposed methods by using an L-shaped array with data collection, and

4) a comparison of proposed methods. Furthermore, computer simulation results for locating unintended emitting devices are given to verify the proposed schemes and to support the experimental results.

The rest of the paper is organized as follows. Section 2, introduces the proposed methods for locating and tracking unintended emissions in 3D by using an L-shaped antenna array. Section 3 gives the computer simulation results for several array and source configurations. Section 4 presents details of the experimental setup and subsequently gives localization and tracking results by evaluating the measurements using the proposed methods. The discussion is finalized with conclusions in Section 5.

2. METHODOLOGY

2.1 3D NEAR-FIELD LOCALIZATION WITH L-SHAPED ARRAY

To establish context, this section starts with the introduction of M_s narrowband-radio-controlled devices, which are stimulated with a continuous RF signal. The unintended emissions from these devices are received with an L-shaped array, which is placed in the *x*-*z* plane consisting of L_x and L_z antennas with inter element spacing *d* as depicted in Figure 2.1.

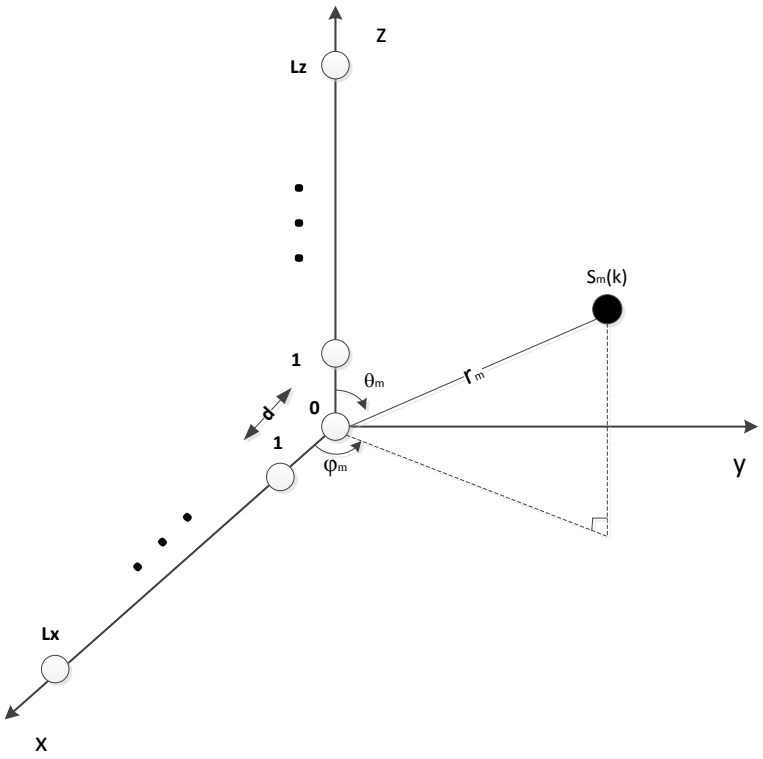

Figure 2.1. L-shaped array configuration.

The array is placed z_h above ground level for better reception. Received signals from M_s near-field signal sources by arrays located in the *x* and *z* axes are expressed in [20] as

$$\mathbf{X}(k)=\sum_{m=1}^{Ms}\mathbf{a}\ (\theta_m,\varphi_m,r_m)s_m(k)+\mathbf{N}_x(k)=\mathbf{A}_x(\theta_m,\varphi_m,r_m)\mathbf{s}(k)+\mathbf{N}_x(k),\quad k=1,...,K_s,\qquad(2.1)$$

where $\mathbf{s}=[s_1,\ldots,s_{M_s}]$ is the vector of signal powers and $\mathbf{A}_x(\theta,\varphi,r)=[\mathbf{a}_x(\theta_1,\varphi_1,r_1),\mathbf{a}_x(\theta_2,\varphi_2,r_2),\ \ldots,\mathbf{a}_x(\theta_{Ms},\varphi_{Ms},r_{Ms})],$ is the manifold matrix of the array located in the *x* axis. These *x* axis elements are the steering vectors of array response to each source, which in the near-field is written as

$$\mathbf{a}_x(\theta_m,\varphi_m,r_m)=[1,\ e^{j(\alpha_{xm}+\beta_{xm})},\ldots,e^{j(l\alpha_{xm}+l^2\beta_{xm})},\ \ldots,e^{j((L_x-1)\alpha_{xm}+(L_x-1)^2\beta_{xm})}],\qquad(2.2)$$

which contains the phase difference of the antennas with respect to the reference point. This phase has two parts which is given by

$$\alpha_{xm}=-2\pi\frac{d}{\lambda}\sin(\theta_m)\cos(\varphi_m)\ \text{ and }\ \beta_{xm}=\pi\frac{d^2}{\lambda r_m}(1-\sin^2(\theta_m)\cos^2(\varphi_m)).\qquad(2.3)$$

where, λ is the wavelength of the signal and *d* is the distance between two successive antennas, θ_m represents the elevation angle, φ_m is the azimuth angle, and r_m is the distance between the array reference and the m^{th} source. The second component contains distance information, which is present due to the near-field effect. Similarly, received signals by the array in the z axis is written as

$$\mathbf{Z}(k)=\sum_{m=1}^{M_s}\mathbf{a}_z(\theta_m,r_m)s_m(k)+\mathbf{N}_z(k)=\mathbf{A}_z(\theta_m,r_m)\mathbf{S}(k)+\mathbf{N}_z(k).\qquad(2.4)$$

where $\mathbf{A}_z(\theta,r)=\left[\mathbf{a}_x(\theta_1,r_1),\mathbf{a}_x(\theta_2,r_2),\ldots,\mathbf{a}_x(\theta_{Ms},r_{Ms})\right]$ is the array response containing steering vectors for each source which is given by

$$\mathbf{a}_z(\theta_m,r_m)=\left[1,\ e^{j(\alpha_{zm}+\beta_{zm})},\ldots,e^{j(l\alpha_{zm}+l^2\beta_{zm})},\ldots,e^{j((L_z-1)\alpha_{zm}+(L_z-1)^2\beta_{zm})}\ \right].\qquad(2.5)$$

Phase components are given by

$$\alpha_{zm} = -2\pi \frac{d}{\lambda} \cos(\theta_m) \text{ and } \beta_{zm} = \pi \frac{d^2}{\lambda r_m} \sin^2(\theta_m). \quad (2.6)$$

As observed from (2.6), the response of the *z* axis array is not a function of the azimuth angle but in the x axis the azimuth and elevation angles are coupled as given in (2.2). Instead of estimating the coupled angles, by estimating elevation angle using the z axis array, then the azimuth angle with the x axis array, the problem turns into solving two independent equations. This simplifies the 3D location estimation.

Proposed Method

Since the array in the z axis is independent of the azimuth angle, the received signal with this array is used to estimate distance between the array and the source, and the elevation angle using 2D MUSIC [11]. Covariance matrix and noise eigen vectors for the array in the *z* axis are calculated as in [11]. Using the orthogonality between the signal and noise subspaces, MUSIC spectrum provides the estimates of elevation angle and range, such as

$$P(\theta, r) = \frac{1}{\mathbf{a}_z^H(\theta, r)\mathbf{U}_{zn}\mathbf{U}_{zn}^H\mathbf{a}_z(\theta, r)}. \quad (2.7)$$

From (2.7), θ and r are estimated, and their estimated values are employed in the 3D MUSIC spectrum of the antenna output which is placed in the *x* plane. Covariance matrix and eigenvectors are calculated as in [11]

$$P(\theta, \varphi, r) = \frac{1}{\mathbf{a}_x^H(\theta, \varphi, r)\mathbf{U}_{xn}\mathbf{U}_{xn}^H\mathbf{a}_x(\theta, \varphi, r)}, \quad (2.8)$$

The first two parameters are provided by (2.7), then (2.8) is simplified to one unknown, such as

$$P(\varphi) = \frac{1}{\mathbf{a}_x^H(\hat{\theta}, \varphi, \hat{r})\mathbf{U}_{xn}\mathbf{U}_{xn}^H\mathbf{a}_x(\hat{\theta}, \varphi, \hat{r})}, \tag{2.9}$$

azimuth angles are estimated with only a 1D search over φ. These polar coordinates are then used to calculate the Cartesian coordinates of the emitting device such as

$$x = \frac{r\sin\theta}{\sqrt{1+\tan^2\varphi}} \tag{2.10}$$

$$y = \frac{r\sin\theta}{\sqrt{1+\tan^2\varphi}}\tan\varphi, \tag{2.11}$$

and

$$z = z_h - \sqrt{r^2 - (r\sin\theta)^2}, \tag{2.12}$$

where z_h is the height of the antenna array when it is placed above for better reception.

Remark 1: Instead of estimating only azimuth angle, the range can also be estimated with a 2D search by the array in *x* axis. Taking the mean of the range parameters estimated by both arrays will increase the localization accuracy.

Next, a 3D near-field tracking method with two-stage EKF is presented for mobile sources using an L-shaped array.

2.2 TRACKING WITH L SHAPED ARRAY USING EKF

For tracking mobile sources in 3D space, the property of the L-shaped array used in localization is also utilized here with a two-stage EKF. During the first stage, elevation angle and the range are estimated with *z* axis array, these results are then used in the

second stage to estimate the azimuth angle using the *x* axis array. The methodology of the proposed method is given in this subsection.

First stage

The time difference between the l^{th} antenna and the reference for the array in *z* axis is written as

$$\tau_{lm} = \alpha_{zm} + \beta_{zm} = -2\pi \frac{d}{\lambda}\cos(\theta_m) + \pi \frac{d^2}{\lambda r_m}\sin^2(\theta_m) \tag{2.13}$$

The state vector for the m^{th} target is defined as $\mathbf{x}_{zm}(k) = [\theta_m(k), \dot{\theta}_m(k), \ddot{\theta}_m(k), \mathrm{r}_m(k), \dot{\mathrm{r}}_m(k), \ddot{\mathrm{r}}_m(k)] \in \Re^6$, [17], which contains the elevation angle, angular velocity and angular acceleration of elevation angle, distance between antennas, and source and change, and acceleration in the distance. The m^{th} target motion $\mathbf{x}_{zm}(k)$ pursues the rule given in [17].

Since the process is a nonlinear function of elevation angle and distance between the source and antenna array, the array output in the *z* axis, $\mathbf{Z}(k)$, can be rewritten as [19]

$$\mathbf{Z}(k) = \mathbf{h}_z(\mathbf{x}_z(k), \mathbf{s}(k))\mathbf{x}_z(k) + \mathbf{v}_z(k) = \mathbf{A}_z(\mathbf{x}_z(k))\mathbf{s}(k) + \mathbf{N}_z(k), \tag{2.14}$$

where $\mathbf{x}_z(k)$ is the compound state vector of the array in the z axis for M_S sources. $\mathbf{v_z}(k)$ is the measurement noise with a variance of σ_v^2. Then, for linearization, a partial derivative matrix of the measurement model is represented as [21]

$$\mathbf{H}_z(k) = \frac{\partial \mathbf{h}_z}{\partial \mathbf{x}_z} = \left[\mathbf{H}_{z1}(k), \ldots, \mathbf{H}_{zM_s}(k)\right], \tag{2.15}$$

where the parameters of (16) is calculated as in [21] such as

$$g_{lm} = -\cos(\tau_{lm})s_m(k) \text{ and } c_{lm} = -\sin(\tau_{lm})s_m(k), \tag{2.16}$$

and derivatives are calculated as

$$\frac{\partial \tau_{lm}}{\partial \theta_m} = -\frac{2\pi d}{\lambda}(l-1)\sin(\theta_m) - \frac{\pi d^2}{\lambda r_m}(l-1)^2 \sin(2\theta_m) \tag{2.17}$$

and

$$\frac{\partial \tau_{lm}}{\partial r_m} = \frac{\pi d^2 (l-1)^2 \sin^2(\theta_m)}{\lambda r_m^2} \tag{2.18}$$

Initially, the target angles and range parameters at two successive time instants $\{\theta_m(-1), \theta_m(0), r_m(-1)\ \mathrm{r}_m(0)\}$ are estimated with the proposed method mentioned in the previous subsection. States are estimated in four steps as described in [17].

Second stage

These estimated values are then used in the second stage of the tracking scheme to estimate the azimuth angle by the same procedure using the array in *x* axis. The state vector for this stage is defined as $\mathbf{x}_{xm}(k) = [\varphi_m(k), \dot{\varphi}_m(k), \ddot{\varphi}_m(k)]$, which contains azimuth angle, change, and acceleration in this angle. The phase between the elements of the array in x axis is written as

$$\tau_{lm} = \alpha_{xm} + \beta_{xm} = -2\pi \frac{d}{\lambda}\sin(\theta_m)\cos(\varphi_m) + \pi \frac{d^2}{\lambda r_m}(1 - \sin^2(\theta_m)\cos^2(\varphi_m)). \tag{2.19}$$

Then the derivative of the phase with respect to the azimuth angle is calculated as

$$\frac{\partial \tau_{lm}}{\partial \varphi_m} = -\frac{2\pi d}{\lambda}(l-1)\sin(\theta_m)\sin(\varphi_m) - \frac{\pi d^2}{\lambda r_m}(l-1)^2 \sin^2(\theta_m)\sin(2\varphi_m). \tag{2.20}$$

The state vector, array output and the derivatives are used in the estimation of the azimuth angle similar to the methodology given in first stage.

Remark 2: The EKF is mostly used for tracking [17]–[19], and it is not generally considered as an estimation method to locate a stationary unintended emitting device.

However, multiple samples are also collected for localization; therefore the initial location estimation can be refined using these samples. Performance evaluation of localization with EKF is given in the discussion section.

2.3 ARRAY PROCESSING WITH GREEN'S FUNCTION

Free space Green's function is used in electromagnetics to express a distance between two points in space. In an array, received signal from the m^{th} source by the l^{th} antenna of uniform linear array (ULA) using the normalized Green's function [16] is given as

$$x_l(k) = \sum_{m=1}^{Ms} \frac{\lambda}{(4\pi R_{lm}(k))^2} e^{(-j\frac{2\pi}{\lambda}R_{lm}(k))} + n(k), \quad k=1,\ldots K_s, \tag{2.21}$$

where $x_l(k)$ is the received power by the l^{th} antenna, λ is the wavelength, and R_{lm} is the distance between l^{th} antenna and m^{th} source which is defined as

$$R_{lm} = \sqrt{(x_l - x_m)^2 + (y_l - y_m)^2 + (z_l - z_m)^2}, \tag{2.22}$$

where (x_l, y_l, z_l) is the position of l^{th} antenna and (x_m, y_m, z_m) is the position of m^{th} source. In matrix form, the received signal by the L element array is written as

$$\mathbf{x}(k) = \mathbf{A}\mathbf{s}(k) + \mathbf{n}(k), \tag{2.23}$$

where $\mathbf{s}(k) = [s_1(k),\ldots,s_{M_s}(k)] \in \Re^{M_s}$ is vector of signal powers, $\mathbf{n}(k) = [n_1(k)\ldots n_L(k)] \in \Re^L$ is the additive noise vector, finally, $\mathbf{A}(R) = [\mathbf{a}(R_1), \mathbf{a}(R_2),\ldots,\mathbf{a}(R_{M_s})]$ is the steering matrix of the array whose elements are the steering vectors for each source. Steering vector for the m^{th} source is expressed as

$$\mathbf{a}(R_m) = [e^{(-j\frac{2\pi}{\lambda}R_{1m})},\ldots,e^{(-j\frac{2\pi}{\lambda}R_{Lm})}]. \tag{2.24}$$

This steering vector can be used in the MUSIC scheme for location estimation. Then, the MUSIC spectrum is rewritten as

$$P_{MUSIC}(x, y, z) = \frac{1}{\mathbf{a}^H(x, y, z)\mathbf{U}_n\mathbf{U}_n^H\mathbf{a}(x, y, z)}, \tag{2.25}$$

where $\mathbf{U}_n \in \Re^{L\times(L-Ms)}$ is the matrix of noise eigenvectors, and $l = Ms+1,\ldots,L$. Peaks of this spectrum show the positions of the unintended emitting sources. Next, the measurement setup details are provided.

3. SIMULATIONS

Computer simulations are performed to verify the performance of the proposed methods described in the previous section. Furthermore, these simulations are performed to validate the experimental results for different array and source configurations as will be shown later. Localization using an L-shaped array is given next. Array consists of 8 antennas, where 4 of them located in *x* plane and 4 located in the *z* plane. In this analysis a point source is simulated and the received signal at the array elements was found by the propagation model outlined in the previous section. Device was placed at (3.6 m, 3.6 m, 1 m) position. Noise is added to the simulated signal to model different SNR levels. Figure 3.1 shows an example of 2D localization, where elevation angle and range estimated by the *z* axis array.

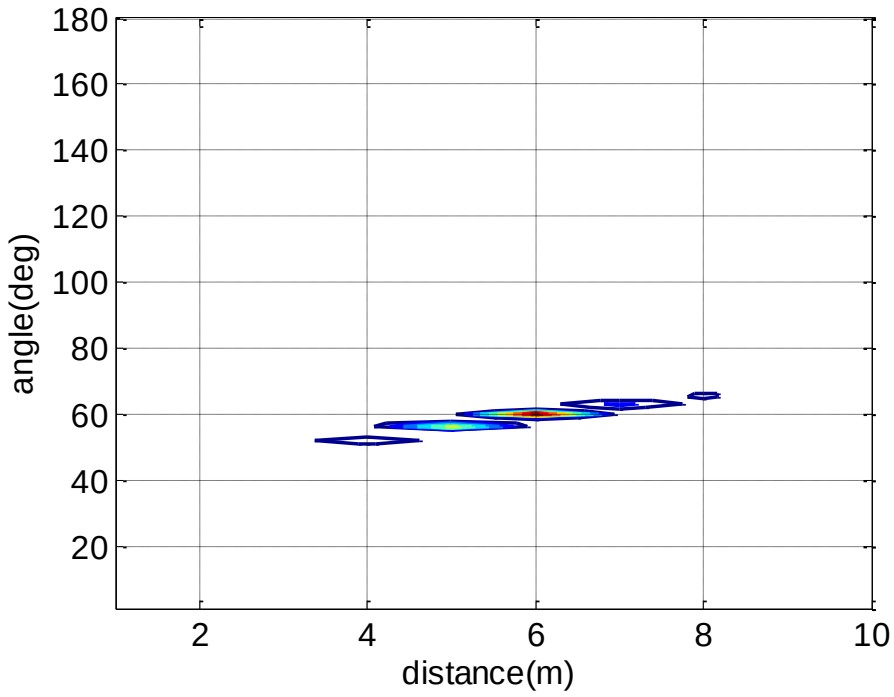

Figure 3.1. Elevation angle and range estimation for unintended emitting source.

Then the 1D spectrum given in Figure 3.2 depicts the azimuth angle which gives the third dimension of location.

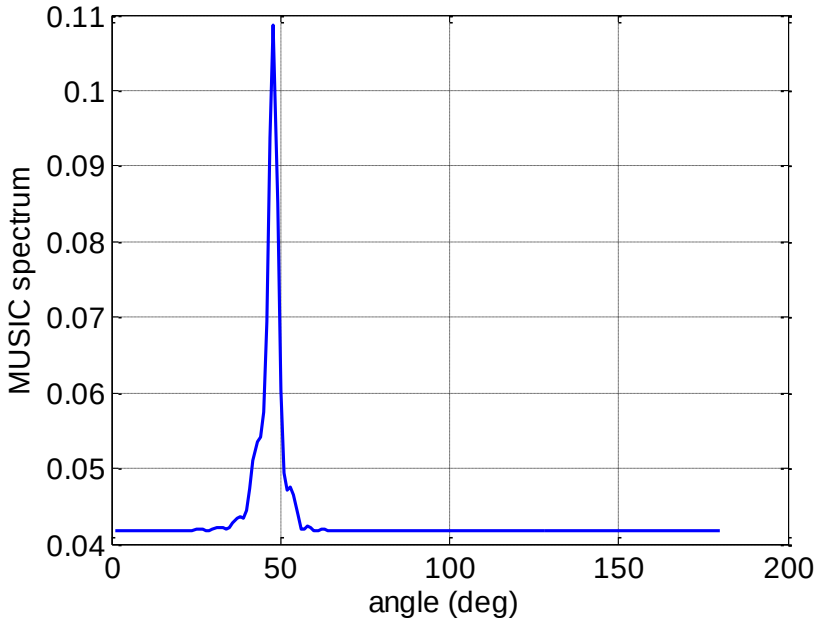

Figure 3.2. Azimuth angle estimation.

The performance of the proposed localization method with respect to SNR is given in Figure 3.3. In this analysis device placed in front of the center of the array in x direction and place in y direction is kept at 7 m. Also device placed 1 m above the ground level where the array placed at 4 m in z direction. As depicted in the figure; the root mean square (RMS) error, calculated between estimated and actual location, is considerably high in low SNR values, which is a drawback of MUSIC scheme. Our measurement system provided such a -95 dB noise level, and the electronic devices that we are tracking emit very low signal and therefore, the SNR is generally low in the region of -10 dB to 30 dB. Therefore, this figure also shows that the near-field approach for localization and

tracking of unintended emissions is as expected. The same analysis is repeated by using Green's function with MUSIC in Figure 3.4.

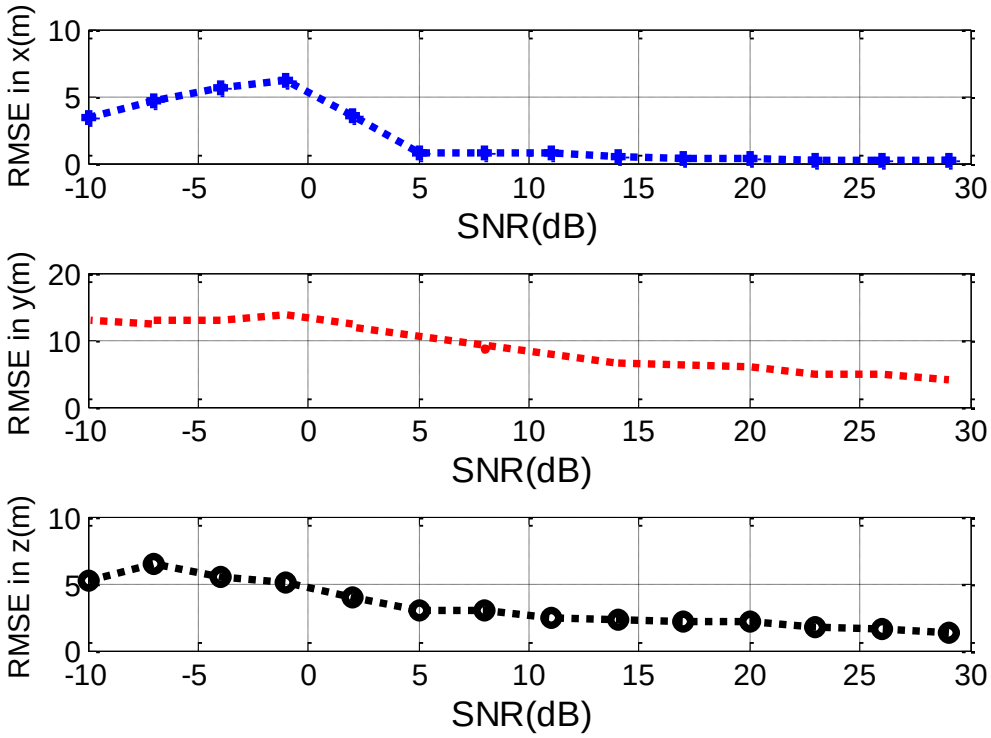

Figure 3.3. RMSE for localization with proposed method with L-shaped array.

Another effect on the estimation accuracy is the number of antennas where the resolution increases with this number. Furthermore, as described in [2], the detection range is also increased with number of antennas. As depicted in Figure 3.5 the error decreases with number of antennas.

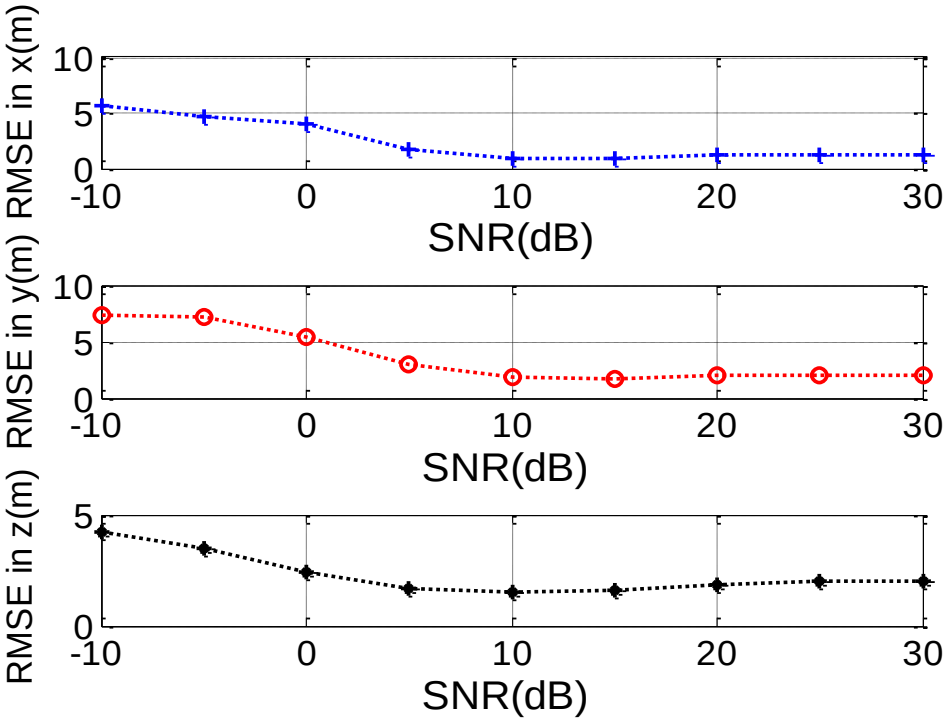

Figure 3.4. RMSE for localization by using Green's function with MUSIC.

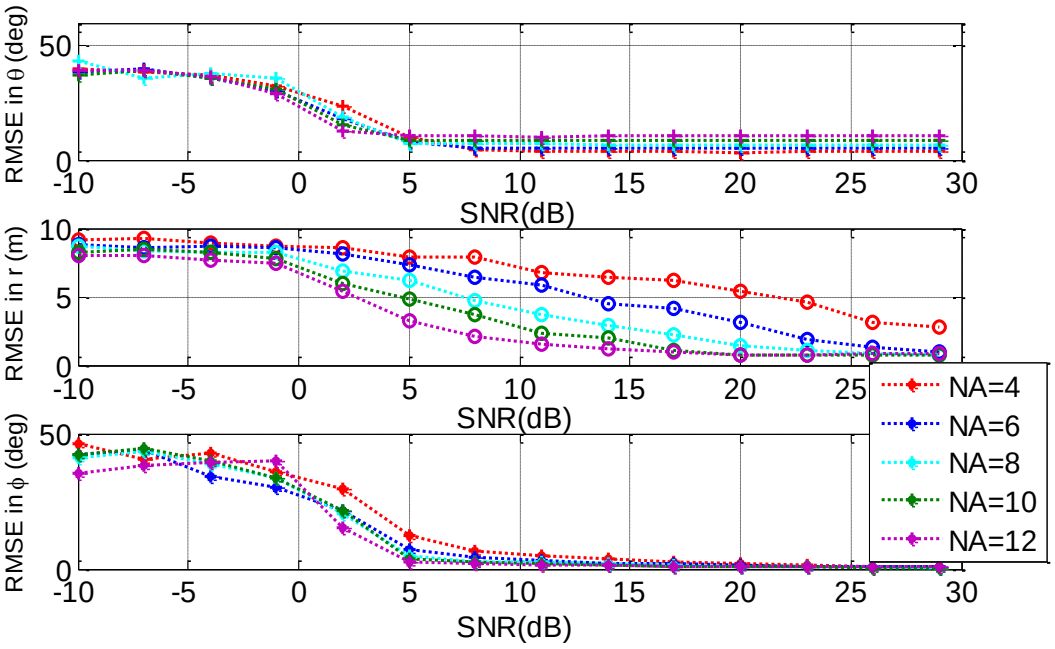

Figure 3.5. RMS estimation errors with L shaped array for different number of antennas.

The placement of the source also has an impact on the accuracy. To show this effect, device is placed on two sides and the center. Distance to the antenna in the *y* direction is changed for each case and location is estimated with L-shaped array using the localization technique built with Green's function. Noise level is kept as −95 dBm. The RMS error calculations for these estimations are given in Figure 3.6. Array center is at 4.6 m. Change in the angle effects estimation in *x* dimension most.

Antenna array can be mounted to a certain height to eliminate the multipath fading and more efficient reception. The L-shaped array placed to a 4m height and the placement of the device is changed in *y* and *z* direction. Figure 3.7 shows that the error in *x* and *y* directions is not affected much with change in the height of the device but error in the *z* direction decreases by putting the device to a higher position because of the increase on the received power level.

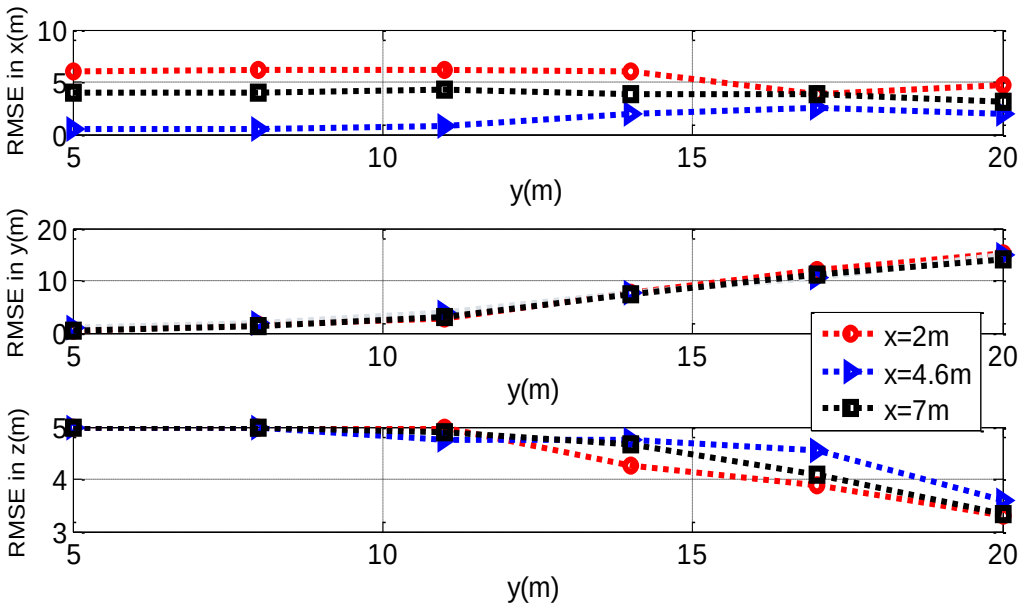

Figure 3.6. Localization error for different positions in x and y directions.

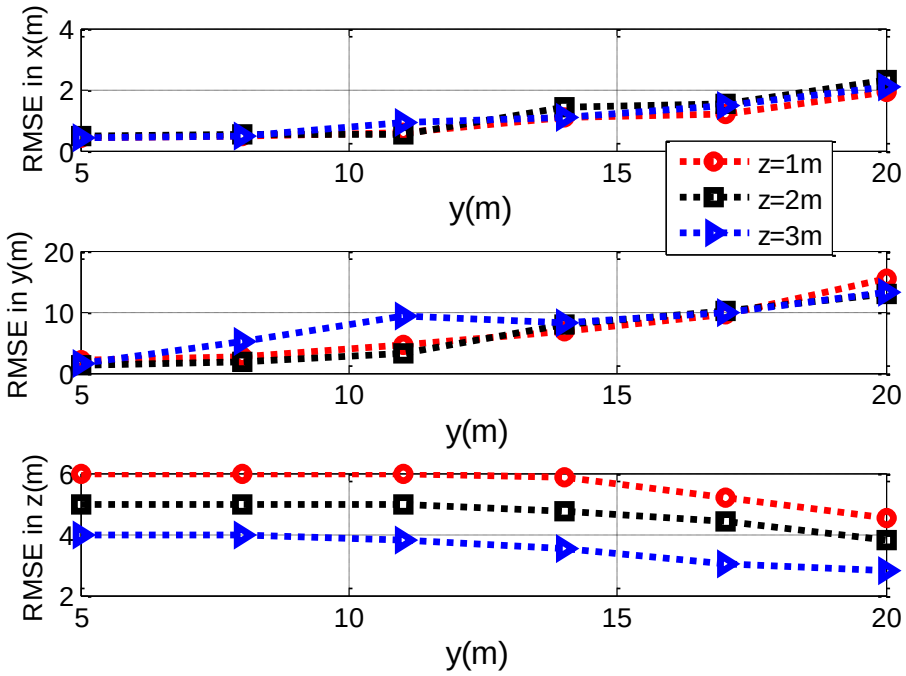

Figure 3.7. Localization error for different positions in z and y directions.

Next the experimental setup and experimental results for the proposed schemes are provided.

4. MEASUREMENTS

4.1 EXPERIMENTAL SETUP

An L-shaped array as shown in Figure 4.1 is used for the experiment. Antennas are omni-directional, unobtrusive, and wideband with an operating bandwidth in the range of 225–2500 MHz (Pharad lightweight wearable antennas). Antennas are connected to 40 dB low noise amplifiers and then to 4-channel Agilent MSO6104A and Agilent MSO7104B oscilloscopes (one oscilloscope for each axis) for data acquisition.

Figure 4.1. Experimental setup.

Four elements of the array are placed along the *x* axis and the remaining four elements are placed along *z* axis. The array is designed with a uniform spacing of λ/2 between the elements. A Walkie-Talkie operating at FRS channel 8 with a frequency of

445.862 MHz is being located. The Walkie-Talkie is operated at FRS channel 8 with a frequency of 445.862 MHz. Agilent N5182A signal generator is used to send the RF stimulating signal at a frequency of 467.5625 MHz and amplitude of -40 dBm to enhance the emissions from the Walkie-Talkie [2].

The oscilloscopes are connected to a PC with a LabView interface to acquire and store data. A total of 200,000 data points are collected each time. The antenna is placed at a height of 4m above ground. Localization accuracy is evaluated by placing the devices at known positions then performance of proposed methods are compared.

4.2 EXPERIMENTAL RESULTS

Performance evaluation of the proposed methods is carried out and described herein to verify the analytical results of Section 2. Experimental results for 3D localization and tracking of unintended emitting sources by using the L-shaped array are given. Further, the experimental data was also processed with free space Green's function for locating the devices using an L-shaped array and results are reported in this section.

Case 1) Device placed at 0.88 m above from ground.

A single Walkie-Talkie was stimulated with an RF signal and the location estimation was performed for multiple positions using the L-shaped array, which is placed 4 m above the ground level. The experiment was held in $10\ \text{m} \times 10\ \text{m}$ area. The device was placed in the (x, y) coordinates with a 0.88 m height. Elevation angle and distance was estimated as given in Figure 3.1, and then these estimated parameters are used to approximate the azimuth angle such as given in Figure 3.2.

The estimated Cartesian coordinates are then calculated with estimated polar coordinates. The RMS errors for localization at each position is calculated with

$$RMSE = \sqrt{E\left[(x-\hat{x})^2 + (y-\hat{y})^2 + (z-\hat{z})^2\right]}, \quad (4.1)$$

and RMSE for each position is shown in Figure 4.2. The mean error for all positions calculated in this case was 0.52 m.

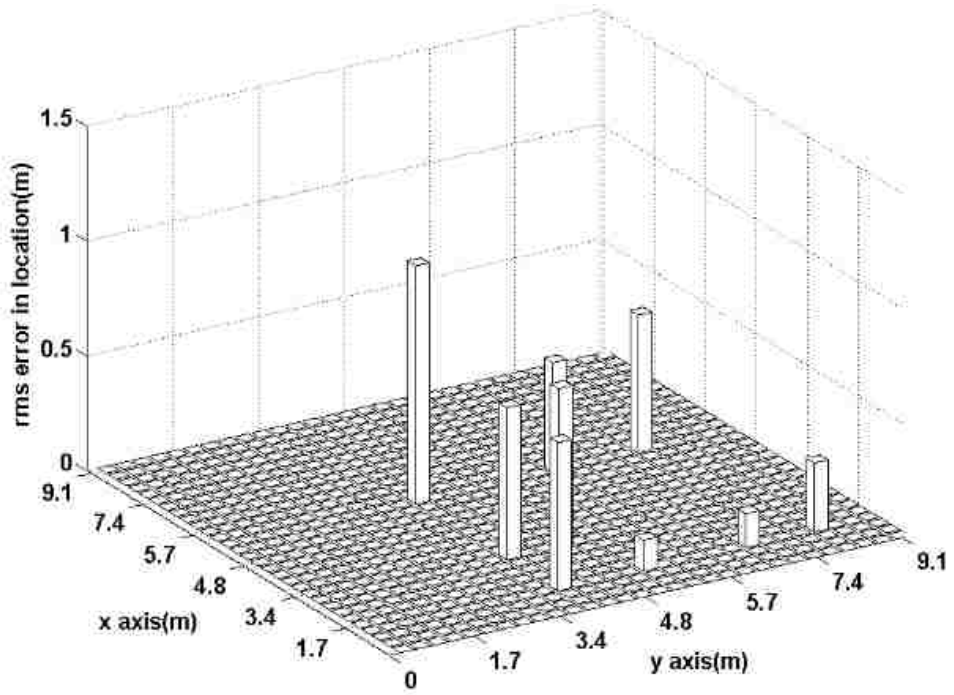

Figure 4.2. Localization errors of a single device with an L-shaped array for different positions when device is at 0.88 m height.

Case 2) Device placed at ground level

The device was placed at the ground level and location estimation was performed. As can be seen from the Figure 4.3, the localization error increased when the device was placed on the ground. Since the emissions of the walkie-talkie are reduced when it is near the ground [2], the mean error calculated in this case was 0.68 m which also verifies the simulation results.

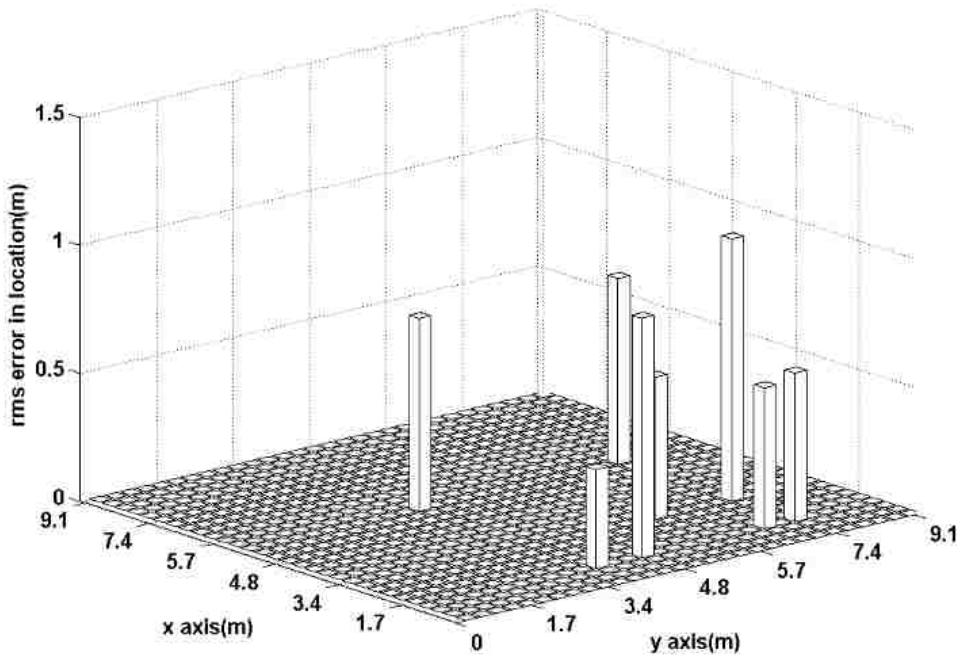

Figure 4.3. Localization errors of a single device with L-shaped array for different positions when device is on the ground.

Case 3) Device placed inside a box

Next, the device was placed inside a cardboard box. Placing the device in a cardboard box reduced the received signal power even though the attenuation coefficient of the cardboard is generally low. The drop in the signal power resulted in an increase in the localization error as observed in Figure 4.4. The calculated mean error was found to be 0.91 m.

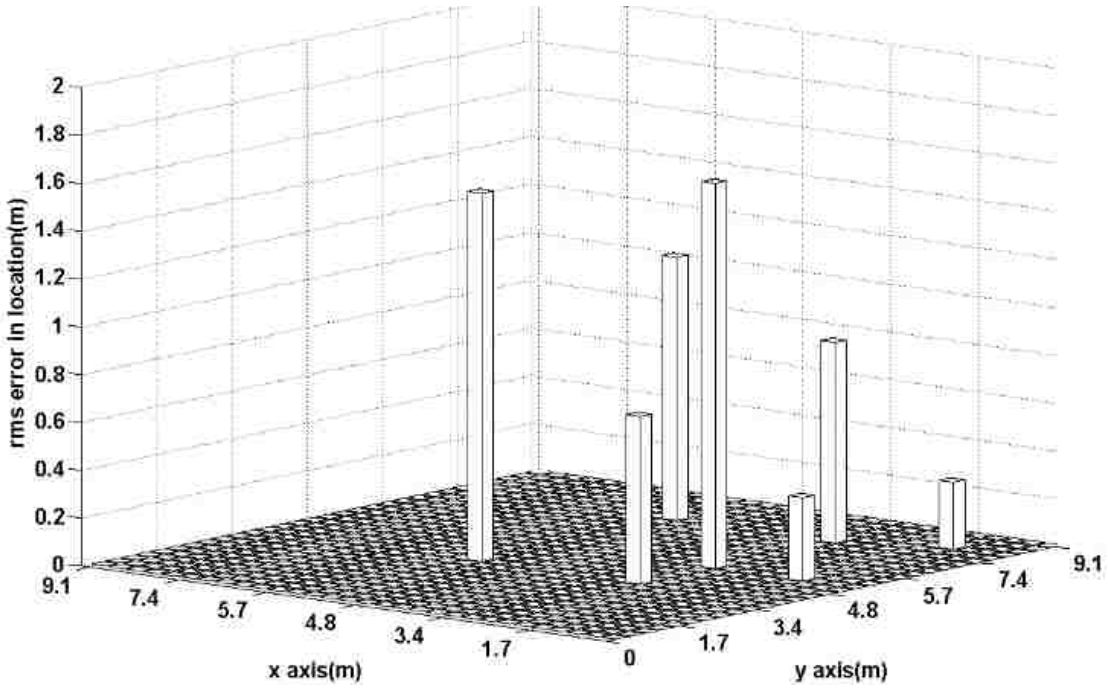

Figure 4.4. Localization errors of a single device with L-shaped array for different positions when device was inside a card board box.

Case 4) Multiple devices

In this case, two devices emitting unintended radiation were considered. Number of antenna elements in the arrays is eight, therefore the localization performance decreased when compared to the single device due to the resolution. Also a smoothing algorithm [11] was needed to separate these two correlated sources. Localization errors for the devices are given in Figure 4.5. The mean errors calculated for these devices were 0.93 m and 1.2 m. The difference in the errors between two devices is because of the different initial power levels of the devices.

Case 5) Estimating range using both arrays

In this case, elevation angle and range was estimated by the *z* axis array but only the estimated elevation angle was employed in the MUSIC spectrum of the array placed in the *x* plane. Then with a 2D search, range and azimuth angle were estimated. Mean of

range parameters estimated by both arrays was considered as the distance between the array and the source. By estimating the range parameter twice, the location accuracy is expected to be higher than estimating the range only with one array. The localization errors for this method are given in Figure 4.6. The mean error calculated for this case was 0.44 m. There was an 18% improvement in the localization accuracy.

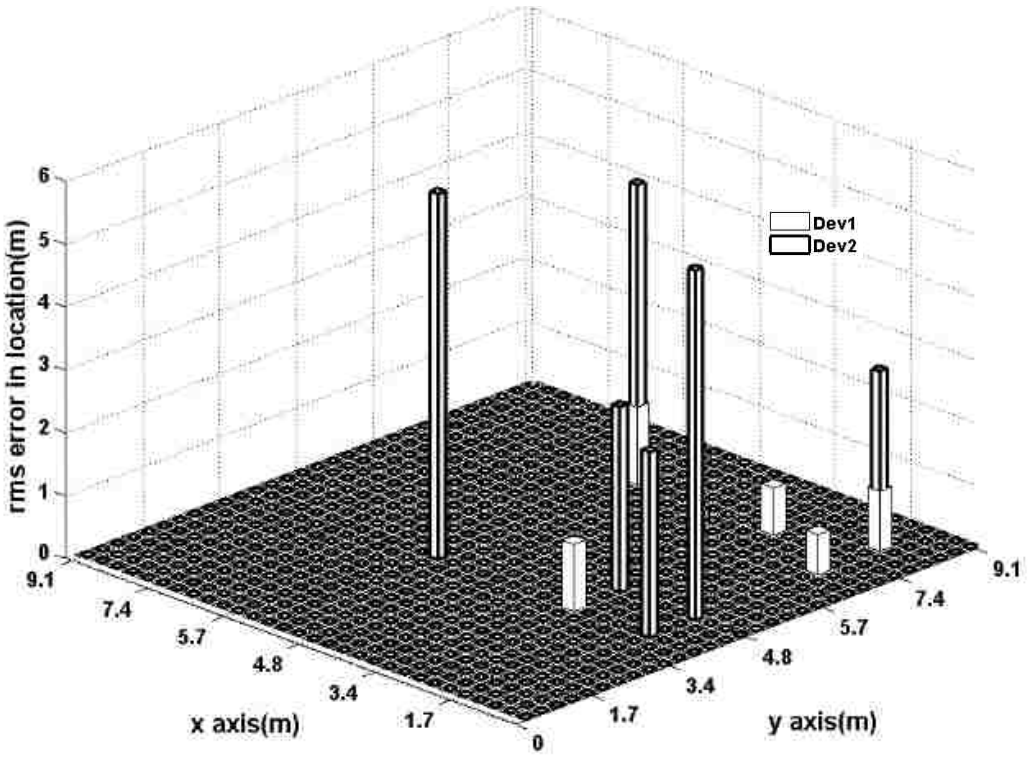

Figure 4.5. Localization errors of two devices with L-shaped array for different positions when devices are at 0.88 m height.

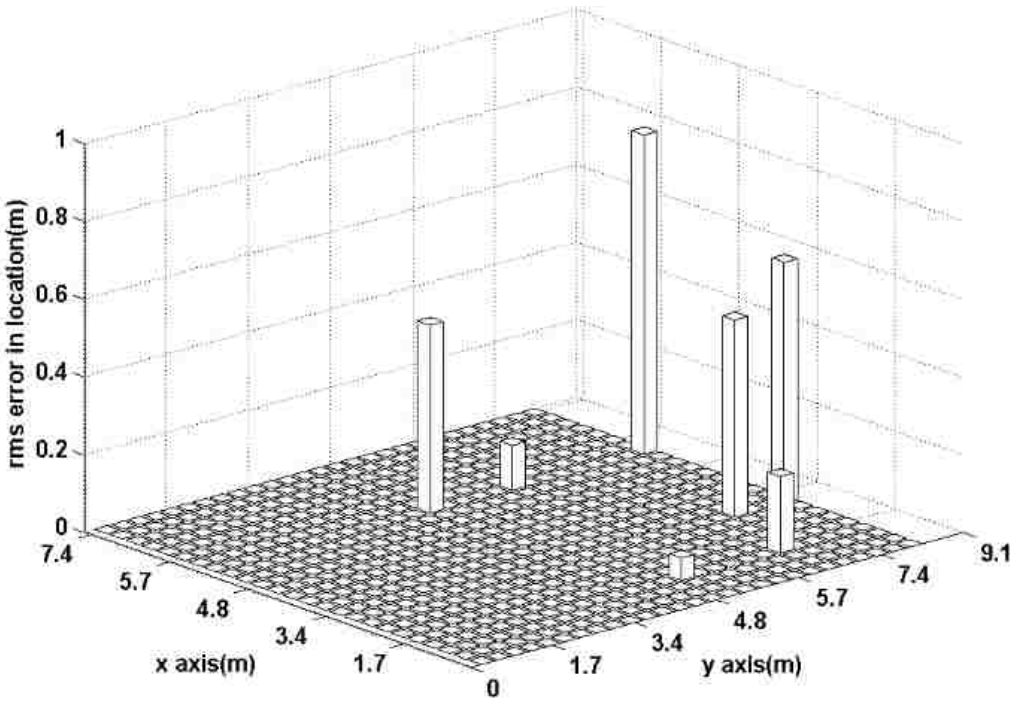

Figure 4.6. Localization errors for a single device when range is estimated by both arrays.

Case 5) Tracking

When an unintended emitting device is mobile, it can be critical to track its motion for security reasons. The tracking results of the mobile target is provided in this subsection using an L-shaped array with the proposed near-field tracking scheme. The elevation angle and the distance between the array and the source were tracked by the array placed in the *z* axis. These estimations were then used in the second-stage EKF to track the azimuth angle. Figures 4.7 and 4.8 depict the tracking performance.

Using the estimated polar coordinates, the Cartesian coordinates of the device were calculated. Initial states were estimated with the 3D localization method proposed in this paper. As shown in Figure 4.9 even if there was an error in the initial estimates, EKF refines the new estimates and the actual trajectory is caught.

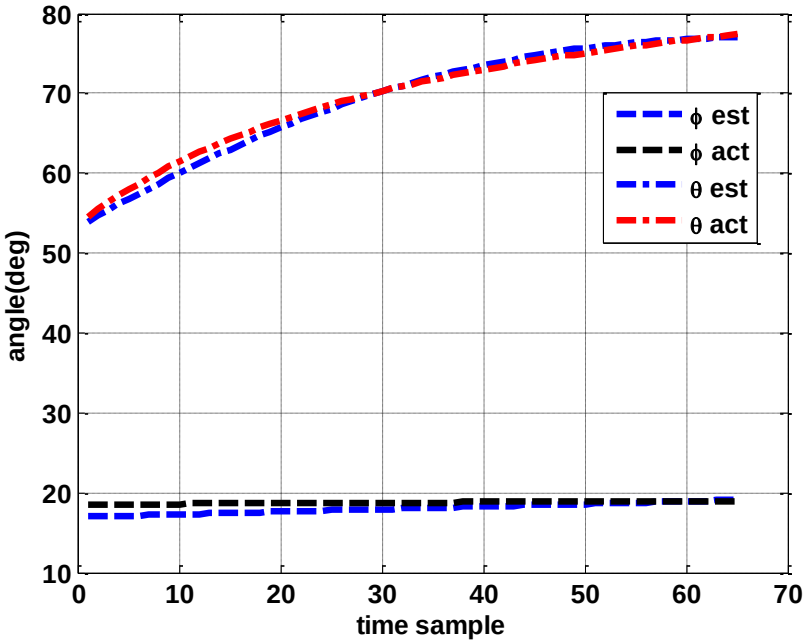

Figure 4.7. Tracking elevation and azimuth angles.

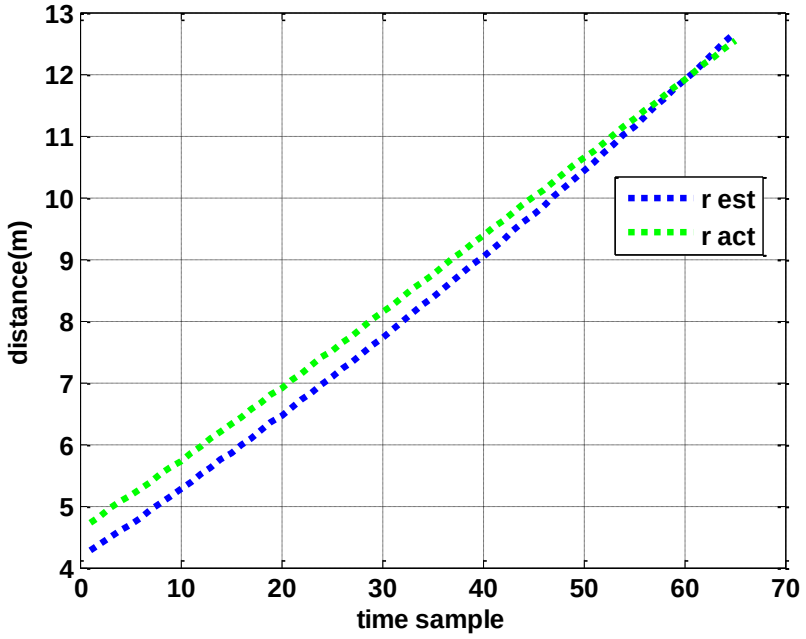

Figure 4.8. Tracking distance between the array and mobile target.

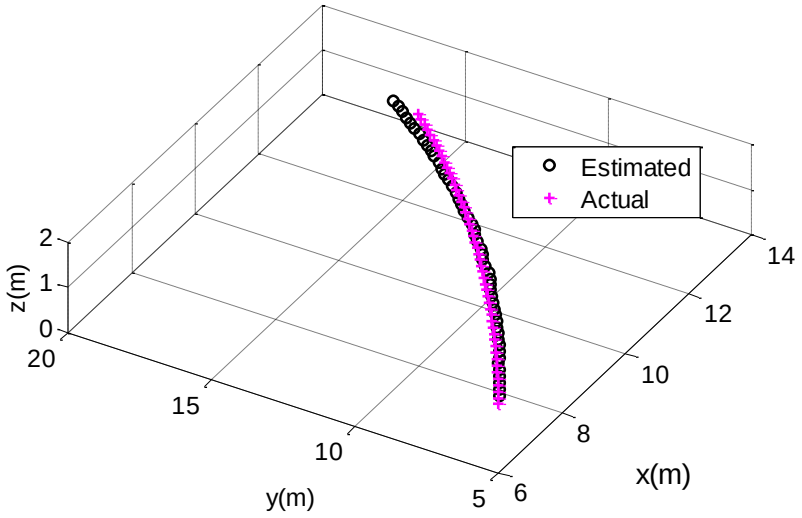

Figure 4.9. Actual and estimated trajectory for single unintended emissions.

If there are multiple devices to be tracked, the EKF solves the data association problem; therefore, an extra data association algorithm is not needed. Estimated and actual trajectories of two mobile devices are given in Figure 4.10.

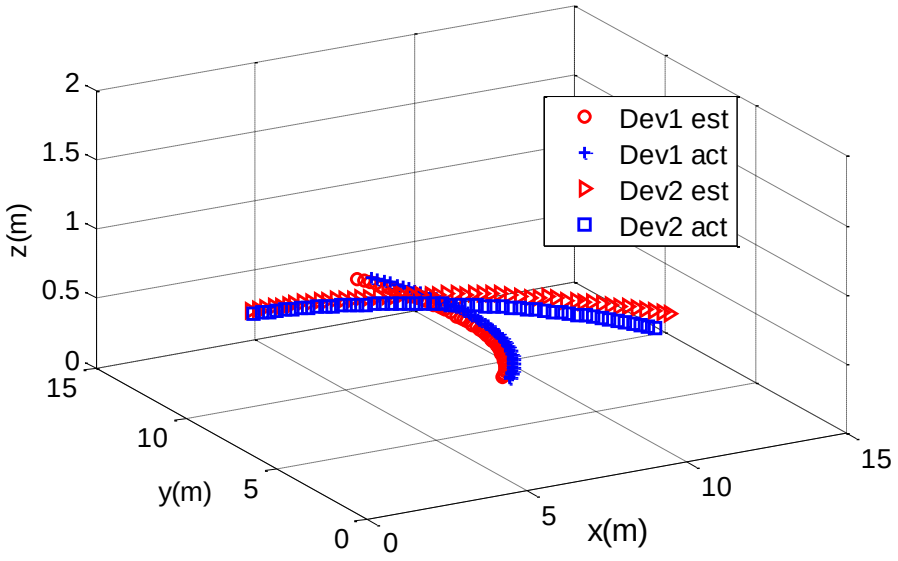

Figure 4.10. 3D tracking performance for two mobile sources.

Case 6) Localization with Kalman filter

In this case, the location of unintended emitting source is estimated using EKF as described in the tracking method mentioned in the previous case. To increase the localization accuracy, 5 samples were taken at each position. These samples were used as memory for the EKF and the initial estimates were refined with the Kalman gain. Figure 4.11 shows that the localization error decreases slightly when Kalman filter is used. For a practical application, the number of samples taken at each position is limited. However, even with only 5 samples, the location estimation improved and localization performance improves with the number of samples

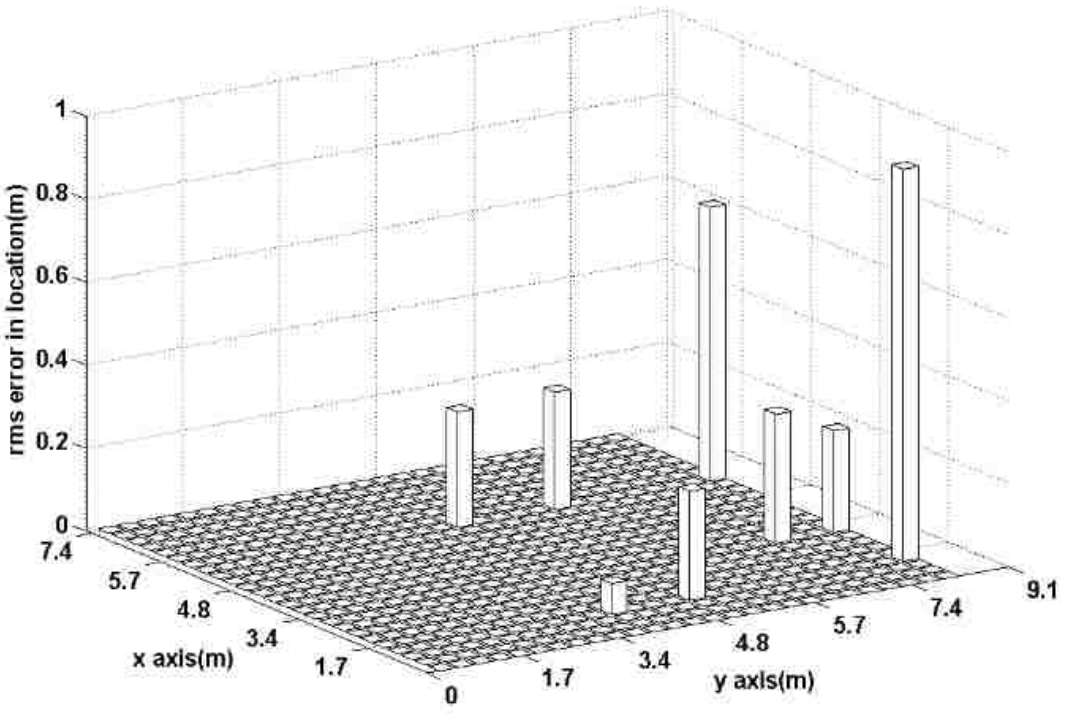

Figure 4.11. Localization errors of a single unintended emitting device by using EKF with a non-uniform measurement model.

Case 7) Localization with Green's Function

Localization of the unintended emissions is provided in this subsection by expressing the phase of the unintended emissions by free space Green's function. The phase of the signal was written in terms of device and antenna position instead of DOA information. Subsequently, the Green's function was employed in MUSIC location estimation scheme which provided the Cartesian coordinates of the device directly. The mean error calculated for this L-shaped array device with Green's function was 0.62 m. The performance of the MUSIC with Green's function is demonstrated in Figure 4.12.

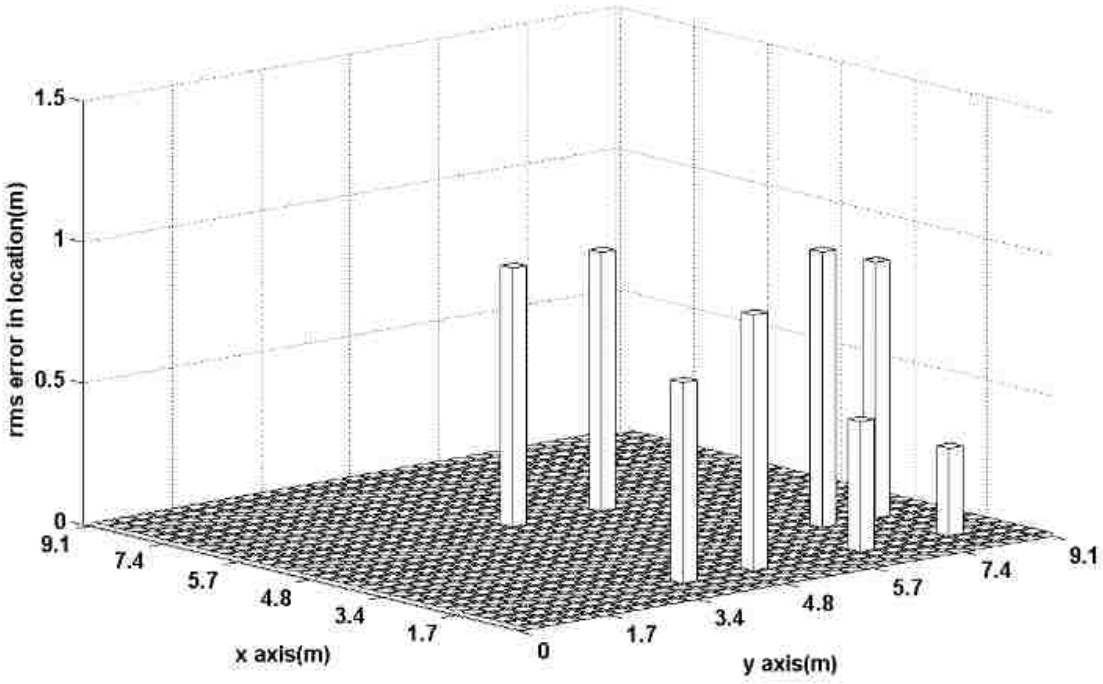

Figure 4.12. Localization errors of a single device with L-shaped array with Green's function when device is at 0.88 m in height.

5. CONCLUSIONS

This paper presents the development and evaluation of novel 3D localization and tracking algorithms for unintended emitting sources in near and far-field regions of the antenna array. Beside the azimuth angle and distance between the array and the source estimated by many near-field localization algorithms, the elevation angle was also estimated in this work to locate the ground-based unintended emissions using an L-shaped array placed to a certain height. Also, to track nonstationary targets, a tracking scheme was demonstrated which uses the L-shaped array with a two-stage EKF. This method does not require an extra data association algorithm due to EKF, and it also does not need signal or noise statistics, which makes it more appropriate for practical applications such as those discussed in this work. Further, in order to calculate the location of a device without DOA estimation, a localization scheme with free space Green's function was presented.

The experimental and simulation results indicate that localization performance increases if the device is placed close to the array, due to higher received power. Also, using an array mounted to a height gives the opportunity to locate and track an unintended emitting device, which is very important especially for surveillance and security applications. Further, if the phase of a signal is calculated with Green's function, and this information is used in MUSIC algorithm, location of the device can be estimated directly.

6. REFERENCES

[1] V. Thotla, M. T. A. Ghasr, M. J. Zawodniok, S. Jagannathan and S. Agarwal, "Detection of Super-Regenerative Receivers Using Hurst Parameter," *IEEE Trans. Instrum. Meas.*, vol.62, no.11, pp.3006-3014, Nov. 2013.

[2] V. Thotla, M. T. A. Ghasr, M. J. Zawodniok, S. Jagannathan and S. Agarwal, "Detection and Localization of Multiple R/C Electronic Devices Using Array Detectors," in *Instrumentation and Measurement, IEEE Transactions on* , vol.64, no.1, pp.241-251, Jan. 2015

[3] Sarah Seguin, "Detection of low cost radio frequency receivers based on their unintended electromagnetic emissions and an active stimulation," Ph.D dissertation, Missouri S&T, Rolla, MO 2009.

[4] R. Roy, A. Paulraj and T. Kailath, "Direction-of-arrival estimation by subspace rotation methods – ESPRIT," *IEEE International Conference on Acoustics, Speech, and Signal Proc.*, vol.11, pp.2495-2498, Apr 1986.

[5] R. Schmidt, "Multiple emitter location and signal parameter estimation," *IEEE Trans. on Ant. and Prop.*, vol.34, no.3, pp. 276- 280, March 1986.

[6] M. Viberg and B. Ottersten, "Sensor array processing based on subspace fitting," *IEEE Trans. on Signal Proc.*, vol.39, no.5, pp.1110-1121, May 1991.

[7] W. Zhi and M. Y. W. Chia, "Near-Field Source Localization via Symmetric Subarrays," IEEE Signal Processing Letters, vol.14, no.6, pp.409-412, June 2007.

[8] N. Yuen and B. Friedlander, "Performance analysis of higher order ESPRIT for localization of near-field sources," *IEEE Transactions on Signal Processing*, vol.46, no.3, pp.709-719, Mar 1998.

[9] R. N. Challa and S. Shamsunder, "High-order subspace-based algorithms for passive localization of near-field sources," *Conference Record of the Twenty-Ninth Asilomar Conference on Signals, Systems and Computers,* vol.2, pp.777-781, Oct. 30 -Nov. 1 1995.

[10] E. Cekli and H. A. Cirpan, "Unconditional maximum likelihood approach for near-field source localization," *8th IEEE International Conference on Electronics, Circuits and Systems,* vol.2, pp.753-756, Sep 2001.

[11] N. Guzey, H. Xu and S. Jagannathan, "Localization of Near-Field Radio Controlled Unintended Emitting Sources in the Presence of Multipath Fading," *IEEE Transactions on Instrumentation and Measurement*, vol.63, no.11, pp.2696,2703, Nov. 2014.

[12] T. Shan, M. Wax and T. Kailath, "On spatial smoothing for direction-of-arrival estimation of coherent signals," *IEEE Transactions on Acoustics, Speech and Signal Processing*, vol.33, no.4, pp. 806-811, Aug 1985.

[13] Y.Hua, T.K. Sarkar and D.D. Weiner, "An L-shaped array for estimating 2-D directions of wave arrival," in *IEEE Transactions on Antennas and Propagation*, vol. 39, no. 2, pp.143-146, Feb. 1991.

[14] N. Tayem and H.M. Kwon, "L-shape 2-dimensional arrival angle estimation with propagator method," in *IEEE Transactions on Antennas and Propagation*, vol. 53, no. 5, pp.1622-1630, May 2005.

[15] L. Bai, C.-Y. Peng, and S. Biswas, "Association of DOA estimation from two ULAs," IEEE Trans. Instrum. Meas., vol. 57, no. 6, pp. 1094–1101, Jun. 2008.

[16] K. F. Warnick and D. V. Arnold, "Electromagnetic Green functions using differential forms," *Journal of Electromagnetic Waves and Applications*, vol.10, no.3, pp. 427-438, 1996.

[17] S. B. Park, C. S. Ryu and K. K. Lee, "Multiple target angle tracking algorithm using predicted angles," *IEEE Transactions on Aerospace and Electronic Systems*, vol.30, no.2, pp.643- 648, Apr 1994.

[18] R.E. Zarnich, K.L. Bell and H.L. Van Trees, "A unified method for measurement and tracking of contacts from an array of sensors," *IEEE Trans. on Signal Processing*, vol.49, no.12, pp.2950-2961, Dec 2001.

[19] J. F. Gu; S. C Chan, W. P. Zhu and M. N. S Swamy, "Joint DOA Estimation and Source Signal Tracking With Kalman Filtering and Regularized QRD RLS Algorithm," *IEEE Transactions on Circuits and Systems II: Express Briefs*, vol.60, no.1, pp.46-50, Jan. 2013.

[20] J. Liang, D. Liu, X. Zeng, W. Wang, J. Zhang, and H. Chen, "Joint azimuth-elevation/(-range) estimation of mixed near-field and far-field sources using two-stage separated steering vector-based algorithm, "Progress In Electromagnetics Research, Vol. 113, 17-46, 2011.

[21] S. H. Chang, S. Y. Hou, S. C. Chang and H. S. Hung, "Novel algorithms for tracking multiple targets," *Journal of Marine Science and Technology*, vol. 18, No. 2, pp. 259-267, March 2010.

2. CONCLUSIONS AND FUTURE WORK

In this dissertation, near-field localization and tracking methods for multiple, narrowband, unintended emitting electronic devices are developed using array antennas. For correlated sources or multipath fading, a smoothing procedure is applied for efficient localization and tracking. Furthermore, general white noise assumption is relaxed by spatial diversity considering the colored noise characteristics of the environment. To locate and track the device in 3D, an L-shaped array is preferred due to its simple configuration and better accuracy. Moreover, to eliminate multipath fading and to assure better reception, the array is placed to a certain height. The performances of the proposed methods are evaluated with a hardware setup. Finally, computer simulations are provided to verify the experimental results.

2.1 CONCLUSIONS

In this dissertation, first, a near-field localization technique for correlated unintended emitting sources was developed. Spatial smoothing procedure was applied and the antenna array was divided into overlapping subarrays to separate the correlated sources and the multipath fading signals. With the random phase modulation, which was a result of spatial smoothing, the signals were separated and the mean of the covariance matrices of the subarrays were employed in a two-dimensional search. Moreover, instead of computer simulations, hardware evaluation of the proposed method, symmetric subarray based localization method and conventional 2D MUSIC provide more realistic results. Finally, the data from the experimental setup demonstrate that Smooth 2-D

MUSIC is more efficient than other near-field localization methods especially in the presence of multipath fading.

Similar to the subspace-based localization schemes, the proposed technique in the first paper assumes a white Gaussian noise which may not always be possible especially in a real environment. The colored characteristics of the environmental noise have to be considered. First, a whitening filter was generated with signal-free measurements. Then, a near-field localization technique with two well separated arrays was developed. With the spatial diversity among the arrays, the locations of the devices were estimated by using generalized correlation decomposition.

The experimental results indicated that the localization accuracy increases with the whitening filter when compared to Smooth 2D MUSIC; however, the accuracy of the whitening filter depends upon the signal-free samples which are limited in practical applications. Hence the spatial diversity of noise on two separate arrays provided better localization accuracy over other methods. In addition noise statistics were not used; therefore, the proposed method is more adaptive to environmental conditions.

Next, a near-field tracking scheme for nonstationary unintended emitting sources is proposed in Paper III. Instead of constructing the covariance matrix of the array output for every time instant as recommended for tracking techniques in the literature, the output of the array was directly used in extended Kalman filter which made the proposed method more practical. The experimental results indicate that the tracking performance increases if the target moves slower since it provides taking more samples during a trajectory which helps in the tuning of the EKF more frequently. In addition, if multiple antenna arrays are used and their mean is considered as the tracking result, the increase in

accuracy is clearly observed. Finally, experimental results show that the proposed method is more efficient than Park's method where a linear measurement model and array output covariance matrix is used for the Kalman filter.

In fourth paper, analysis of the proposed methods provided with computer simulations. Results show that, since the power of the emissions are very low, it is more appropriate to use near-field techniques. By this analysis, the performance of the proposed methods, which were supported with experimental data, is verified and the computer simulations show that the near-field approach for localization of unintended emissions is highly satisfactory.

In the fifth paper, a suite of near-field, 3D localization and tracking schemes are presented for unintended emissions by using an L-shaped array. This chapter shows that multipath fading and reflections can be eliminated by placing the array at a certain height. The experimental evaluation show how localization performance increases if the source is close to the array because of the weak nature of emissions. Furthermore, when manipulating the phase of the signals with Greens function, the errors in the DOA estimation do not affect the location calculation. Also, this method is suitable for every array configurations.

2.2 FUTURE WORK

As a part of future work, noise cancelation for the localization can be considered. Since the power of the emissions is very weak, it is very difficult to distinguish signal and noise eigen values for subspace based DOA estimation algorithms. By noise cancelling, signal and noise subspaces can be separated efficiently, which results in a more accurate localization.

In this dissertation, the antennas in the array were identical and the spacing between the elements was uniform. If a problem occurs in one of the antennas, an adaptive localization method can be developed by considering this issue.

Furthermore, although an L-shaped array can be placed to a height for better reception and used for 3D localization, instead of array antennas, an unmanned aerial vehicle (UAV) flying above the target can synthesize an array in any configuration. In this way, ground-based targets can be located and tracked efficiently.

REFERENCES

[1] D. G. Beetner, S. Seguin and T. Hubing, "Electromagnetic emissions stimulation and detection system," U.S. Patent 7,464,005, Dec. 9, 2008.

[2] C. Stagner, A. Conrad, C. Osterwise, D. G. Beetner and S. Grant, "A practical superheterodyne-receiver detector using stimulated emissions," *IEEE Transactions on Instrumentation and Measurement*, Vol. 60, No. 4, April 2011.

[3] J. Hertenstein and S. Jagannathan, "Simulation and Detection of Unintended Electromagnetic Emissions From Super-Regenerative Receivers," *IEEE Transactions on Instrumentation and Measurement*, vol.62, no.7, pp.2093-2100, July 2013.

[4] V. Thotla, M.T.A. Ghasr, M. Zawodniok, S. Jagannathan and S Agarwal, "Detection of Super-Regenerative Receivers Using Hurst Parameter," *IEEE Transactions on Instrumentation and Measurement*, vol.62, no.11, pp.3006,3014, Nov. 2013.

[5] Sarah Seguin, "Detection of low cost radio frequency receivers based on their unintended electromagnetic emissions and an active stimulation," Ph.D dissertation, Missouri University of Science and Technology, Rolla, MO 2009.

[6] A. Shaik, H. Weng, X. Dong, T.H. Hubing and D.G. Beetner, " Matched filter detection an identification of electronic circuits based on their unintentional radiated emissions," *IEEE International Symposium on In Electromagnetic Compatibility*, vol. 3, pages 853-856, August 2006.

[7] N. Salman, M. Ghogho and A.H. Kemp, "On the Joint Estimation of the RSS-Based Location and Path-loss Exponent," *IEEE Wireless Communications Letters*, vol.1, no.1, pp.34-37, February 2012.

[8] A.Kushki, ; K.N. Plataniotis and A.N. Venetsanopoulos, "Kernel-Based Positioning in Wireless Local Area Networks," *IEEE Transactions on Mobile Computing*, vol.6, no.6, pp.689-705, June 2007.

[9] B. B. Peterson, C. Kmiecik, R. Hartnett, P. M. Thompson, J. Mendoza, and H. Nguyen, "Spread spectrum indoor geolocation," *J. Inst. Navigat*., vol. 45, no. 2, pp. 97–102, 1998.

[10] X. Li, K. Pahlavan, M. Latva-aho, and M. Ylianttila, "Comparison of indoor geolocationmethods in DSSS and OFDM wireless LAN," in Proc. *IEEE Veh. Technol. Conf.*, Sep. 2000, vol. 6, pp. 3015–3020.

[11] S. Correal, S.Kyperountas,Q. Shi, and M.Welborn, “An ultrawideband relative location system,” in Proc. *IEEE Conf. Ultra Wideband Syst.Technol*, pp. 394–397, Nov. 2003.

[12] Y. Zhu, D.Huang, A. Jiang; “Network localization using angle of arrival,” *IEEE International Conference on Electro/Information Technology*, pp.205-210, 18-20 May 2008.

[13] C. Balanis, Antenna Theory Analysis and Design, John Wiley and Sons, 2nd ed. 1997.

[14] R. Schmidt, "Multiple emitter location and signal parameter estimation," *IEEE Transactions on Antennas and Propagation*, vol.34, no.3, pp. 276- 280, Mar 1986.

[15] R. Roy and T. Kailath, “ESPRIT-estimation of signal parameters via rotational invariance techniques,” *IEEE Transactions on Acoustics, Speech and Signal Processing*, vol.37, no.7, pp.984-995, Jul 1989.

[16] M.F. Khan and M. Tufail, “Comparative analysis of various Matrix Pencil methods for direction of arrival estimation,” *International Conference on Image Analysis and Signal Processing (IASP)*, pp.496-501, 9-11 April 2010.

[17] J. Xin and A. Sano, “Computationally efficient subspace-based method for direction-of-arrival estimation without eigendecomposition,” *IEEE Transactions on Signal Processing*, vol.52, no.4, pp. 876- 893, April 2004.

[18] B. D. Steinberg, Principles of Aperture and Array System Design: Including Random and Adaptive Arrays. New York, NY, USA: Wiley, 1976, pp. 9–10.

[19] N. Yuen and B. Friedlander, “Performance analysis of higher order ESPRIT for localization of near-field sources,” *IEEE Transactions on Signal Processing*, vol.46, no.3, pp.709-719, Mar 1998.

[20] E, Cekli and H. A. Cirpan, “Unconditional maximum likelihood approach for near-field source localization,” *8th IEEE International Conference on Electronics, Circuits and Systems*, vol.2, pp.753-756 Sep 2001.

[21] R.N. Challa and S. Shamsunder, “High-order subspace-based algorithms for passive localization of near-field sources,” *Conference Record of the Twenty-Ninth Asilomar Conference on Signals, Systems and Computers*, 1995. vol.2, pp.777,781 vol.2, Oct. 30 1995-Nov. 1 1995.

[22] L. Fu and R. J. Vaccaro, “Performance degradation of DOA estimators due to unknown noise fields,” *IEEE Transactions on Signal Processing*, vol.40, no.3, pp.686-690, Mar 1992.

[23] V. Nagesha and S. Kay, "Maximum likelihood estimation for array processing in colored noise," *IEEE International Conference on Acoustics, Speech, and Signal Processing*, vol.4, pp.240-243, 27-30 April 1993.

[24] H. Ye and R. D. DeGroat, "Maximum likelihood DOA estimation and asymptotic Cramer-Rao bounds for additive unknown colored noise," *IEEE Transactions on Signal Processing*, vol.43, no.4, pp.938-949, Apr 1995.

[25] B. Goransson and B. Ottersten, "Direction estimation in partially unknown noise fields," *IEEE Transactions on Signal Processing*, vol.47, no.9, pp.2375-2385, Sep 1999.

[26] B. Friedlander and A. J. Weiss, "Direction finding using noise covariance modeling," *IEEE Trans. on Signal Proc.*, vol.43, no.7, pp.1557-1567, Jul 1995.

[27] M. Viberg, P. Stoica and B. Ottersten, "Maximum likelihood array processing in spatially correlated noise fields using parameterized signals," *IEEE Trans. on Signal. Proc.*, vol.45, no.4, pp.996-1004, Apr 1997.

[28] K. Werner and M. Jansson, "Optimal Utilization of Signal-Free Samples for Array Processing in Unknown Colored Noise Fields," *IEEE Trans. on Signal Processing*, vol.54, no.10, pp.3861-3872, Oct. 2006.

[29] G. C. Carter, "Coherence and time delay estimation," *Proceedings of the IEEE*, vol.75, no.2, pp.236- 255, Feb. 1987.

[30] J. F. Yang and M. Kaveh, "Adaptive eigen subspace algorithms for direction or frequency estimation and tracking," *IEEE Transactions on Acoustics, Speech and Signal Processing*, vol.36, no.2, pp.241-251, Feb 1988.

[31] C. K. Sword, M. Simaan and E. W. Kamen, "Multiple target angle tracking using sensor array outputs," *IEEE Transactions on Aerospace and Electronic Systems* , vol.26, no.2, pp.367- 373, Mar 1990.

[32] C. R. Rao, C. R. Sastry and B. Zhou, "Tracking the direction of arrival of multiple moving targets," *IEEE Transactions on Signal Processing*, vol.42, no.5, pp.1133-1144, May 1994.

[33] J. Sanchez-Araujo and S. Marcos, "An efficient PASTd-algorithm implementation for multiple direction of arrival tracking," *IEEE Transactions on Signal Processing*, vol.47, no.8, pp.2321-2324, Aug 1999.

[34] S. B. Park, C. S. Ryu and K. K. Lee, "Multiple target angle tracking algorithm using predicted angles," *IEEE Transactions on Aerospace and Electronic Systems*, vol.30, no.2, pp.643- 648, Apr 1994.

[35] C. S. Ryu, S. H. Lee and K. K. Lee, "Multiple target angle tracking algorithm using angular innovations extracted from signal subspace," *IEEE Electronics Letters*, vol.35, no.18, pp.1520-1522, 2 Sep 1999.

[36] W. Zhi and M. Y.W. Chia, "Near-Field Source Localization via Symmetric Subarrays," *IEEE Signal Processing Letters*, vol.14, no.6, pp.409,412, June 2007.

[37] Y. D. Huang and M , Barkat, "Near-field multiple source localization by passive sensor array, " *IEEE Transactions on Antennas and Propagation*, vol.39, no.7, pp.968,975, Jul 1991.

[38] Y.Hua, T.K. Sarkar and D.D. Weiner, "An L-shaped array for estimating 2-D directions of wave arrival," in IEEE Transactions on Antennas and Propagation, vol. 39, no. 2, pp.143-146, Feb. 1991.

[39] N. Tayem,and H.M. Kwon, "L-shape 2-dimensional arrival angle estimation with propagator method," in IEEE Transactions on Antennas and Propagation, vol. 53, no. 5, pp.1622-1630, May 2005.

[40] L. Bai, C.-Y. Peng, and S. Biswas, "Association of DOA estimation from two ULAs," IEEE Trans. Instrum. Meas., vol. 57, no. 6, pp. 1094–1101, Jun. 2008.

[41] S. Kikuchi, H. Tsuji, and A. Sano, "Pair-matching method for estimating 2-D angle of arrival with a cross-correlation matrix," IEEE Antennas Wireless Propag. Letters, vol. 5, no. 1, pp. 35–40, Dec. 2006.

VITA

Nurbanu Guzey was born in Yozgat, Turkey in 1984. She earned her bachelor's degree in Electronics and Communication Engineering from Yildiz Technical University, Istanbul Turkey in 2006. She received a fellowship from Turkish Ministry of Education for graduate education in the USA.

She started her master's degree in Electrical Engineering at University of Texas at Dallas in September 2009 and earned her degree in August 2011. During her education she completed a thesis entitled "Effects of Random Delay Errors in Transversal Filters". In September 2011 she started her Doctorate of Philosophy in Electrical Engineering at Missouri University of Science and Technology. She worked as a research assistant with Dr. Jagannathan Sarangapani. Her work was based on localization and tracking of electronic devices using their unintended emissions. She received the degree of Doctor of Philosophy in Electrical Engineering from Missouri University of Science and technology in December 2015.